Università degli Studi di Cagliari
Facoltà di Scienze Matematiche Fisiche Naturali
Dipartimento di Chimica Inorganica e Analitica

Near-Infrared Luminescent Lanthanide Complexes of Quinolinol Ligands: Structure/Properties Relationship

PhD thesis of:

Flavia Artizzu

Supervisor:
Prof. Paola Deplano

Coordinators:
Prof. I. Ferino
Prof. V. Lippolis

Dottorato di Ricerca in Chimica
Settore Scientifico Disciplinare CHIM03

XX Ciclo
2004-2007

Alla mia famiglia

"These elements (lanthanides) perplex us in our researches, baffle us in our speculations and haunt us in our dreams. They stretch like an unknown sea before us, mocking, mystifying and murmuring strange revelations and possibilities"

Sir William Crookes

Address to the British Association, 1887

Table of Contents

Chapter 5

Chapter 6

Chapter 1

Introduction

A general overview on the development of new-generation optical devices based on lanthanide complexes, pointing out the importance of NIR-emissive compounds in several technological applications, is given here.

1.1 Introduction

Since the first report by Tang and VanSlyke[1-3] of efficient green electroluminescence from aluminium quinolinolates (AlQ_3, Q=8-quinolinolato), extensive work has been performed to improve the properties of organic light emitting devices based on "small molecules" (*Low molecular weight molecule* - OLEDs), till the development of flat panel displays and other emitting devices.[4-6] Emission from AlQ_3 is due to an intra-ligand transition which is strongly enhanced by ligand coordination to the metal ion.

In these last years, many efforts have been made to improve the luminescence properties of this class of emitting molecules and to "fine-tune" the emission wavelength by varying the metal ion or the nature and the position of the substituents on the ligands.[2,7]

In the earlier 1990s,[8-9] lanthanide ions* were proposed as luminescent materials for electroluminescent devices, because their emission is long-lived and can be considered as nearly monochromatic.

Due to their unique photochemical properties, with emission wavelengths that span from the UV to the near-infrared (NIR), and also to their paramagnetic properties, lanthanides are currently finding numerous

*Given the relatively high natural abundance and distribution of lanthanide elements on Earth's crust (for instance Nd is more abundant than Pb), the trivial term "rare-earth" with which lanthanides are often referred to, has somewhat lost his meaning, and its use is strongly discouraged by IUPAC. Therefore, in this thesis, f-block elements will be always referred to as "lanthanides".

applications in many different fields ranging from optoelectronics to biology. In particular, interest is growing for their potential applications as: (i) phosphors for lighting industry;[10] (ii) electroluminescent and/or photoluminescent materials for organic light emitting diodes and optical fibres for display technology and telecommunications;[11] (iii) functional complexes for biological assays and medical imaging purposes.[12-14]

The three NIR-emitting ions, Nd^{III}, Er^{III}, Yb^{III} (and, in part, Pr^{III}), are recently gaining much popularity because, besides their several potential applications in telecommunications and biomedical analysis, recent advances in electronics and detector technology allow the detection of weak NIR emission by means of readily available and modestly priced equipment.[15]

Among the NIR-emitting lanthanide ions, Er^{III} plays a special role in telecom technologies, since it displays a sharp emission occurring at the wavelength of 1.55 μm (0.8 eV), thus covering a spectral window in which glass optical fibres show high transparency (the so-called third-communication window). Doped silica fibres such as EDFAs (Erbium Doped Fiber Amplifiers) are at the heart of the optical amplification technology used in the long-haul communication systems operating in the 1.5-μm spectral window. Also other lanthanide ions such as Yb^{III}, Pr^{III} and Nd^{III}, are being used as dopants in optical amplifiers since they can strengthen the signal in the first and second-communication windows, at 1 μm and 1.33 μm wavelengths.

A disadvantage of this technology stems from the weak absorptivity of lanthanide ions and their very low solubility in all inorganic matrices, resulting in long and expensive amplifiers. A promising strategy to overcome these drawbacks is to encapsulate the lanthanide ion by a "light harvesting" organic ligand which allows optical pumping and provides good solubility in the host material. Moreover, the ligand can shield the ion from additional coordination from the solvent or impurities in the matrix, which could quench the luminescence. Such lanthanide complexes could enable the realisation of a new generation of low-cost optical amplifiers in the centimeter-length scale, featuring superior optical and mechanical figures of merit,[16-17] and are suitable for the fabrication of photonic integrated circuits.[16-17]

A brief description of organic light emitting diodes (OLEDs) and of optical fibres is given in the Appendix Section of this thesis (A.1).

Finally, it is worth mentioning that NIR-emitting lanthanide complexes are also finding many applications as luminescent probes and sensors for biological assays especially for *in vivo* time-resolved imaging of biological tissues (e.g. cancer detection), which are highly transparent in part of the NIR spectral range (0.9-1.5 μm approximately). This is of special interest since, given that NIR-emission from lanthanide complexes can be obtained after long-wavelength (in the Visible region) excitation of the ligand chromophore, UV irradiation of biological tissues, which can be harmful for *in vivo* applications, could be avoided.[18-19]

1.2 Aim of the work

Lanthanide quinolinolates represent a class of compounds which have been proposed as low cost emitting materials in the visible and near-infrared region.[20-25] Among the several organo-erbium complexes extensively investigated as emitting materials in the last decade, the ErQ_3 complex[#] can be considered as a prototype organo-lanthanide system for 1.5-μm telecom applications and has gathered much attention especially after the demonstration of the first electrically excited organic IR emitter.[20-21]

Despite the interest of physicists into these compounds, since recently, literature lacked completely in optimised synthetic procedures, and the structures of lanthanide quinolinolates were not available. This has so far led to questionable assignments of the deactivation mechanisms affecting the luminescence properties of lanthanide quinolinolates. Therefore, a detailed understanding of the structure/property relationship was strongly demanded.

This work has been primarily focused on finding reliable structure-property relationships of lanthanide quinolinolato complexes to be used as potential emitters in telecom technology. This should also allow to draw up the guidelines to design new lanthanide complexes with improved luminescence efficiency.

[#] This complex is commercialised by Sigma Aldrich as ErQ_3, Tris(8-hydroxyquinolinato)erbium(III) Empirical Formula: $C_{27}H_{18}ErN_3O_3$, Formula Weight: 599.71, Product no. 658502.

In particular the research has been addressed to:

I. a reinvestigation of the synthetic procedures of lanthanide complexes of 8-hydroxyquinoline and its halogen-substituted derivatives to deepen the knowledge of the chemistry of these complexes, so far limited by experimental difficulties in obtaining analytically pure products and by the absence of structural characterisation. Efforts have been focused on finding detailed experimental conditions to provide pure products useful for optical devices and on determining the structural features and properties of these complexes.

II. an exploration of the processing potential of this class of compounds which have been proposed by physicists as emitters for numerous applications in photonics. Among the several techniques with which organo-lanthanides can be processed to obtain new materials suitable for optical applications, the sol-gel method to prepare innovative lanthanide-doped sol-gel glasses appears to be one of the most promising. This processing method has therefore been selected for the preparation of a series of highly transparent and homogeneous glasses incorporating lanthanide quinolinolates whose photophysical properties are to be deeply investigated.

III. find, on the basis of the obtained results, the guidelines to obtain NIR-emitting lanthanide complexes with improved luminescence

properties. These include the use of deuterated or perfluorinated ligands and solvents,[26-27] to minimise the deactivation pathways trough high-frequency oscillators such as OH or CH groups (see Chapter 2), as well as the use of metal-d complexes as ligands toward the lanthanide ion.[28-29]

References

[1] C. W. Tang, S.A. Van Slyke, *Appl. Phys. Lett.* **1987**, *51*, 913.

[2] C. H. Chen, J. Shi, *Coord. Chem. Rev.* **1998**, *171*, 161.

[3] C. W. Tang, S. A. VanSlyke, C. H. Chen, *J. Appl. Phys.* **1989**, *65*, 3610.

[4] U. Mitscke, P. Bauerle, *J. Mater. Chem.* **2000**, *10*, 1471.

[5] T. W. Kelley, P. F. Baude, C. Gerlach, D. E. Ender, D. Muyres, M. A. Haase, D. E. Vogel, S. D. Theiss, *Chem. Mater.* **2004**, *16*, 4413.

[6] J. Kido, Y.Okamoto*, Chem. Rev.* **2002**, *102*, 2357.

[7] R. Ballardini, G. Varani, M. T. Indelli, F. Scandola, *Inorg. Chem.***1986**, *25*, 3858.

[8] J. Kido, K. Nagai, Y. Ohashi, *Chem. Lett.* **1990**, 657.

[9] J. Kido, K. Nagai, Y. Okamoto, *Chem. Lett.* **1991**, 1267.

[10] T. Jüstel, H. Nikol, C. Ronda, *Angew. Chem., Int. Ed. Engl.* **1998**, *37*, 3084.

[11] S. Capecchi, O. Renault, D.-G. Moon, M. Halim, M. Etchells, P. J. Dobson, O. V. Salata, V. Christou, *Adv. Mater.* **2000**, *12*, 1591.

[12] P. Caravan, J. J. Ellison, T. J. McMurry, R. B. Lauffer, *Chem. Rev.* **1999**, *99*, 2293.

[13] D. Parker, *Coord. Chem. Rev.* **2000**, *205*, 109.

[14] V. W. W. Yam, K. K. W. Lo, *Coord. Chem. Rev.* **1999**, *184*, 157.

[15] J.-C. G. Bunzli, C. Piguet, *Chem. Soc. Rev.* **2005** *34*, 1048-1077.

[16] K. Kuriki, Y. Koike Y. Okamoto, *Chem. Rev.* **2002**, *102*, 2347-2356.

[17] L. H. Slooff, A. Van Blaaderen, A. Polman, G. A. Hebbink, S. I. Klink, F. C. J. M. Van Veggel, D.N. Reinhoudt, J. W. Hofstraat, *J. Appl. Phys.* **2002**, *91*, 3955-3979.

[18] A. V. Chudinov, V. D. Rumyantseva, A. V. Lobanov, G. K. Chudinova, A. A. Stomakhin, A. F. Mironov, *Russ. J. Bioorg. Chem.* **2004**, *30*, 89.

[19] M. H. V. Werts, R. H. Woudenberg, P. G. Emmerink, R. van Gassel, J. W. Hofstraat, J. W. Verhoeven, *Angew. Chem., Int. Ed.* **2000**, *39*, 4542 and references therein.

[20] R. J. Curry, W. P. Gillin, *Appl. Phys. Lett.* **1999,** *75,* 1380.

[21] W. P. Gillin, R. J. Curry, *Appl. Phys. Lett.* **1999**, *74,* 798.

[22] O. M. Khreis, R. J. Curry, M. Somerton, W. P. Gillin, *J. Appl. Phys.* **2000**, *88*, 777.

[23] M. Iwamuro, T. Adachi, Y. Wada, T. Kitamura, S. Yanagida, *Chem. Lett.* **1999**, 539;

[24] M. Iwamuro, T. Adachi, Y. Wada, T. Kitamura, N. Nakashima, S. Yanagida, *Bull. Chem. Soc. Jpn.* **2000**, *73*, 1359-1363.

[25] O. M. Khreis, W. P. Gillin, M. Somerton, R.J. Curry, *Org. Electron.* **2001**, *2*, 45.

[26] G. A. Hebbink, D.N. Reinhoudt, F. C. J. M. van Veggel, *Eur. J. Org. Chem.* **2001**, 4101-4106.

[27] G. Mancino, A. J. Ferguson, A. Beeby, N. J. Long, T. Jones, *J. Am. Chem. Soc.* **2005**, *127*, 524-525.

[28] D. Imbert, M. Cantuel, J.-C. G. Bünzli, G. Bernardinelli, C. Piguet *J. Am.Chem. Soc.* **2003**, *125*, 15698.

[29] S. Torelli, D. Imbert, M. Cantuel, G. Bernardinelli, S. Delahaye, A. Hauser, J.-C.G. Bünzli, C. Piguet *Chem. Eur. J.* **2005**, *11*, 3228.

Chapter 2

Background

The luminescent properties of lanthanides and the emission mechanism of complexes with suitable "antenna" ligands, are described here. Principles of quenching phenomena that may affect the luminescent emission of trivalent near-infrared emitting lanthanide ions are also discussed. A general overview on the coordination chemistry of the lanthanide ions is also given, pointing out the peculiar chemical behaviour of Ln^{III} ions arising from the $[Xe]4f^{n}5s^{2}5p^{6}$ configurations and their position in the periodic table.

2.1 Introduction

The lanthanide (or lanthanoid) series comprises the 15 elements with atomic numbers 57 through 71, from lanthanum to lutetium, and occupies a unique position in the periodic table, which correspond to the first period of f-block elements, having $[Xe]4f^n5d^16s^2$ general configurations. Due to their specific electronic configurations and the low electronegativity, lanthanide atoms tend to lose three electrons, usually $5d^1$ and $6s^2$, to attain their most stable oxidation state as trivalent ions. The lanthanide trications possess characteristic $4f^n5s^2p^6$ openshell configurations, featuring a Xe core electronic configuration with the addition of n 4f electrons, with n varying from 0 (for La^{III}) to 14 (for Lu^{III}). This $4f^n$ sub-shell lies inside the ion, shielded by the $5s^2$ and $5p^6$ closed sub-shells. Thus, lanthanide ions are sometimes referred to as “triple-positively charged noble gases”.

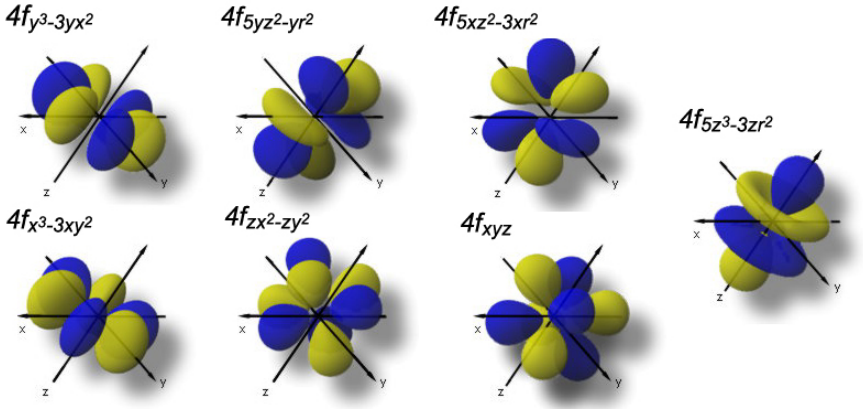

Fig. 2.1: The 4f orbitals.

Since all the changes take place two shells in, even removing the 6s shell does not bring the 4f electrons to the outer layer. Therefore, all these elements are very similar chemically, since their outer shells, even as ions, are virtually identical.

The partially filled 4f shell, with several unpaired electrons, gives unique properties to the lanthanide ions, which show special luminescent and magnetic behaviour, that are of interest for several potential applications.

2.2 Lantanide luminescence

The narrow emission bands of the lanthanide ions originate from intrashell f→f transitions that, being Laporte-forbidden, are also characterised by low absorption coefficients and relatively long lifetimes (up to several milliseconds). Lanthanide ions with completely filled (Lu^{III}) or empty (La^{III}) 4f orbitals are not luminescent, whereas, for the other ions, emission ranges from UV to NIR. Due to the fact that the 5s and 5p shells have a larger radial dispersion than 4f orbitals, they effectively shield the latter from environmental effects and ligand perturbation. Thus, lanthanide ions retain to a great extent the spectroscopic and magnetic properties of the free ions and the electronic spectra of tripositive lanthanide compounds can be considered as derived from the spectra of the gaseous ions by a fairly small perturbation and feature a line-like nature.[1]

Each 4f electron is characterised by the 4 quantum numbers: n=4, l=3, m_l and m_s, and the degeneracy of each configuration in the absence of any interaction is given by:[2]

$$\frac{(4l+2)!}{n!(4l+2-n)!}\text{; with } l = 3 \qquad \text{Eq. 1}$$

The energy levels originating from the electronic terms of the $4f^n$ configurations are written $^{(2S+1)}\Gamma_J$ (where S is the spin multiplicity, Γ represents the orbital angular momentum and J is the total angular momentum) following the *Russell-Saunders L, S, J coupling scheme* in which the spin-orbit coupling originates J levels from the $^{(2S+1)}\Gamma$ terms. In principle, this is just a rough approximation for the lantanide ions whose levels are more appropriately described on the basis of the *j-j coupling scheme* which takes into greater account the spin-orbit interaction rather than the interelectronic repulsion, or, even better, with the *intermediate coupling scheme* in which coulombic and spin-orbit interactions have the same importance and terms with the same J but different L and S could mix. However, the Russell-Saunders scheme still represents a convenient way to label the energy levels of a lanthanide ion.

According to Hund's rule, the ground term for the free ion is derived from the largest values of L and S quantum numbers while the spin-orbit coupling quantum number, J, ranges from $L-S \leq J \leq L+S$ and takes, for the fundamental level, the value J = L–S for $n < 7$ (La-Eu) and J = L+S for $n \geq 7$ (Gd-Lu).

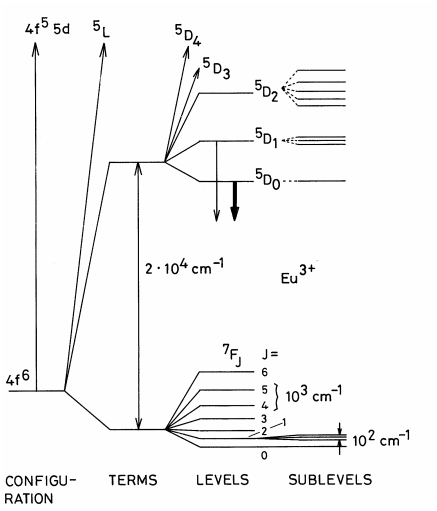

Fig. 2.2: Spectroscopic terms and energy levels of Eu^{3+}.

With respect to $^{(2S+1)}\Gamma$, the energy of a $^{(2S+1)}\Gamma_J$ level is:[2]

$$E_{SO} = \tfrac{1}{2}\lambda[J(J+1) - L(L+1) - S(S+1)] \text{ (Landé's rule)} \qquad \text{Eq. } \mathbf{2}$$

The energy separation between $^{(2S+1)}\Gamma$ terms induced by the coulombic effect is about 10^5-10^4 cm^{-1} while the gap between J-levels induced by spin-orbit coupling is about 10^3 cm^{-1}.[2] Therefore, since this energy gap is much greater than the thermal energy at ambient temperature ($kT \cong 200$ cm^{-1}), J levels other than the fundamental level are hardly populated.[3]

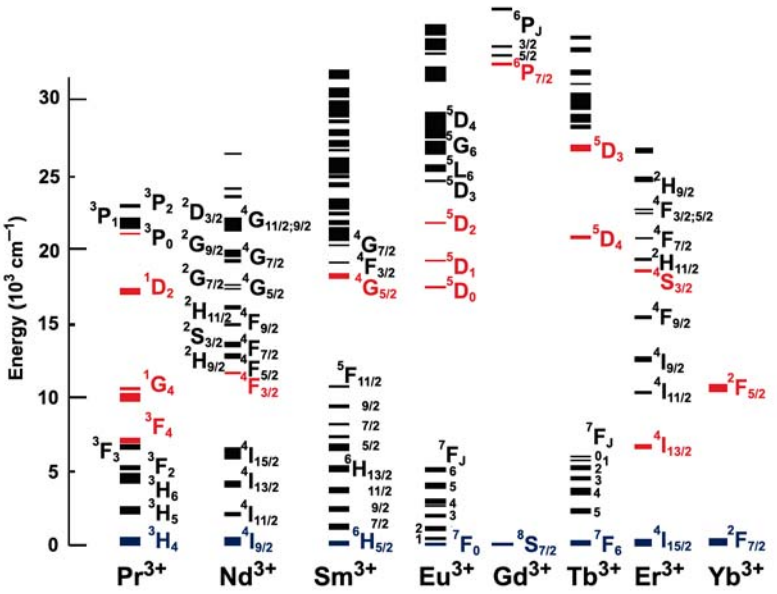

Fig. 2.3: *Diecke diagram of the energy levels of some trivalent lanthanide ions. The main emissive levels are depicted in red while the ground levels are drawn in blue.*[3]

From the Diecke diagram reported in fig. 2.3 it is quite evident that the energy levels of the emissive lanthanide ions are often markedly subdivided into two main groups consisting of closely spaced levels. The f–f transitions which originate the luminescent emission of lanthanide ions usually occur from the lowest level of the higher multiplet (populated by non-radiative cascade decay from the excited upper levels) to the ground manifolds.

These parity-forbidden intrashell transitions can be classified as follows:

- Transitions between states with different spin multiplicity (spin-forbidden) which give rise to UV and visible emission (e.g. $^5D_x \rightarrow {}^7F_x$ for Eu^{III} and Tb^{III});

- Transitions between levels that differ only in the value of the total spin-orbit coupling costant J, which correspond to near-infrared emission (e.g. $^4I_{13/2} \rightarrow {}^4I_{15/2}$ for Er^{III}).

In principle, according to IUPAC's rules, one can refer to the first class of transitions by using the term "phosphorescence" and to the second with the term "fluorescence",[3] but, due to the fact that emission arises from f orbitals of heavy lanthanide ions with high spin-orbit effects (L and S quantum numbers somehow lose their meanings), some authors prefer to use the general term "luminescence" to indicate the radiative emission from these ions.[4]

When a lanthanide ion is surrounded by ligands, the 4f electron distribution is perturbed both by *nephelauxetic* effects (a drift of ligand electron density into the lanthanide ion causes an expansion of the 4f shell and reduces the 4f - 4f interactions) and *crystal field* (CF) effects. In the latter case, the surrounding ligands, in a point negative charge model, destroy the spherical symmetry of the "free-ion" inducing a partial removal of the degeneracy of individual 4f terms (which are split into 2J+1 levels in a C_1

symmetry, less in a CF of higher symmetry, depending on the possible representations of the J vector in the symmetry point group), thus making f–f transitions slightly allowed. Due to the shielding by the external 5s and 5p orbitals the magnitude of this splitting is moderate and the average energy gap between the levels is only about 100 cm^{-1}.[2,5] Given the rather low perturbation due to crystal field or ligand field on the 4f orbitals, the position of both the absorption and emission bands of the lanthanide ions does not change significantly upon coordination with respect to the free ion spectra, thus each band can be easily recognised and provides the fingerprints for the corresponding lanthanide ion. However, in some cases, a fine structure arising from this Crystal Field or Ligand Field splitting (*Stark splitting*) could be clearly observed in the absorption and luminescence spectra of low-symmetry lanthanide complexes, and could thus be useful to probe the metallic environment.[3]

The 4f - 4f transitions could be either electric dipolar (ED) or magnetic dipolar (MD), or even quadrupolar in character. The ED transitions are strongly forbidden by parity rules (Laporte's rule: $\Delta l = \pm 1$) while MD transitions are allowed but unlikely and therefore have an intrinsic low intensity. The fact that the ED transitions are strongly forbidden by selection rules ensures long emission lifetimes. However, ED transitions in a lanthanide complex could be slightly permitted as the selection rules are somewhat relaxed by several mechanisms such as the Crystal Field effect, the coupling with vibrational states (i.e. the symmetry of the system is transiently changed allowing the so-called *vibronic transitions*), the J mixing,

and the mixing with opposite-parity wavefunctions (e.g. 5d orbitals, ligand orbitals, charge transfer states).[3,6-7]

The oscillator strengths of certain 4f - 4f transitions appears to be particularly sensitive to the ligand environment. These transitions are often referred to as "*hypersensitive transitions"* and their intensity is significantly increased as the symmetry of the lanthanide complex is lowered or the polarizability of the ligands increased. For that reasons, given that the position of the 4f bands does not change significantly upon complexation, the *hypersensitive transitions* of Er^{III} and Nd^{III} have revealed to be extremely useful as a marker to monitor the complex formation in aqueous solution.[8,9] These transitions are, in principle, quadrupolar in character (selection rules $\Delta J=\pm 2$) but, actually, their mechanism can be described as follows: the electric dipolar component of the radiation induces a set of transient electric dipoles in the ligand environment that couples to the 4f-electron distributions via electrostatic quadrupolar (Ln)-dipolar (ligand) interactions. In a non-centrosymmetric complex, or a complex subject to an *ungerade* vibrational mode, these quadrupole-induced dipolar interactions can lead to large amplifications of the 4f-4f electric quadrupolar transition probabilities. Hypersensitive transitions are therefore often referred to as "pseudoquadrupolar".

2.3 Sensitised lanthanide luminescence

In the previous paragraph it has been pointed out that most of the 4f transitions are forbidden by selection rules, and, although several mechanisms, such as the coupling with vibrational states, may relax them to some extent, the absorption cross section (molar extinction coefficient: $\varepsilon < 10$ mol^{-1} dm^3 cm^{-1}) and the emission intensity after a direct excitation of the lanthanide ion remain, however, very low.

A way to overcame this drawback, first proposed by Weisseman in 1942,[10] is to encapsulate the lanthanide ion with a suitable organic "light harvesting" ligand (chromophore) which can allow indirect excitation of the lanthanide ion by populating its higher levels by means of an energy transfer mechanism (sensitized emission). In the earlier 1990s, the interest on lanthanide complexes as luminescent materials was renewed, since Lehn[11] proposed that such compounds could be seen as *light conversion molecular devices* (LMCDs), coining the term "antenna effect" to denote the absorption, energy transfer, emission sequence involving distinct absorbing (the ligand) and emitting (the lanthanide ion) components, thus overcoming the very small absorption coefficient of the lanthanide ions.[12] This indirect excitation process allows to obtain, for example, narrow-band near infrared radiation by exciting the "antenna" (sensitizer), which should have a broad and intense absorption band in the UV-visible region, with a low-cost visible source (photoluminescence, PL) or by means of an electric pulse (electroluminescence, EL) in OLED devices. The two-step excitation process

permits the achievement of a large excited-state population using light fluences (J/cm^2) four to five orders of magnitude lower than those required for bare ions. Furthermore, the considerable Stokes shift between the excitation and the emission wavelengths allows to separate well the "spurious" wavelengths due to scattered radiation or ligand photoluminescence.

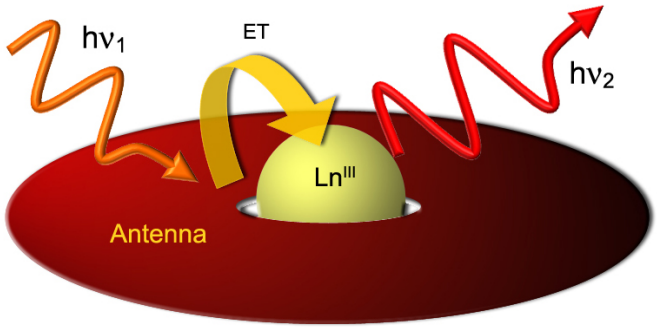

Fig. 2.4: *Scheme of indirect excitation mechanism of a Ln^{III} ion through an "antenna" ligand ($h\nu_1$= excitation wavelength; ET=energy transfer; $h\nu_2$=emission wavelength).*

The 4f emission mechanism obtained from indirect excitation of a lanthanide complex usually occurs trough several stages. First, ligand energy absorption leads to the formation of an excited singlet state ($S_0 \rightarrow S_1$). This is followed by an intersystem crossing (ISC) radiationless process to the ligand triplet states (T_1, T_2) that competes with organic fluorescence (PL) and radiationless deactivation (NR) of the excited singlet as thermal energy. The

third step consists of a radiationless direct energy transfer from the ligand long-lived triplet states to the nearest low-lying 4f levels of the lanthanide ion (triplet energy transfer, ET_T), which becomes excited and could produce luminescence, if necessary, after previous radiationless decay to a lower 4f emitting level.

The lanthanide ion could also be excited by energy transfer from the S_1 state (singlet energy transfer, ET_S) but this state is short-lived and the process is much less probable than ISC or radiative or non-radiative decays. In other words, energy is transferred from the triplet state because energy transfer via the singlet state is not fast enough to compete with fluorescence or intersystem crossing.

In a simplified model, the luminescence quantum yield Q_{Ln}^{L} of sensitized luminescence from a lanthanide complex can thus be written:

$$Q_{Ln}^{L} = \eta_{ISC}\eta_{ET}Q_{Ln}^{Ln} \qquad \text{Eq. } \mathbf{3}$$

where Q_{Ln}^{Ln} is the quantum yield for direct excitation of the lanthanide ion, η_{ISC} represents the efficacy of the intersystem crossing process and η_{ET} is the effectiveness of the $^3\pi\pi^*$–Ln transfer.[3]

The entire ligand-to-Ln^{III} energy transfer process can be schematically depicted in the Jablonsky diagram:

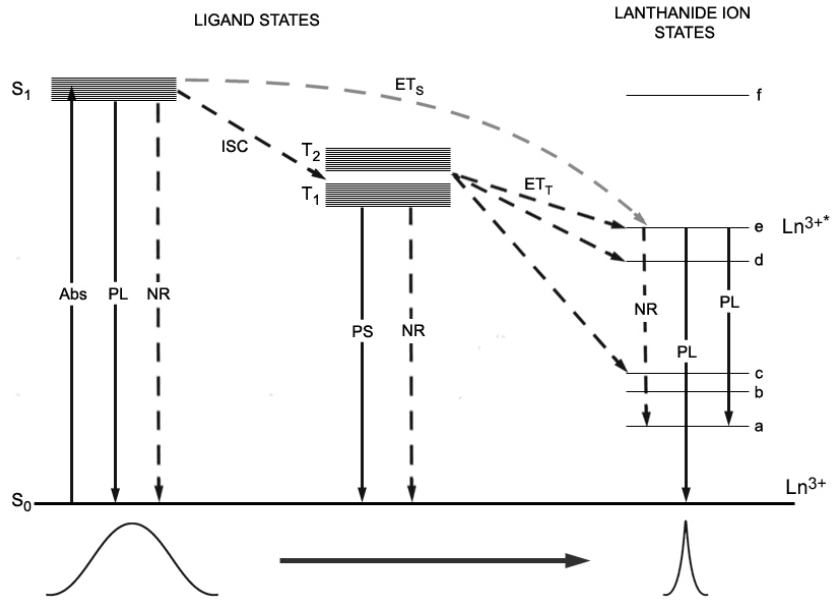

Fig. 2.5: *Jablonsky diagram reporting the energy flow from the organic ligand to the emitting lanthanide ion (ABS = absorption; PL = luminescence; PS = phosphorescence; NR = non- radiative decay; ISC = Intersystem Crossing; ET = Energy Transfer; a,b,c,d,e,f = Ln^{3+} energy levels).*

The high spin-orbit coupling between the heavy, paramagnetic, lanthanide ion and the ligand, considerably favours the ISC mechanism (*heavy atom effect*) which populates the ligand triplet state (usually $^3\pi\pi^*$) and produces an intramolecular energy transfer to the 4f states rather than a radiationless thermal decay that usually takes place in the absence of the lanthanide ion.

The ligand-to-metal energy transfer can be described on the basis of two theoretical models considering different dipolar-multipolar donor (ligand)-acceptor (Ln^{III}) interactions. The exchange mechanism or Dexter mechanism of transfer,[13] is an electron exchange process implying an overlap between the ligand and the metal orbitals. On the other hand, the Förster mechanism of transfer,[14] is a coulombic interaction through space involving a coupling between the dipole moments associated with the T_1 state and the 4f orbitals, strongly dependent on the spectral overlap between the emission spectrum of the donor and the absorption spectrum of the acceptor. In the Dexter mechanism, the spectral overlap is independent of the oscillator strength of the transitions (emission and absorption spectra are normalized such that the areas of the spectra are unity).

These mechanisms are schematically depicted in Figure 2.6:

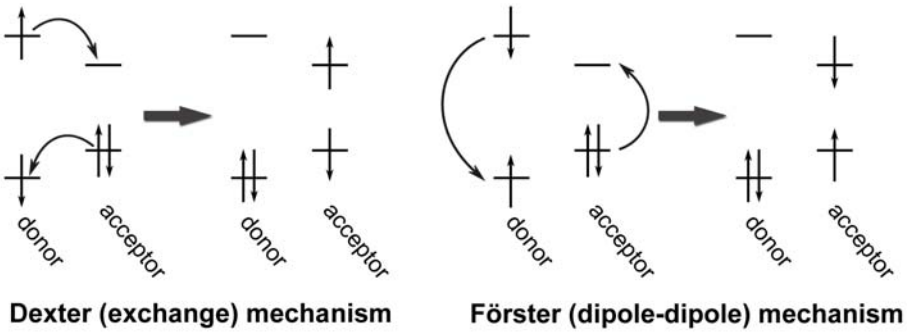

Fig. 2.6: *Schematic representation of Dexter (left) and Förster (right) mechanisms of energy transfer.*

Both mechanisms are distance (r)-dependent but in the case of the Dexter mechanism this dependence is exponential while in the Förster mechanism it is proportional to $1/r^6$. For this reason, the Dexter energy transfer is a short-range mechanism, whereas Förster energy transfer occurs over longer distances.[15,16]

Accepting levels of the lanthanide ions are also selected according to the following selection rules:

- $\Delta J = 0, \pm 1$ ($J = J' = 0$ excluded) for a Dexter mechanism;
- $\Delta J = \pm 2, \pm 4, \pm 6$ for a Förster mechanism;

where ΔJ is referred to a transition from the lanthanide ground state.

In general, the sensitisation of the lanthanide ion seems to occur from the ligand triplet state via a Dexter mechanism[12] although, in some cases, energy transfer from singlet states cannot be ruled out.[17-18] For efficient energy transfer to the lanthanide ion, the triplet states of the ligand must be closely matched to or slightly above the metal ion's emitting resonance levels[19-20] even though this is a complex process involving numerous rate constants.[12,21]

In some cases, the ligand-to-metal energy transfer can be *phonon-assisted*, and occurs through a molecular vibration, thus the overlap between the ligand and the lanthanide ion orbitals is no longer necessary.

An important detrimental phenomenon for the sensitisation of lanthanide ions is *energy back transfer* occurring from the excited lanthanide ion to the

sensitizer. This happens in cases where the donating sensitizer level is (too) close to the accepting lanthanide ion level, which makes thermally activated energy back transfer possible. An energy gap of at least 1000-2000 cm^{-1} is then necessary to completely prevent energy back transfer.[22-24] However, energy back transfer has been only demonstrated for visible emitters (Eu^{III}, Tb^{III}) but it has never been detected in the case of NIR-emitting complexes.[23]

There exist at least two other ways by which lanthanide ions can be excited.

The first one occurs trough ligand-to-metal charge transfer states (LMCT), provided that they lie well above the emitting levels of the lanthanide ion in order to be suitable to transfer the energy without quenching the metal emission. This mechanism trough CT states has the advantage that it can allow photo-excitation of the lanthanide ion by using long-wavelength (in the visible-near infrared spectral region), relatively inexpensive, light sources.

The second possibility is sensitisation through energy transfer from a complex of a transition d-metal ion such as, for instance, Cr^{III}, Pt^{II}, Ru^{II}.[24-28] Transition d-metal complexes represent a class of promising chromophores which can act as sensitizers toward lanthanide ions. It is in fact possible to find stable complexes with strong absorption maxima at almost any wavelength ranging from UV to NIR. Thus, for each luminescent lanthanide, an accurate selection of the proper energy donor, on the basis of its spectral properties (i.e. spectral overlap between the donor and the acceptor bands), is possible. Heavy d-metals also favour the intersystem-crossing mechanism leading to a high triplet quantum yield, and the resulting long-lived excited

state enhances the energy transfer rate to a covalently-attached lanthanide.[24] In some cases, a remarkable improvement of the lanthanide emission lifetime in the near-infrared may result when population of the lanthanide upper levels occurs by energy transfer from a particularly long-lived excited d-state of the transition metal (e.g. $Cr^{III}(^2E) \rightarrow Nd^{III}(^4F^{3/2})$).[27]

Furthermore, metal-d complexes can exhibit good photochemical stability and kinetic inertness and, in most cases, d-f systems can be prepared in a very convenient way by using suitable metal-d coordination compounds as "complex ligands" towards the lanthanide ion.

In conclusion, for efficient lanthanide emission, complexes should have a high absorption coefficient, a high intersystem crossing rate, an efficient energy transfer, and an efficient lanthanide luminescence quantum yield. Several organic dyes and chromophores which can act as ligands towards the lanthanide ion possess a high absorption coefficient, while the intersystem crossing quantum yield of a sensitizer should, in principle, be close to 100% provided that it is enhanced by the introduction of heavy atoms (the lanthanide itself but also atoms like bromine or iodine in the dye system). However, according to the Förster-Dexter theory, the energy transfer rate is mainly determined by the distance between the sensitizer and the lanthanide ion as well as by their normalised spectral overlap.

2.4 Quenching of lanthanide luminescence

Several non-radiative deactivation processes exist which can severely limit the emission quantum yield of lanthanide complexes whatever efficient is the sensitization process through the antenna ligand. These quenching effects lead to observed luminescent lifetimes (τ_{obs}) some orders of magnitude shorter than the natural radiative emission lifetime (τ_r) of the free lanthanide ion. The overall rate constant (κ_{obs}) for such deactivation processes, is inversely proportional to the measured lifetime, and is given by:[29,2]

$$\kappa_{obs} = \frac{1}{\tau_{obs}} = \kappa_r + \sum_i \kappa_i^{nr} \qquad \text{Eq. 4}$$

where κ_r (= $1/\tau_r$) represents the radiative rate constant whereas κ_i^{nr} is the single rate constant for competing non radiative processes.

The quantum yield of a luminescent lanthanide ion Q_{Ln}^{Ln} essentially depends on the energy gap between the lowest-lying excited (emissive) state of the metal ion and the highest sublevel of its ground multiplet. The smaller this gap, the easier is its de-excitation by non-radiative deactivation processes, for instance through vibrations of bound ligands, particularly high energy vibrations such as O–H or C–H.

In NIR-emissive organolanthanide systems, the efficiency of the Ln ion luminescence is severely limited by quenching phenomena mainly due to the

resonance energy transfer from the lanthanide ion to the molecular stretching vibrations of C–H and O–H groups present in the surrounding (*deactivation via vibrational excitation*).

Resonance energy transfer (RET) is a radiationless transmission of an energy quantum from a donor, atom or molecule, previously excited, to an acceptor (atom, molecule or groups of atoms/molecules), by resonance interaction between the donor and acceptor, without conversion to thermal energy, and without the donor and acceptor coming into kinetic collision. The donor is the dye initially excited, the acceptor is the system to which the energy is subsequently transferred.[30]

In the NIR-emitting lanthanide ions (Nd^{III}, Er^{III}, Yb^{III}), the energy gap of the radiative (f–f) transition matches well the energy of the first and second vibrational overtones of O–H and C–H groups (with vibrational quanta ν=2 and ν=3) which therefore act as efficient quenchers via vibrational excitation (see Fig. 2.7). According to the energy gap theory, the vibrational transition probability is proportional to the Franck-Condon factor, i.e. overlap integrals between the energy gap and vibrational energy.[31] The Franck-Condon factor is inversely proportional to the vibrational quantum number ν, thus the quenching via vibrational excitation drastically decreases for superior harmonics of deactivating oscillators.

Water molecules are undoubtedly the most powerful quenchers for NIR-luminescence, especially in the case of erbium emission at 1.5 μm, since the first overtone of the H–O–H stretching vibration falls around 1.42 μm. This represents a challenging problem to solve to obtain efficient NIR emission

from lanthanide complexes, given the strong tendency of lanthanide ions to coordinate water molecules. However, the entity of such quenching effect strongly depends on the number of H_2O molecules in the surrounding of the lanthanide ion, and the comparison of luminescence lifetimes and quantum yield measurements in H_2O and D_2O has been used as a tool to identify the coordination sphere of hydrated lanthanide ions.[32-33]

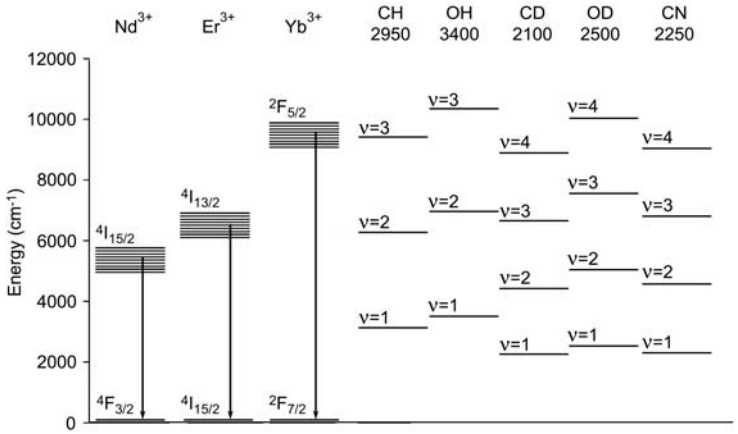

Fig. 2.7: *Energy gaps of emitting levels of NIR-emissive lanthanide ions compared to the energy of vibrational modes of C–H, O–H, C–D, O–D, C–N bonds and their superior harmonics.*

Substitution of C–H and O–H bonds with C–D and O–D bonds, for instance using deuterated solvents and ligands, has led, in some cases, to a slight improvement of the NIR luminescence lifetimes, especially in cases where deuterated DMSO molecules replace coordinated H_2O molecules.[31,34-35] However, the effect of substitution remains insufficient for highly efficient NIR emission since quenching could occur through vibrations of vibrational

quanta only one unit higher than those of C–H and O–H groups. Moreover, replacing hydrogen atoms with heavier deuterium atoms in the molecule could affect its stability and raise its sublimation point, that is detrimental for the fabrication of thin films for optoelectronic devices.

The theory of resonance energy transfer (RET) was developed by T. Förster in the 1940s-1950s.[36,14] From a classic viewpoint the RET process could be summarised in three basic steps: (i) excited donor acts as oscillating dipole; (ii) acceptor molecules interact with this oscillating field; (iii) excitation transfer occurs from donor to acceptor without photon emission through a multipolar-dipolar interaction mechanism trough space. As already pointed out in the previous paragraph, this mechanism (schematically depicted in Figure 2.6b) is strongly dependent on the distance (**r**) between the donor, namely the emitting lanthanide ion, and the acceptor, that is the oscillating O–H or C–H group, and this relationship is proportional to r^{-6}. Moreover, the RET mechanism requires a spectral overlap between the emission spectrum of the donor and the absorption spectrum of the acceptor (*resonance condition*).

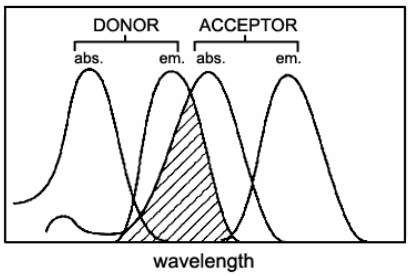

Fig. 2.8: *Resonance condition: spectral overlap between the emission band of the donor and the absorption band of the acceptor.*

The transfer rate k_{nr}, describing the energy transfer between a donor and an acceptor, is given by:

$$k_{nr}(r) = \frac{1}{\tau_r}\left(\frac{R_0}{r}\right)^6 = \frac{Q_y \kappa^2}{\tau_r r^6}\left[\frac{9000(\ln 10)}{128\pi^5 N n^4}\right]\int F_D(\lambda)\sigma_A(\lambda)\lambda^4 d\lambda; \quad \left(\frac{1}{\tau_r} = k_r\right) \qquad \text{Eq. 5}$$

where N is the Avogadro number, τ_r and Q_y are, respectively, the radiative lifetime and the quantum yield of the donor in the absence of the acceptor, n is the refractive index of the medium, r is the donor-acceptor distance, κ^2 is a factor that accounts for the relative orientation of transition dipole moments of the donor and the acceptor. R_0 is the Förster distance, at which the donor-to-acceptor energy transfer and the donor natural radiative decay have the same probability and is proportional to the integral representing the spectral overlap between the emission spectrum of the donor $F_D(\lambda)$, normalised to unity, and the absorption cross-section of the acceptor $\sigma_A(\lambda)$.

The radiative decay constant k_r ($=1/\tau_r$) can be evaluated from the donor emission cross-section $\sigma_D(\lambda)$ through the Strickler-Berg law:[37]

$$k_r = 8\pi n^2 c \int \frac{\sigma_D(\lambda)}{\lambda^4} d\lambda \qquad \text{Eq. 6}$$

where c is the speed of light in the vacuum.

The transfer rate is thus affected by the donor-acceptor distance, the resonance condition, and the relative orientations of donor and acceptor transition dipole moments.

The orientation factor κ^2 is given by:

$$\kappa^2 = (\cos\vartheta_T - 3\cos\vartheta_D \cos\vartheta_A)^2 \qquad \text{Eq. 7}$$

where (**T** is the angle between the transition dipole moments of the donor and the acceptor (**d** and **a**), θ_D and θ_A are, respectively, the angles between the donor transition moment and the connecting vector **r** and between the latter and the acceptor transition moment.

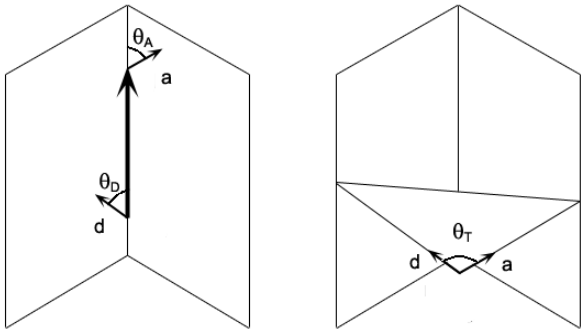

Fig. 2.9: *Illustration of the angles θ_D, θ_A and θ_T. **r** is the vector connecting the centre of the donor to the centre of the acceptor, **d** and **a** are, respectively, the transition dipole moments of the donor and the acceptor.*

The maximum value of κ^2 is obtained for collinear transition dipole moments ($\kappa^2 = 4$); for parallel transition dipole moments is $\kappa^2 = 1$. If dipole moments are oriented perpendicular to each other then κ^2 takes the minimum value available: $\kappa^2 = 0$. In Figure 2.10 examples of relative orientation of donor and acceptor dipole transition moments are shown; the

central segment represents the donor dipole, the segments depicted along the circles represent possible acceptor dipole orientations.

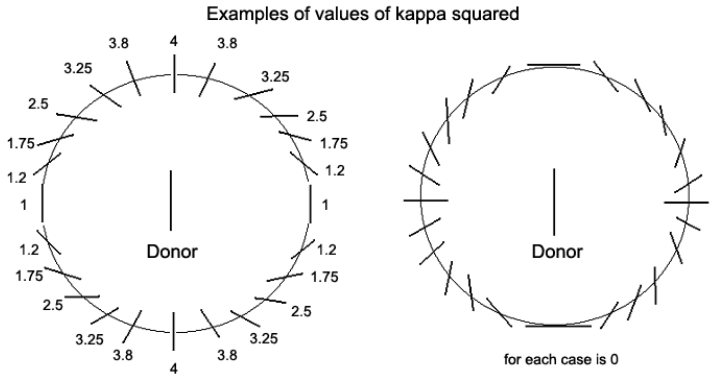

Fig. 2.10: Examples of cases in which κ^2 is maximum or minimum.[30]

The mechanism of quenching trough vibrational excitation, although the most effective, especially for NIR emitters, is not the only one responsible for lanthanide radiationless decay. Other deactivation mechanisms could occur trough a Förster-type dipole-dipole energy transfer between two neighbouring lanthanide complexes. These non-radiative processes can be easily induced by diffusional collision of complex molecules, especially in a liquid medium.[31]

The *cross-relaxation* mechanism consists of an energy sharing between two lanthanide ions, one of them initially in an excited state, that came into close contact, leaving both of them in a lower-lying non-emissive state. The *excitation migration* mechanism is a rapid exchange of energy between two

lanthanide ions, that does not imply a radiationless deactivation by itself, but may increase the quenching probability by favouring the transfer of excitation where more quenching processes may take place. It is evident that both mechanisms are greatly enhanced by concentration, and the reduced luminescent lifetimes observed in highly concentrated media are generally ascribed to the so-called *concentration quenching* effect.

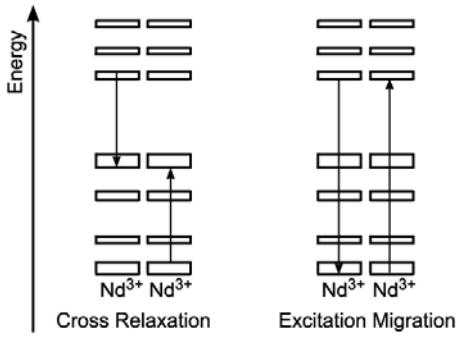

Fig. 2.11: *Sketches of the Cross Relaxation and Excitation Migration mechanisms for* Nd^{3+}.[31]

Another process that may affect the luminescence quantum yield of a lanthanide complex in a non-inert atmosphere is quenching by oxygen. Oxygen molecules ($^3O_2$) are in fact known to be efficient phosphorescence quenchers and may deactivate the excited triplet state of the organic chromophore thus preventing the sensitization of the lanthanide ion via energy transfer from the triplet state of the sensitizer.[29,38]

2.5 Lanthanide coordination chemistry

As already mentioned at the beginning of this Chapter, lanthanides possess $4f^n5d^16s^2$ configurations, and, as a result of the low electronegativity of these elements and the increasing stabilisation of the 4f, 5d, and 6s orbitals (4f > 5d > 6s) occurring upon successive removals of electrons from the neutral Ln metal, the +3 oxidation state is by far the most stable (although also +2 and +4 states exist for some lanthanide elements). Therefore, the coordination chemistry of lanthanides is based almost exclusively on their trivalent cations, Ln^{III}.

The progressive filling of the 4f orbitals with 14 electrons across the lanthanide series, which causes only a poor screening to the increasing nuclear charge, results in a continuous and smooth decrease in the atomic and ionic radii, a phenomenon known as “lanthanide (or lanthanoidic) contraction”. This trend is responsible for some important effects on the chemical behaviour of these elements (and, of course, on the properties of the following third-row transition elements that are smaller than what would be normally expected in the absence of the f-block). The ionic radius of trivalent lanthanide ions drops from 1.061 Å for La^{III} to 0.848 Å for Lu^{III} with a relative maximum (cusp) in the graph corresponding to the half-filled $4f^7$ shell of Gd^{III} (fig. 2.12). However, the entity of this contraction is only about 15% on going from La^{III} to Lu^{III}, while the difference in the ionic radius between two successive lanthanides is about 1%.

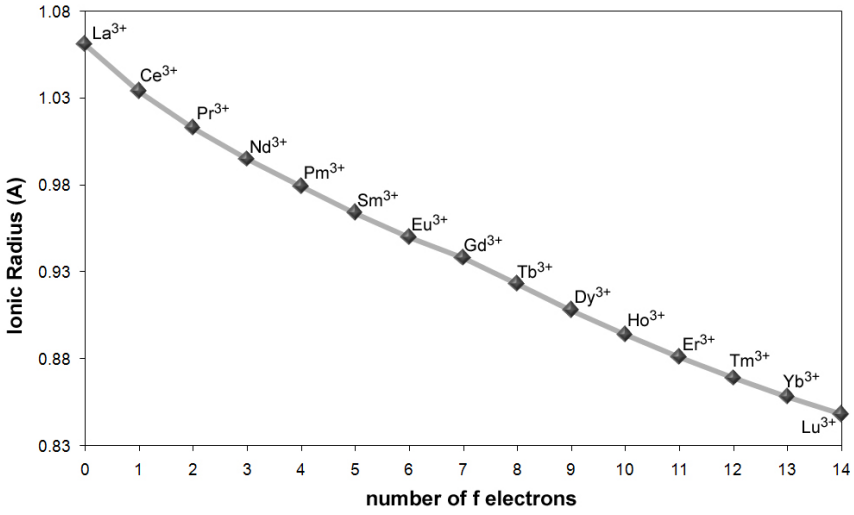

Fig. 2.12: *Graphical plot of the ionic radius of trivalent lanthanide ions Ln^{3+} versus atomic number.*

The shielding effect played by the outward filled $5s^2p^6$ shell toward 4f electrons is so effective that the latter can be referred to as *core-like* electrons. Thus, lanthanide ions resemble each other very markedly in their chemical behaviour even though they exhibit interesting variability of the coordination characteristics across the lanthanide series, (but this variability is much less pronounced than that found among transition-metal ions).[1]

Due to the fact that 4f electrons are contracted into the core, they almost do not participate in bonding and coordination occurs predominantly via ionic interactions whereas covalence plays a little role in Ln-ligand dative bonds. As a direct consequence, no π-backbonding is possible and the chemistry of

the M^0 state almost lacks completely (i.e. carbonyls…). The nature of the coordination sphere, and consequently the geometry of the complex, is therefore controlled by a subtle interplay between electrostatic interactions (i.e. minimisation of repulsive terms, particularly ligated atoms-ligated atoms repulsions) and interligand steric constraints.[39,40]

Furthermore, given the diffuse radial dispersion of the core-like f orbitals, it is evident that the coordination geometry of the lanthanide complexes, unlikely that of the d-block transition elements, is not governed by orbital directionality at all. Actually, it is mainly ruled by steric reasons involving the ligand steric hindrance and the size of the cation. The large lanthanide ions show a strong tendency to attain high coordination numbers ranging from C.N.=6 (extremely unusual and only with ligand of particular steric hindrance) to C.N.=12. The preferred coordination number varies along the lanthanide series and, while the first terms of the series (La-Nd) usually show preference for C.N.=9, the heavier (and smaller) lanthanide ions (Gd-Lu) tend to saturate their coordination sphere by reaching octa-coordination. This can be readily explained on the basis of the lanthanide contraction, even though the variation in size along the series is so smooth that often no precise estimation on the lanthanide coordination sphere could be done in advance, and many examples of coordination equilibria in solution (especially for mid-term lanthanides) exist.[41]

Anyhow, it is possible to assert, without relevant uncertainties, as observed by Byrne and Li,[43] that the mid-term lanthanide element, namely Gd (and, to a smaller extent, Eu), shows a rather “anomalous” coordination

behaviour, which is intermediate between that of the lighter and of the heavier lanthanide elements. Thus, the old subdivision of the lanthanide series into two groups, “of cerium” (La-Pr) and “of yttrium” (Sm-Lu), doesn’t seem to reflect exactly their chemical trend.

Finally, lanthanides are strong Lewis acids displaying typical *a-class* (*hard*) properties leading to a strong preference for *hard* donors, especially negatively charged donor groups.[40-41] This hard-acid behaviour, and therefore the ionic character of the bonding, increases along the lanthanide series and is particularly effective for the heavier lanthanide ions which possess smaller ionic radii. O-donors undoubtedly display the most effective coordinating properties toward lanthanides, but also N-based ligands form stable complexes, whereas the coordination chemistry of lanthanides with S-donors and other chalcogens, is so far very limited. Many examples of Ln-complexes are known with O-based or even N-based neutral ligands, either monodentate or multidentate, with the metal-ligand bond strength increasing as increasing the dipolar character of the ligand itself. In particular, water molecules show very good affinity to lanthanide ions and provide very strong coordination to the lanthanide center, often readily filling the metal coordination sphere and making nearly impossible to isolate complexes without directly Ln-bounded H_2O molecules, from aqueous solutions (lanthanide ions possess very high hydration energies). Unfortunately, this is extremely detrimental for lanthanide emission, especially in the near-infrared, since water is the most powerful luminescence deactivator. Thus, this is an

inconvenient that must be taken into account while attempting to prepare Ln complexes with improved luminescence.

In general, due to this strong affinity for H_2O molecules, the synthesis of lanthanide complexes from aqueous solutions (or even when reacting common hydrated lanthanide salts) is often an entropy-driven process. Complexation with a chelating ligand will in fact result in a decrease in hydration of the lanthanide ion, with a positive entropy change (chelating effect) that is partially offset by the strongly endothermic dehydration process. Thus, for a favourable Gibbs free energy change upon complex formation, it is necessary to use ligands either of excellent coordinating properties or, at least, suitable to provide several binding sites (i.e. macrocyclic ligands) in order to take valuable advantage from the entropy raise.[3]

References

[1] F. A. Hart, "Scandium, Yttrium and the Lanthanides", *Comprehensive Coordination Chemistry*, chap.39.

[2] J.-C. G. Bunzli, *Electronic Levels and Spectroscopy of 4f Elements*, Lecture, Summer School 2005 on *"Advanced Luminescent Materials Based on Lanthanide Organic/Inorganic Complexes"*, Krutyn, Poland, 2005.

[3] J.-C. G. Bunzli, C. Piguet *Chem. Soc. Rev.* **2005** *34*, 1048-1077.

[4] G. J. Palenik, *'Systematics and the Properties of the Lanthanides'*, ed. S. P. Sinha, Reidel, Dordrecht, **1983**, 153.

[5] J. Kido, Y. Okamoto, *Chem. Rev.* **2002**, *102*, 2357-2368.

[6] B. R. Judd, *Phys. Rev.* **1962**, *127*, 750.

[7] G. S. Ofelt, *J. Chem. Phys.* **1962**, *37*, 511.

[8] S. A. Davis, F. S. Richardson, *Inorg. Chem.* **1984**, *23,* 184-189.

[9] E. M. Stephens, K. Schoene, F. S. Richardson, *Inorg. Chem.* **1984**, *23*, 1641-1648.

[10] S. I. Weissman, *J. Chem. Phys.* **1942**, *10*, 214–217.

[11] J. M. Lehn, *Angew. Chem. Int. Ed. Engl.* **1990**, *29*, 1304.

[12] G. F. de Sà, O. L. Malta, C. de Mello Donegá, A. M. Simas, R. L. Longo, P. A. Santa-Cruz, E. F. da Silva, *Coord. Chem. Rev.* **2000**, *196*, 165-195; N. Sabbatini, M. Guardigli, J.-M. Lehn, *Coord. Chem. Rev.* **1993**, *123*, 201.

[13] D. L. Dexter, *J. Chem. Phys.* **1953**, *21*, 836.

[14] T. Förster, *Discuss. Faraday Soc.* **1959**, *27*, 7.

[15] W. DeW. Horrocks, M. J. Rhee, A. P. Snyder, D. R. Sudnick, *J. Am. Chem. Soc.* **1980**, *102*, 3650.

[16] F. Quochi, R. Orrù, F. Cordella, A. Mura, G. Bongiovanni, F. Artizzu, P. Deplano, M. L. Mercuri, L. Pilia, A. Serpe, *J. Appl. Phys.* **2006**, *99*, 053520.

[17] M.P. Lowe, D. Parker, *Inorg. Chim. Acta* **2001**, *317*, 163

[18] F. Vögtle, M. Gorka, V. Vicinelli, P. Ceroni, M. Maestri, V. Balzani, *Chem. Phys. Chem.* **2001**, 769.

[19] R. D. Archer, H. Y. Chen, L. C. Thompson, *Inorg. Chem.* **1998**, 37, 2089.

[20] F. Gutierrez, C. Tedeschi, L. Maron, J. P. Daudey, R. Poteau, J. Azema, P. Tisnes, C. Picard, *Dalton Trans.* **2004**, 1334.

[21] F. R. Gonçalves e Silva, O. L. Malta, C. Reinhard, H. U. Güdel, C. Piguet, J. E. Moser, J.-C. G. Bünzli, *J. Phys. Chem. A* **2002**, *106*, 1670.

[22] J. Kido, Y. Okamoto *Chem. Rev.* **2002**, *102,* 2357-2368; G. Hebbink, *Luminescent Materials based on Lanthanide Ions*, PhD thesis, Twente University, The Netherlands, **2002;** S. Sato, M. Wada, *Bull. Chem. Soc. Jpn.* **1970**, *43*, 1955.

[23] M. Latva, H. Takalo, V. M. Mukkala, C. Matachescu, J. C. Rodriguez-Ubis, J. Kankare, *J. Luminesc.* **1997**, *75*, 149.

[24] M. D. Ward, *Coord. Chem. Rev.* **2007**, *251*, 1663-1677.

[25] M. D. Seltzer, *J. Chem. Educ.* **1995**, *72*, 886.

[26] N. M. Shavaleev, G. Accorsi, D. Virgili, Z. R. Bell, T. Lazarides, G. Calogero, N. Armaroli, M. D. Ward, *Inorg. Chem.* **2004**, *44*, 61.

[27] D. Imbert, M. Cantuel, J.-C. G. Bünzli, G. Bernardinelli, C. Piguet, *J. Am. Chem. Soc.* **2003**, *125*, 15698.

[28] G. M. Davis, S. J. A. Pope, H. Adams, S. Faulkner, M. D. Ward, *Inorg. Chem.* **2005**, *44*, 4656-4665.

[29] D. Parker, J. A. G. Williams, *J. Chem. Soc., Dalton Trans.* **1996**, 3613-3628.

[30] B. W. Van der Meer, G. Coker, S. Y. S. Chen, *Resonance Energy Transfer Theory and Data,* Wiley-VCH, New York, **1994**.

[31] S. Yanagida, Y. Hasegawa, K. Murakoshi, Y. Wada, N. Nakashima, T. Yamanaka, *Coord. Chem. Rev.* **1998**, *171*, 461-480.

[32] W. D. Horrocks Jr., D. R. Sudnick, *J. Am. Chem. Soc.* **1979**, *101*, 334.

[33] A. Beeby, I. M. Clarkson, R. S. Dickins, S. Faulkner, D. Parker, L. Royle, A.S. de Sousa, J. A. G. Williams, M. Woods, *J. Chem. Soc.*, *Perkin Trans. 2* **1999**, 493–503.

[34] A. Beeby, S. Faulker, *Chem. Phys. Lett.* **1997**, *266*, 116-122.

[35] Y. Hasegawa, Y. Kimura, K. Murakoshi, Y. Wada, J.Ho. Kim, N. Nakashima, T. Yamanaka, S. Yanagida, *J. Phys. Chem.* **1996**, *100*, 10201-10205.

[36] T. Förster, *Annalen der Physik* **1948**, *2*, 55-75; english translation (1993).

[37] S. J. Strickler, R. A. Berg, *J. Chem. Phys.* **1962**, *37*, 814.

[38] D. Parker, *Coord. Chem. Rev.* **2000**, *205*, 109.

[39] H. Tsukube, S. Shinoda, *Chem. Rev.* **2002,** *102,* 2389-2403.

[40] J.-C. G. Bunzli, C. Piguet *Chem. Rev.* **2002,** *102,* 1897.

[41] N. N. Greenwood, A. Earnshaw, *Chemistry of the Elements*, 2nd ed., Butterworth-Heinman, London, **1997**, Ch. 30, 31.

[42] F. A. Cotton, G. Wilkinson, *Advanced Inorganic Chemistry*, 5th ed., Wiley, N.Y., **1988**, Ch. 20, 21.

[43] R. H. Byrne, B. Li, *Geochim. Cosmochim. Acta* **1995**, *59*, 4575-4589.

Chapter 3

Lanthanide Quinolinolates

The synthesis and the characterisation of lanthanide complexes with quinolinolato ligands, with a full investigation of the structure/property relationship, are described here. The spectroscopic properties are discussed with the view to provide suitable tools to identify and characterise univocally the structural features of this class of complexes which shows a wide variety of coordination modes.

3.1 Introduction

As already mentioned in the first Chapter of this thesis, the *tris*(8-quinolinolato) erbium(III) (ErQ_3) can be considered as a prototype organo-lanthanide system for 1.5-μm telecom applications since Gillin and Curry, in 1999,[1-4] first proposed it as a potential material for silicon-compatible 1.5-μm electroluminescence (EL) emitters. ErQ_3 has been used as emitting material deposited by vacuum deposition either on quartz glass for photoluminescence studies[5-6] or on a silicon substrate[4] or on indium-tin-oxide coated glass[1,3] in the production of OLEDs emitting electroluminescence at 1.5 μm. Moreover, the same material has been processed incorporated in a polymer host as a thin-film blend in polycarbonate.[7] The research on new organo-lanthanide materials that can emit in the near-infrared was then extended to NdQ_3 whose bright infrared electroluminescence at 900, 1064 and 1337 nm was demonstrated,[8-9] and to YbQ_3, which emits at 977 nm.[5,10-11]

Quinolinol ligands, for long known as very good coordinating agents toward trivalent lanthanide ions,[12-15] have therefore been selected as suitable antenna ligands to prepare lanthanide-containing materials for electroluminescence applications.

In addition, lanthanide complexes with some derivatives of 8-hydroxy-quinoline, especially dihalo-substituted quinolinols, have been prepared with the aim to fully investigate the photo-physical characteristics of this class of

complexes and to improve their emission efficiency by reducing the number of CH quenching groups in the complex.[16-18]

The first report of a lanthanide quinolinato compound by Pirtea goes back to 1936.[19] In the light of previous results on the structure of quinolinolates of trivalent metals[20] the author assumed a tris-chelated octahedral structure for LaQ_3. Since then, several papers have reported controversial assumptions on the stoichiometry of complexes with 8-hydroxy-quinolinol (HQ) and its derivatives.[1-18,21-22] One of the most frequently used literature procedures for the preparation of these complexes was described by Aly et al. in 1971.[14] According to this synthetic method, an ethanolic solution of HQ is added to a solution of lanthanide nitrate in water. The crude product which precipitates after addition of a slight excess of an ammonium hydroxide solution corresponds to 1:3 metal-to-ligand ratio. This conclusion is supported by CHN analysis and vibrational spectroscopy. In 2001 Khreis et al.[10] reported a study on the emission properties of YbQ_3 used as emitting centre in an electroluminescence device (OLED). The complex was prepared following a slightly different method in which a water solution of lanthanide chloride in water is slowly added to a solution of the ligand in methanol/water mixture without addition of a base.

Recently, Van Deun and coworkers[23] have deeply reinvestigated these commonly used synthetic procedures in order to clarify the nature of the products obtained by these reactions. On the basis of NMR and mass spectra performed on the obtained samples it has been concluded that they actually do not consist of single pure products bur rather of mixtures of

species having different stoichiometries. One of these species contains three lanthanide ions bridged by the Q ligands (“trimeric” complex), and is the predominant product in the case of 8-hydroxy-quinoline and 5-chloro-8-quinolinol. Instead, by using 5,7-dihalo-quinolinol ligands, mixtures of *tris* and *tetrakis* complexes with metal-to-ligand ratios of 1:3 and 1:4 have been found. Structural characterisation performed on some samples confirmed these stoichiometries. This work by Van Deun et. al is particularly relevant since it demonstrated that this class of compounds actually possesses a rich structural chemistry. However, the reported improved methods, aimed at obtaining pure products, have proven to be successful only in the case of saline *tetrakis*-type compounds, while the isolation of pure “trimeric” and *tris* species was taken as unfeasible.

The study reported in this thesis was being independently carried out while Van Deun’s group was performing its research.[24-26]. The obtained complementary results have allowed to achieve a deeper knowledge of this class of complexes and to provide the procedures to obtain neutral pure products suitable to be processed for optical devices. Moreover, the structural and spectroscopic characterisation of these products have allowed to find a reliable structure/property relationship.[24-26]

3.2 Erbium quinolinolates: synthesis and crystal structure description

The development of the synthetic pathways to obtain pure and well defined products, has been done by carefully considering several parameters such as pH range, temperature, solvents and reaction times. As a matter of fact, a strict control of these factors is necessary to ensure the completion of the complexation reaction and the formation of the desired complex in high yields; otherwise, a mixture of undefined products results.

The quinolinol ligand undergoes several protic equilibria in solution, involving neutral, anionic and protonated forms (Scheme 3.1). A tautomeric equilibrium also exists which leads to the zwitterionic form bearing the proton on the nitrogen atom of the pyridine ring.

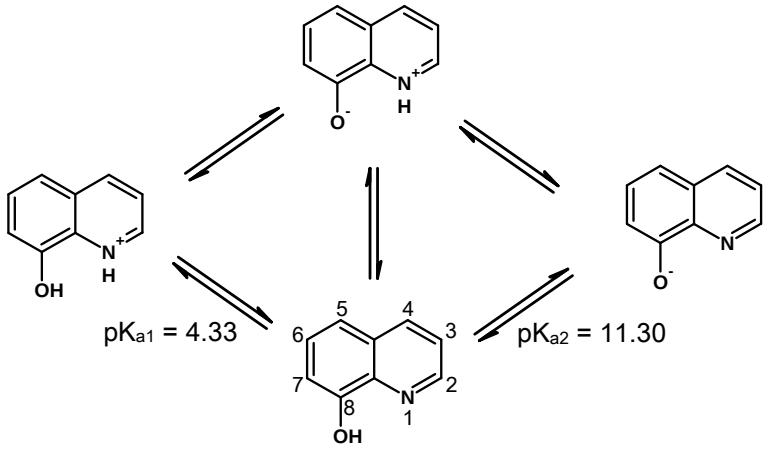

Scheme 3.1: *Protic equilibria of 8-hydroxy-quinoline.*[27-28]

The acidic character of the ligand is remarkably increased by the presence of electron-withdrawing substituents, especially in the *para*- and *ortho*- positions with respect to the phenolic group, whereas an electron-donating group, such as a methyl substituent, on the pyridine ring, will increase the pK values of both the dissociations.[27]

Ligand	pK_{a1}	pK_{a2}
HQ	4.33	11.30
H5,7ClQ	1.70 ± 0.02	8.90 ± 0.02
H5,7BrQ	1.00 ± 0.02	8.95 ± 0.02
H2MeQ	4.45	11.63

Table 3.1: *pK_a values of some quinolinol derivatives (HQ=8-hydroxy-quinoline; H5,7ClQ=5,7-dichloro-8-quinolinol; H5,7BrQ=5,7-dibromo-8-quinolinol; H2MeQ=2-methyl-8-quinolinol).*[27]

In the case of syntheses made in aqueous solution, the weak base NH_3 is added to deprotonate the quinolinol ligand, before the addition of the metal ion, in order to obtain the lanthanide complex with the anionic form of the ligand. The addition of a strong base, such as NaOH, to the reaction mixture, often leads to an impure final product. This may be also due to a possible nucleophilic attack of the OH^- group on the 2 position of the pyridine ring forming 2-hydroxy-carbostyril.[29]

On the other hand, trivalent lanthanide cations are strong Lewis acids, displaying the tendency to form insoluble hydroxides and oxides (Ln_2O_3), even at rather low pH. For instance, Er^{III} hydroxides or oxides precipitate from perchlorate solution at pH = 6.61 ($K_{ps} = 4.1 \cdot 10^{-24}$ $mol^5\,l^{-5}$).[30]

Therefore, a careful control of the pH conditions is a primary requirement to obtain a pure final product. However, this also strongly depends on the nature of the substituents on the quinoline ring since they considerably affect its chemical behaviour (i.e. acid-base and coordinating properties).

Furthermore, it has to be remarked that reaction times are of great importance to ensure the completion of the complexation reaction to obtain a pure product.

In Scheme 3.2 a summary of the synthetic procedures used to obtain three different kinds of neutral erbium complexes in high yields is reported. As shown, apparently small differences in the reactions' conditions produce different products: i) the *trinuclear*[*] complex Er_3Q_9 (**1**) which is obtained when Q is the unsubstituted ligand deprotonated by NH_3 either in water or ethanol/water mixtures; ii) the *tris* dimeric complexes where the mononuclear unit consists of $[Er(5,7XQ)_3(H_2O)_2]$ [X = Cl (**2**) and Br (**3**)] where the ion is octacoordinated to three deprotonated ligands and to two water molecules; iii) the *tetrakis* mononuclear $[Er(5,7XQ)_2(H5,7XQ)_2Cl]$ [X = Cl (**4**) and Br (**5**)] complexes, where only two of the four coordinated ligands are deprotonated, obtained by mixing the erbium chloride with H5,7XQ in organic solvents without addition of a base.

[*] Since the compounds of general formula Ln_3Q_9 do not consists of repeating structural units they cannot be referred to as "trimeric" complexes, therefore the more proper term "trinuclear" is used in this thesis. Conversely, compounds of general formula $[Ln(XQ)_2(HXQ)_2Cl]$, which bear two different ligand forms, are, for convenience' sake, referred to as "tetrakis"-type complexes.

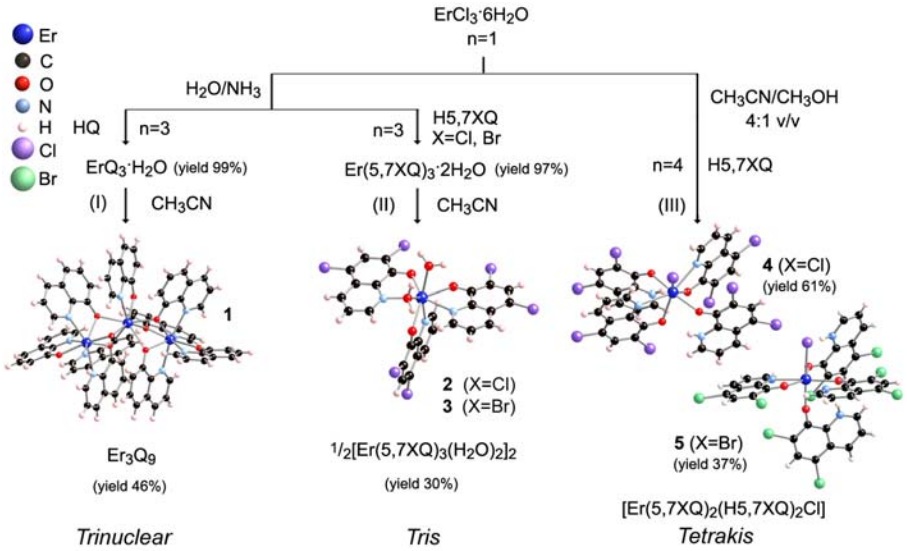

Scheme 3.2: *Reaction pathways.*

In conclusion, the reaction conditions and the nature of the ligand strictly determine the nature of the final product.

3.2.1 *Trinuclear* Er_3Q_9

The pathway I of Scheme 1 follows a modification of the most conventional literature procedure reported to obtain the assumed to be ErQ_3.[14] Accordingly, as described in detail in the Experimental part, few drops of NH_3 28% were added to a HQ in H_2O mixture under mixing (scheme 3.1, pathway I). After 30 min a water solution of $Er(NO_3)_3 \cdot 5H_2O$ or

$ErCl_3 \cdot 6H_2O$ (in the 3:1 ligand to metal molar ratio) was added to the above mixture, which was allowed to react for two days. The yellow precipitate formed was collected by filtration, washed with water, NaOH 0.1 M, water and dried in oven. Elemental analysis of this solid is in agreement with an $ErQ_3 \cdot H_2O$ formulation. The same product is obtained by using ethanol (or methanol) to dissolve HQ and erbium chloride in spite of the nitrato salt. Yellow crystals, suitable for a diffractometric X-ray study, were obtained on recrystallisation of the crude product from warm CH_3CN.

Structural results show that the obtained product is a *trinuclear* species $Er_3Q_9 \cdot CH_3CN$ (**1**), as reported in reference 25. A similar *trinuclear* structure is exhibited also by $[Ho_3Q_9] \cdot HQ$.[31] The ESI-Mass Spectra of the crude product analysed as $ErQ_3 \cdot H_2O$ and of $Er_3Q_9 \cdot CH_3CN$ show the presence of $Er_3Q_8^+$ cation in both samples proving that the *trinuclear* structure is the reaction product, that is not formed on recrystallisation in organic solvents, and that is preserved in solution. In reference 23 the corresponding reaction in water is reported to produce crude products with analytical results in agreement with a metal to ligand ratio 1:3, ESI-mass corresponding to $Ln_3Q_8^+$ and ^{1}HNMR spectra showing more peaks than expected for a LnQ_3 formulation. However, the crystals isolated by using ethanol as solvent showed to be $NH_4[Er_3Q_8Cl(OH)] \cdot 4C_4H_8O_2$. On the basis of the reported experimental details, it may be suggested that the crude products of reference 23 correspond to Er_3Q_9 (ESI-Mass Spectra and analytical results match perfectly with our findings). The fact that $NH_4[Er_3Q_8Cl(OH)] \cdot 4C_4H_8O_2$ was isolated in ethanol in spite of **1**, may be related to the reaction times (10

min) shorter with respect to those used in our experiments to collect Er_3Q_9. Low soluble ionic intermediates can precipitate in organic solvents before the reaction is gone to completion.

The X-ray data analysis of the obtained crystals of **1** shows that the *trinuclear* complex Er_3Q_9, depicted in Figure 3.1, is formed.[24-25]

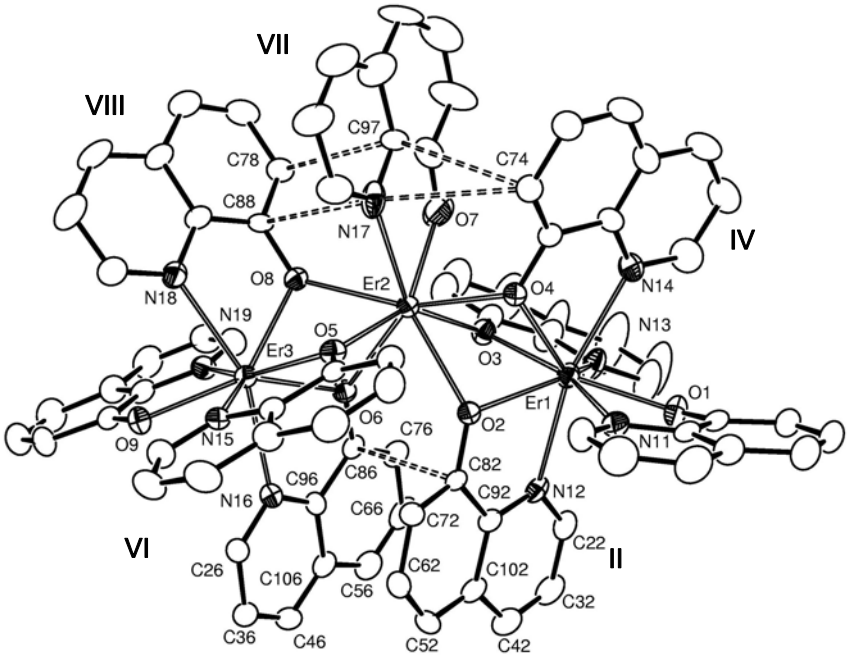

Fig. 3.1: *Perspective view of Er_3Q_9. Dashed bonds represent π interactions. Thermal ellipsoids are drawn at the 25% probability level.*

Each metal presents a distorted square anti-prismatic geometry with the two outer metals bound by four nitrogen and four oxygen atoms whereas the inner erbium is octa-coordinated by a nitrogen and seven oxygen atoms [bond length ranges: Er–O_{bridge} = 2.306(4)-2.480-(3) Å, Er–O = 2.243(5)-2.276(3) Å, Er–N = 2.456(5)-2.533(7) Å]. The molecule is bent [Er(1)–Er(2)–Er(3) angle = 133.48(1)°], and the intermetallic distances between the erbium atoms are 3.478 Å for Er(1)···Er(2) and 3.495 Å for Er(2)···Er(3). In the inner pocket the II and VI quinolinolate anions are π stacked [II-IV dihedral angle=2.0(1)°]. The minimum distance is exhibited by the C(82) and C(86) atoms [3.201(3) Å]. On the opposite side of the molecule, the VII quinolinolate is also interacting with the IV and VIII quinolinolate anions [minimum distances: N(17)–C(74) = 3.155(8) Å and N(17)–C(88) = 3.067(7) Å], but the quinolinolate molecules are skewed with respect to each other with the dihedral angles between the planes of 34.7(1)°(IV-VII) and 30.2(1)° (VII-VIII).

A summary of crystallographic data is reported in Table 3.2.

Crystallographic data for Er_3Q_9	
Empirical formula	$C_{83}H_{57}Er_3N_{10}O_9$
Formula weight	1840.17
Colour, habit	Yellow, Block
Crystal size (mm)	0.15 x 0.10 x 0.10
Crystal system	Triclinic
Space group	P-1
a, b, c (Å)	12.352(1), 16.775(1), 18.199 (1)
α, β, γ (deg.)	83.488(1), 79.302(1), 83.831(1)
V (Å³)	3667.0(4)
Z	2
ρ(calc) (Mg/m³)	1.667
T (K)	293(2)
μ (mm^{-1})	3.468
θ range (deg.)	1.23 to 27.03
No.of rflcn/obsv F>4σ(F)	31568/15582
GooF	0.926
R1 [a]	0.0390
wR2 [b]	0.1064

Table 3.2: Summary of X-ray crystallographic data for **1**.
[a] $R1 = \Sigma||F_O|-|F_C||/\Sigma|F_O|$; [b] $wR2 = [\Sigma[w(F_O^2-F_C^2)^2]/\Sigma[w(F_O^2)^2]]^{½}$, $w = 1/[\sigma^2(F_O^2) + (aP)^2 + bP]$, where $P = [max(F_O^2,0) + 2F_C^2]/3$

The crystal packing reveals the presence of partial π-stack between adjacent *trinuclear* complexes involving quinoxaline ligand with interligand spacings in the 3.307-3.407 Å range. The minimum distance in these stack is between C22 and C42' (3.307(8) Å), C44 and C64''' (3.48(1) Å) and C49 and C49'' (3.407(9) Å) that involves the II, IV and IX quinoline molecules, Figure 3.2.

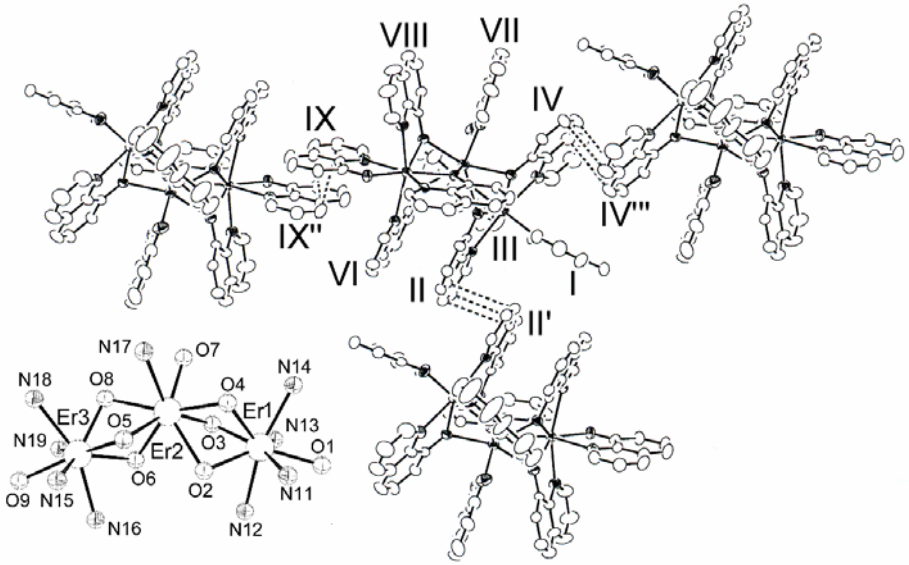

Fig. 3.2: *Crystal packing of Er_3O_9 (**1**) together with the coordination environment of the erbium atoms. Dashed bonds represent inter-molecular π interactions; '=-x; -y; 1-z, ''=-x; 1-y; 1-z, '''=1-x; -y; -z. Thermal ellipsoids are drawn at the 25% probability level. Solvent molecules have been removed for clarity.*

As concluding comments, it can be remarked that the structural characterisation of $(ErQ_3)_n$ is openly in contrast with the common assumption of a tris-chelated octahedral coordination geometry for this complex (Figure 3.3). It was generally assumed that, in this unsaturated structure, the Er coordination sphere can be easily fulfilled by water molecules, which are supposed to be the most important IR quenchers especially when directly bounded to the metal ion. Moreover, some authors[17-18] have argued that these directly coordinated water molecules can be easily displaced by the more coordinating DMSO molecules, leading to better luminescence efficiency when performing measurements on dymethylsulfoxide solutions.

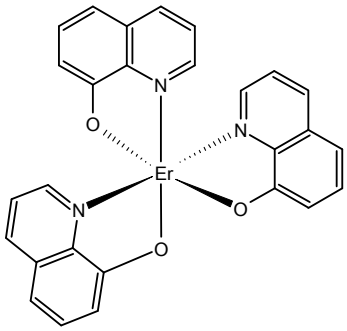

Fig. 3.3: *Tris*-chelated octahedral structure of ErQ_3, as reported in ref. 5.

3.2.2 *Tris* [$Er(XQ)_3(H_2O)_2$]

By using as ligand 5,7-dihalo-8-quinolinol (H5,7ClQ) and (H5,7BrQ), the reaction described above for Er_3Q_9 produces the mononuclear species $[Er(5,7ClQ)_3(H_2O)_2]$ (**2**), and $[Er(5,7BrQ)_3(H_2O)_2]$ (**3**), (Scheme 1, pathway II) which on recrystallisation from warm CH_3CN do not lose the water molecules, that are coordinated to the erbium ion. The three quinolinolato ligands act as bidentate chelating donors, thus the metal ion results octa-coordinated. The crystal structure of **2** shows that two octa-coordinated units form a dimer through four hydrogen bonds $[Er(5,7ClQ)_3(H_2O)_2]_2 \cdot 3H_2O \cdot CH_3CN$. **2** differs from the dimer described in reference 23 for the non-coordinated solvent molecules. Unfortunately, due to crystal thinness, the crystal structure of **3** has not been solved. However, analytical data are in agreement with the $[Er(5,7BrQ)_3(H_2O)_2]$ formulation while spectroscopic results and comparisons with the reported data of analogous compounds[23] allow to infer that this complex is most likely isostructural with complex **2**.

In the crystal structure of **2**, the metal adopts a square antiprismatic geometry with the square faces defined by the N(11)-O(11)-O1w-O2w and N(12)-N(13)-O(12)-O(13) atoms. The coordinated O1w molecule acts as a hydrogen bond donor with respect to the O(11) and O(12) oxygen atoms of a centro-symmetric molecular unit generating a dinuclear entity, in which only a partial stack between the I and II quinoline molecules is present (C(61)-C(52)'=3.45(1) Å and C(81)-C(72)'=3.60(1) Å; '= -x, -y, -z). Figures 3.4a and 3.4b. In the crystal packing, intermolecular interactions are determined by a

partial superimposition of I and III quinoline molecules (C(71)-C(33)''=3.433(9) Å and C(91)-C(43)''=3.41(1) Å, ''= -y, x-y, z). Figure 3.5.

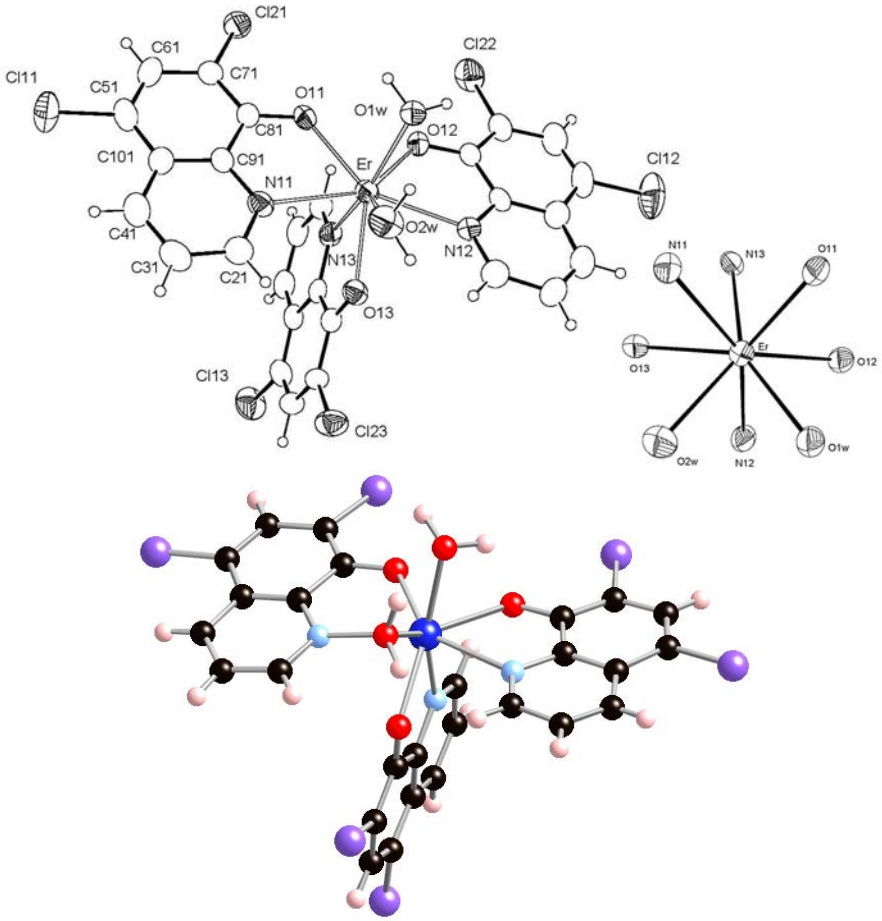

Fig. 3.4a: Crystal structure of $[Er(5,7ClQ)_3(H_2O)_2]\cdot 1.5H_2O\cdot 0.5CH_3CN$ together with the Archimede's antiprism coordination of the erbium ion. Solvent molecules (three water molecules with occupancy factor 1.5 and one acetonitrile molecule with occupancy factor 0.5 per molecular unit) have been removed for clarity.

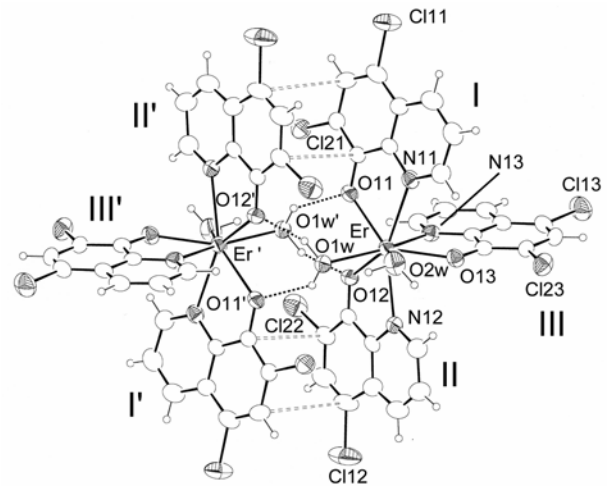

Fig. 3.4b: *Ortep drawing of the dimeric entity* $[Er(5,7ClQ)_3(H_2O)_2]_2 \cdot 3H_2O \cdot CH_3CN$ (**2**) *at the 30% ellipsoids level. ' = -x; -y; -z. Dotted lines represent hydrogen bonds exchanged by the two units whereas dashed bonds represent intermolecular π interactions.*

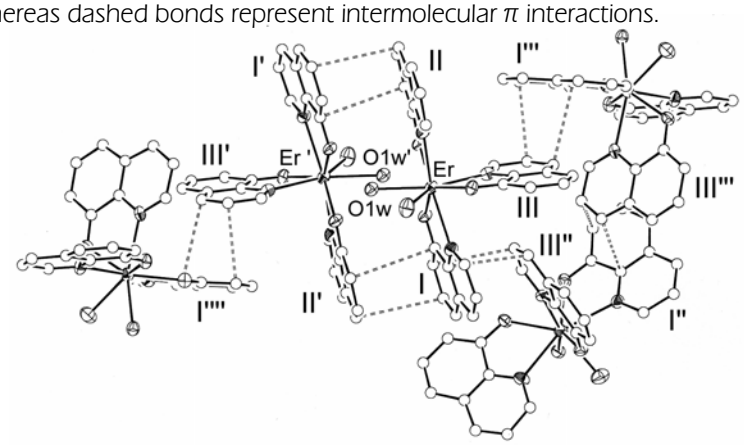

Fig. 3.5: *Crystal packing of the dimer* $[Er(5,7ClQ)_3(H_2O)_2]_2 \cdot 3H_2O \cdot CH_3CN$ (**2**) *at the 30% ellipsoids level. ' = -x; -y; -z, '' = -y; x-y; z, ''' = y-x; -x; z,'''' = x-y; x; -z. Dashed bonds represent intermolecular π interactions. Solvent molecules have been removed for clarity.*

Crystallographic parameters and selected bond lengths are reported in Tables 3.3 and 3.4.

Crystallographic data for $[Er(5,7ClQ)_3(H_2O)_2]$	
Empirical formula	$C_{28}H_{20.50}Cl_6ErN_{3.50}O_{6.50}$
Formula weight	889.94
Colour, habit	Yellow, Block
Crystal size (mm)	0.10×0.10×0.05
Crystal system	Trigonal
Space group	R-3
a, b, c (Å)	21.679(1), 21.679(1), 37.224(2)
α, β, γ (deg.)	90, 90, 120
V (Å³)	15150(1)
Z	18
T (K)	293
ρ(calc) (Mg/m³)	1.756
μ (mm⁻¹)	3.016
θ range (deg.)	1.64 to 26.05
No.of rflcn/obsv F>4σ(F)	53113 / 3391
GooF	1.011
R1 [a]	0.0361
wR2 [b]	0.0546

Table 3.3: Summary of X-ray crystallographic data for **2**.
[a] $R1 = \Sigma||F_O|-|F_C||/\Sigma|F_O|$; [b] $wR2 = [\Sigma[w(F_O^2-F_C^2)^2]/\Sigma[w(F_O^2)^2]]^{½}$, $w = 1/[\sigma^2(F_O^2) + (aP)^2 + bP]$, where $P = [max(F_O^2,0) + 2F_C^2]/3$

Bond lengths (Å) of $[Er(5,7ClQ)_3(H_2O)_2]$			
Er-N(11)	2.542(5)	**Er-O(11)**	2.287(4)
Er-N(12)	2.500(5)	**Er-O(12)**	2.317(4)
Er-N(13)	2.449(4)	**Er-O(13)**	2.296(4)
Er-O1w	2.364(4)	**Er-O2w**	2.414(4)

Table 3.4: *Selected bond lengths for* **2**.

As stated in reference 23, the formation of a mononuclear species instead of the *trinuclear* complex resulting when using the unsubstituted 8-hydroxy-quinoline ligand, is probably due to the steric hindrance of the halogen atom in the 7 position of the quinoline ring which prevents the bridging arrangement.

3.2.3 *Tetrakis* $[Er(5,7XQ)_2(H5,7XQ)_2Cl]$

The complexes $[Er(5,7XQ)_2(H5,7XQ)_2Cl]$ (X=Cl, Br) were prepared by reacting 5,7-dichloro-8-quinolinol (HClQ) or 5,7-dibromo-8-quinolinol (HBrQ) with $ErCl_3 \cdot 6H_2O$ in CH_3CN/CH_3OH 4:1 solvent mixture without addition of a base to deprotonate the ligand hydroxy group (Scheme 1, pathway III). Given the increased acidity of the dihalo-substituted 8-hydroxy-quinolines (due to the presence of electron-withdrawing groups especially on the 5-position of the phenoxy-ring) with respect to the unsubstituted one,[27] partial ligand deprotonation, evidenced by the sudden colour change, immediately

takes place upon addition of the Er^{III} ion to the ligand solution to form the chelated complex. The reaction mixture was then stirred under gentle heating (50-60°C) for approximately 1 day and the solution has been carefully roto-evaporated until saturation (color turned to orange). Well-shaped red crystals suitable for X-ray structural analysis were obtained after slow evaporation of the solvent for few days.

X-ray diffractometric studies performed on suitable crystals of $[Er(5,7XQ)_2(H5,7XQ)_2Cl]$ [X=Cl (**4**); X=Br (**5**)] have demonstrated that the metal ion results epta-coordinated to four ligands, two N,O chelated in deprotonated form as anions, and two that can be formally considered as zwitterionic ligands (N^+–H and O^-) and therefore act as monodentate oxygen donors. The charge of the metal ion is balanced by one coordinating halogenide. These compounds belongs to the class of *tetrakis*-type lanthanide complexes with 5,7-dihalo-8-quinolinol ligands, first reported by Van Deun et al.,[23] which correspond to 1:4 metal-to-ligand ratio. Whereas the *tetrakis* complexes in reference 23 are octa-coordinated to four ligands in the anionic form, and thus bear a negative charge balanced by a small cation, the synthetic method reported in this work has led to the isolation of uncharged complexes having different geometrical arrangements.

In the unit cell of **4**, two independent molecules are present, which are related by a *pseudo* center of symmetry. The two independent molecules interact through a partial stack between the III-VIII and IV-VII quinoline molecules with the minimum distance between these stacks of 3.422(8) [C(93)···C(108)] and 3.439(8) Å [C(97)···C(104)]. The coordination geometry

of **4** and **5** can be described as distorted pentagonal bipyramidal with the equatorial positions defined by Cl(1)-O(11)-O(13)-N(11)-N(13) for Er(1) in **4**, Cl(2)-O(15)-O(17)-N(15)-N(17) for Er(2) in **4** and O(11)-O(13)-O(14)-N(11)-N(14) for Er in **5**, Figures 3.6a,b, 3.7 and 3.8.

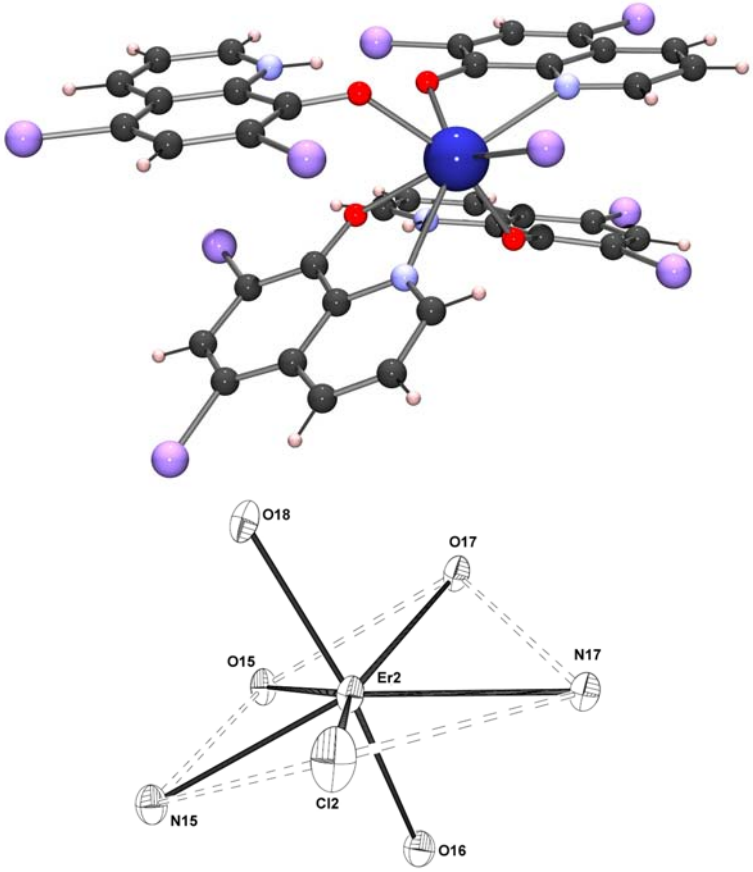

Fig. 3.6a,b: Crystal structure and metal coordination environment of $[Er(5,7ClQ)_2(H5,7ClQ)_2Cl]$ (**4**).

The molecular geometry of **4** and **5** differs in the spatial disposition of the quinoline molecules with respect to each other and in the hydrogen bonds that the protonated quinolines (N^+–H as hydrogen bond donor) exchange with the surrounding groups. In **4**, the N–H are directed toward the oxygen atoms of the opposite and N,O chelated quinoline, whereas in **5** one N–H interacts with the chlorine ions and the second with the oxygen atom of a quinoline. In the crystal structure of **5** there is an uncoordinated CH_3CN molecule per molecular unit.

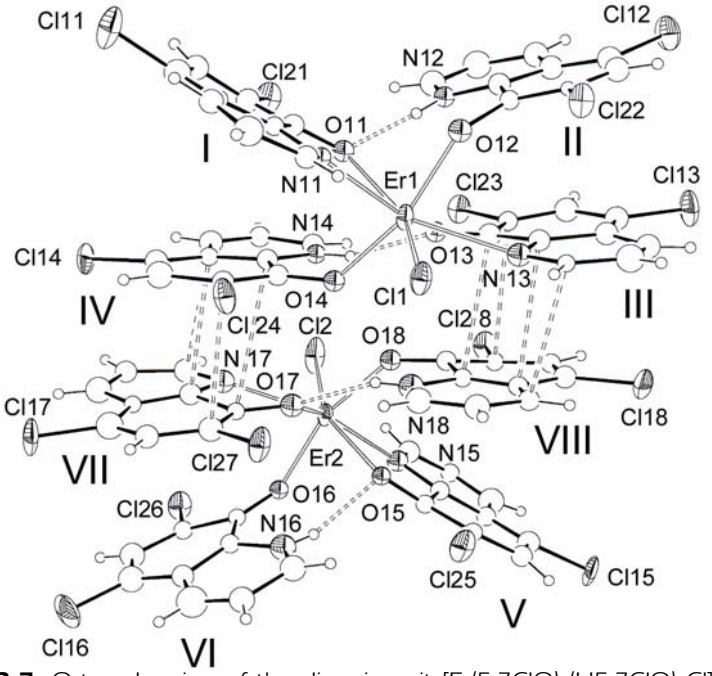

Fig. 3.7: Ortep drawing of the dimeric unit $[Er(5,7ClQ)_2(H5,7ClQ)_2Cl]_2$ (**4**) at the 30% ellipsoids level. Roman numbers refer to the quinoline molecules. Dotted lines represent hydrogen bonds, dashed lines represent intermolecular π-interactions.

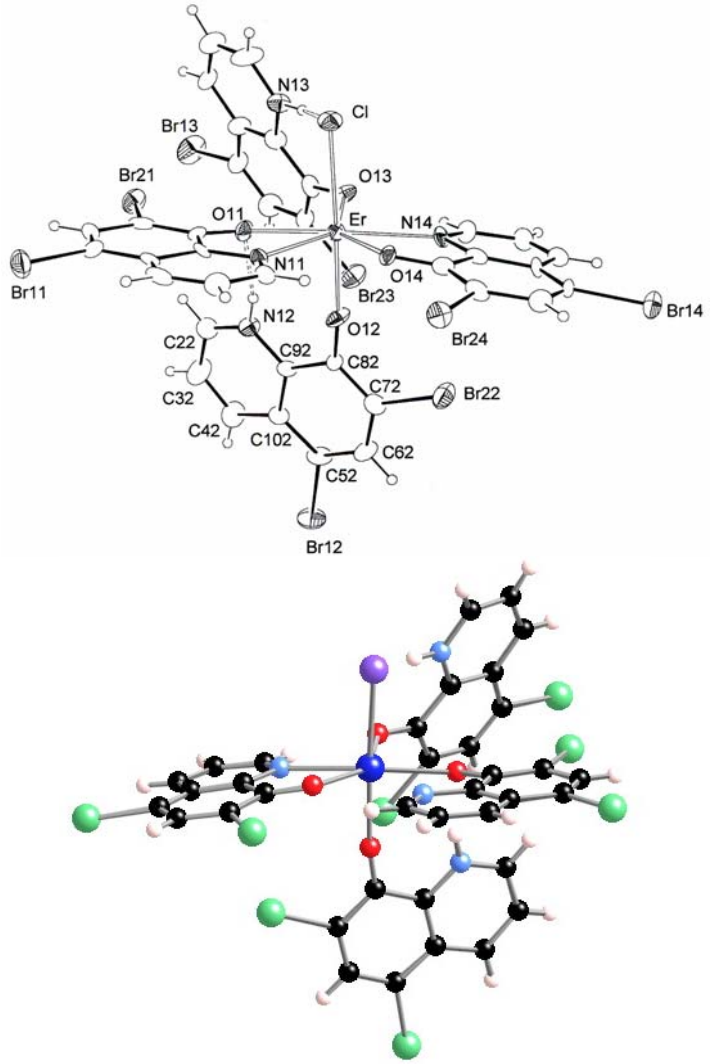

Fig. 3.8: Crystal structure of $[Er(5,7BrQ)_2(H5,7BrQ)_2Cl]\cdot CH_3CN$ (**5**). Dotted lines represent hydrogen bonds. The CH_3CN solvent molecule has been removed for clarity.

The crystal packing of **4** reveals the presence of two interconnected layers in the *ac* and *bc* crystallographic planes, respectively. These layers are determined by the partial stack of I and VI quinoline molecules (*bc* layer) and by the partial stack of the I-VI and II-V quinoline molecules (*ac* layer), Figure 3.9.

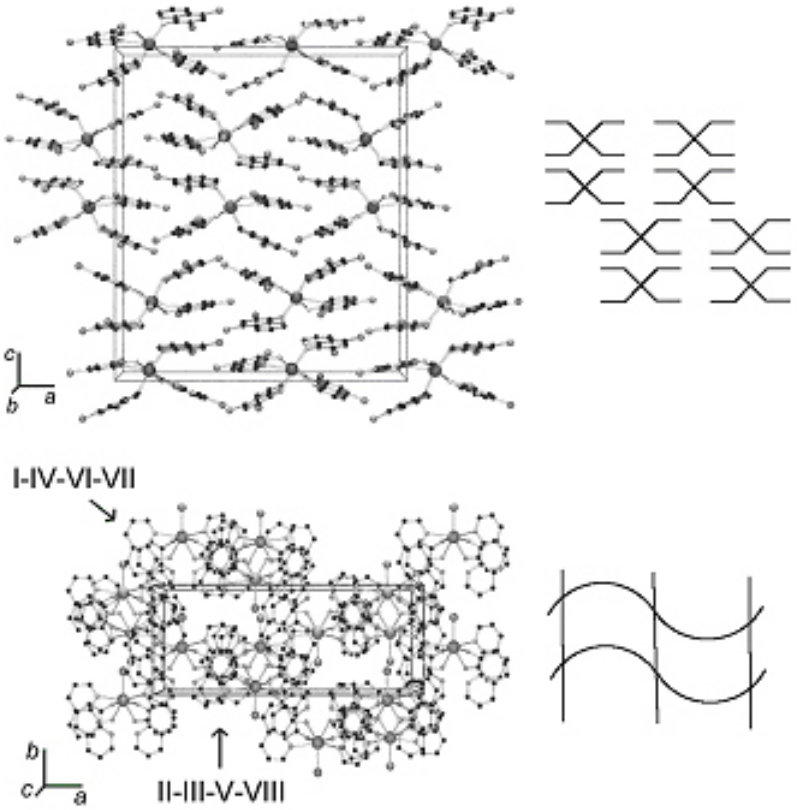

Fig. 3.9: Crystal packing of $[Er(5,7ClQ)_2(H5,7ClQ)_2Cl]$ (**4**) projected along the *b* (above) and *c* (below) crystallographic axes together with a schematic description of the packing.

In the crystal packing of **5**, the molecular unit interacts through the I, II and IV quinoline groups with symmetry related units. The partial π-stack that involves the II and II' quinolines is limited to the juxtaposition of the peripheral part of the ligands (min. distance: C(42)-C(102)'=3.69(2) Å; '=-x; -y; -z) whereas the interaction between the I and IV'' quinolines is more extensive and determines a closer contact between the two molecular entities (min. distance: C(41)-C(24)''=3.36(2) Å; ''=1-x; y-1/2; ½-z). Figure 3.10.

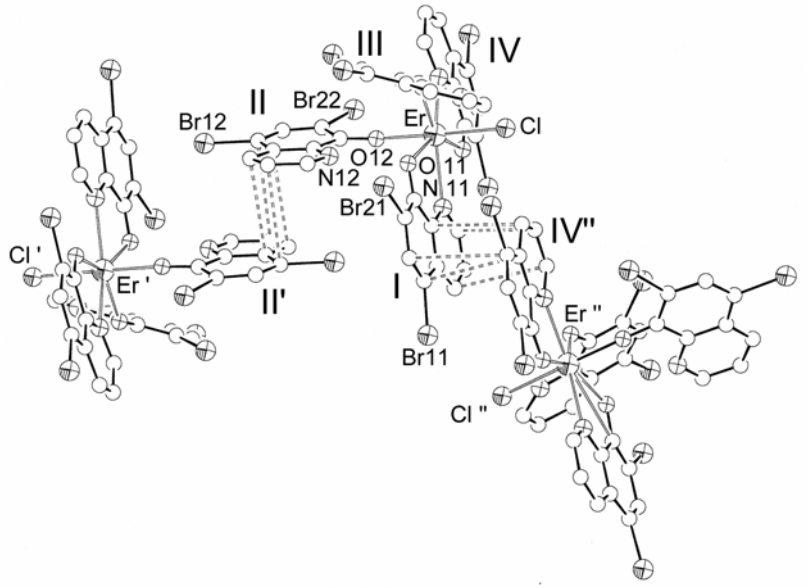

Fig. 3.10: Crystal packing of $[Er(5,7BrQ)_2(H5,7BrQ)_2Cl]\cdot CH_3CN$ (**5**) at the 30% ellipsoids level. The CH_3CN solvent molecule has been removed for clarity.

A summary of X-ray crystallographic data for **4** and **5** is reported in Table 3.5. Selected bond lengths of compounds **4** and **5** are reported in Table 3.6.

Geometric parameters of the hydrogen bonds of **4**-**5** are reported in Table 3.7.

Crystallographic data for $[Er(5,7ClQ)_2(H5,7ClQ)_2Cl]\cdot$ and $[Er(5,7BrQ)_2(H5,7BrQ)_2Cl]\cdot$		
Empirical formula	$C_{72}H_{36}Cl_{18}Er_2N_8O_8$	$C_{38}H_{21}Br_8ClErN_5O_4$
Formula weight	2113.71	1453.59
Colour, habit	Orange, Block	Orange, block
Crystal size (mm)	0.10×0.08×0.05	0.55×0.35×0.25
Crystal system	Orthorhombic	Monoclinic
Space group	$Pca2_1$	$P2_1/c$
a, b, c (Å)	25.570(9), 9.750(7), 29.490(9)	13.493(9), 17.295(9), 18.151(9)
α, β, γ (deg.)	90, 90, 90	90, 97.16(3), 90
V (Å³)	7352(6)	4203(4)
Z	4	4
T (K)	293	293
ρ(calc) (Mg/m³)	1.910	2.297
μ (mm^{-1})	2.985	9.713
θ range (deg.)	1.38 to 24.02	3.05 to 25.00
No.of rflcn/obsv F>4σ(F)	34926 / 4465	7580 / 4096
GooF	0.929	1.001
R1 [a]	0.0659	0.0655
wR2 [b]	0.1123	0.1414

Table 3.5: Summary of X-ray crystallographic data for **4** and **5**.
[a] $R1 = \Sigma||F_O|-|F_C||/\Sigma|F_O|$; [b] $wR2 = [\Sigma[w(F_O^2-F_C^2)^2]/\Sigma[w(F_O^2)^2]]^{½}$, $w = 1/[\sigma^2(F_O^2) + (aP)^2 + bP]$, where $P = [\max(F_O^2,0) + 2F_C^2]/3$

Bond lengths (Å) of $[Er(5,7ClQ)_2(H5,7ClQ)_2Cl]$			
Er(1)-O(11)	2.26(2)	**Er(2)-O(15)**	2.37(2)
Er(1)-O(12)	2.12(2)	**Er(2)-O(16)**	2.20(2)
Er(1)-O(13)	2.36(2)	**Er(2)-O(17)**	2.24(2)
Er(1)-O(14)	2.12(2)	**Er(2)-O(18)**	2.16(2)
Er(1)-N(11)	2.48(2)	**Er(2)-N(15)**	2.52(2)
Er(1)-N(13)	2.50(2)	**Er(2)-N(17)**	2.56(2)
Er(1)-Cl(1)	2.611(7)	**Er(2)-Cl(2)**	2.621(7)
Bond lengths (Å) of $[Er(5,7BrQ)_2(H5,7BrQ)_2Cl]$			
Er-O(11)	2.316(8)	**Er-N(11)**	2.52(1)
Er-O(12)	2.182(8)	**Er-N(14)**	2.478(9)
Er-O(13)	2.294(8)	**Er-Cl**	2.687(3)
Er-O(14)	2.223(8)		

Table 3.6: Selected bond lengths for **4** and **5**.

	d(Å)	N-H···X (deg.)
$[Er(5,7ClQ)_2(H5,7ClQ)_2Cl]$		
N(12) ··O(11)	2.89(3)	154(2)
N(14) ··O(13)	2.91(3)	160(2)
N(16) ··O(15)	2.73(3)	166(2)
N(18) ··O(17)	2.96(3)	162(2)
$[Er(5,7BrQ)_2(H5,7BrQ)_2Cl]$		
N(13) ··Cl	3.10(1)	154.2(7)
N(12) ··O(11)	2.81(1)	167.6(7)

Table 3.7: Geometric parameters of the hydrogen bonds of **4-5**.

It can be inferred that the formation of the "zwitterionic" complex from the reaction mixture under neutral conditions undergoes competitive prototropic equilibria between the different forms of the quinolinol, strongly influenced by the presence of the metal ion.[28] Those equilibria involve both the quinolinolium ($H_2$5,7XQ$^+$) and the quinolinolate (5,7XQ$^-$) ions along with the zwitterionic form of the ligand, although the acidic character of the lanthanide ion probably shifts the equilibrium toward the protonated form. The UV-Visible absorption spectrum of the reaction mixture reported in Figure 3.11 seems to indicate the coexistence of both the protonated (H_2ClQ$^+$) and the anionic (5,7ClQ$^-$) form of the 5,7-dichloro-8-quinolinol.

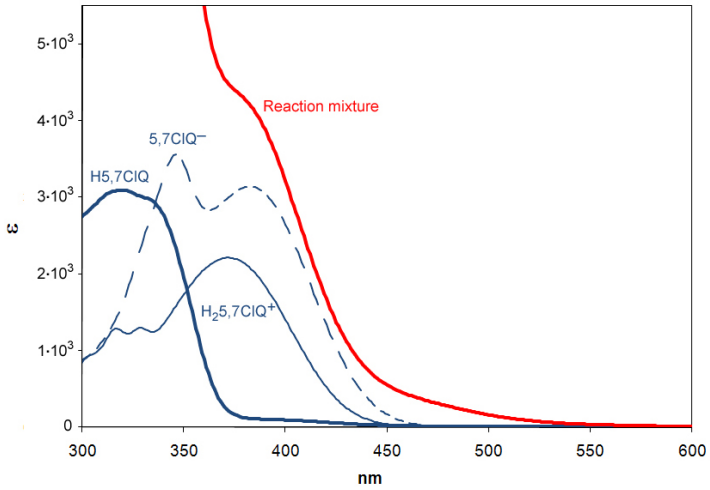

Fig. 3.11: Comparison of UV-Vis absorption spectra of the reaction solution of [Er(5,7ClQ)$_2$(H5,7ClQ$_2$)Cl] (red line) and of differently protonated forms of the 5,7-dichloro-8-quinolinol ligand (blue lines).

Concentration of the solution results in the formation and subsequent crystallisation of the tetrakis complex where two quinolines are in the anionic form and two are zwitterionic. The tautomeric rearrangement of the neutral quinolinol in the complex is probably due to the preference of the strong Lewis acid Ln^{III} for anionic oxygen donor atoms.

3.3 Spectroscopic studies

3.3.1 Electronic spectroscopy

The electronic spectra of the ligands, either in neutral or in deprotonated form, and of complexes **1** and **2**-**4**, in the 300–500 nm spectral region, are reported in Figure 3.12 and 3.13, respectively. Compounds **3** and **5** display spectral features that are very similar to those of **2** and **4** and their spectra are reported in the Appendix Section of this thesis (A.2).

The lowest energy absorption band of the quinolinol ligand is red shifted in the anion, and this shift is higher for the halogen-substituted ligands.

In the absorption spectrum of Er_3Q_9 (**1**) a broad band having a shoulder at lower wavelengths appears, whereas the spectra of compounds **2**, **3**, **4** and **5** consist of two distinct prominent bands. All the spectra of the compounds studied in this work are qualitatively similar to those of the free ligands and therefore the absorption bands are assigned to ligand-centred

transitions.[32-33] The position of the high-energy peak is modestly affected by the presence of the metal ion whereas the lowest energy peak is red-shifted in the complexes to an extent comparable to that generally observed in complexes with closed-shell metal ions which are characterised by little covalent character of the metal-ligand bond. On the other hand, the shift is larger and more sensitive to the metal ion in complexes with open-shell transition metals.[32] Moreover this band is red shifted as the polarity of the solvent increases.

Absorption maxima of compounds **1**-**5** and of the ligands are listed in Table 3.8.

Complex	λ_{1max} (nm)	λ_{2max} (nm)
Er_3Q_9 (1)	335 (shoulder)	369
$[Er(5,7ClQ)_3(H_2O)_2]$ (2)	343	396
$[Er(5,7BrQ)_3(H_2O)_2]$ (3)	344	397
$[Er(5,7ClQ)_2(H5,7ClQ)_2Cl]$ (4)	340	394
$[Er(5,7BrQ)_2(H5,7BrQ)_2Cl]$ (5)	342	396
Q^-	337	363
$5,7ClQ^-$	346	381
$5,7BrQ^-$	347	382

Table 3.8: *Absorption maxima of compounds* **1**-**5** *and of quinolinolate ligands in MeOH solution.*

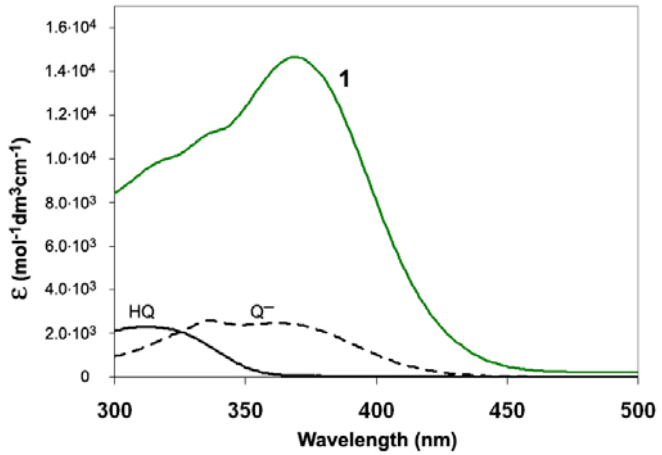

Fig. 3.12: UV-visible spectrum of **1** (green line) in MeOH solution. The spectra of the ligand both in the neutral (continuous line) and in the anionic form (dashed line) are reported for comparison.

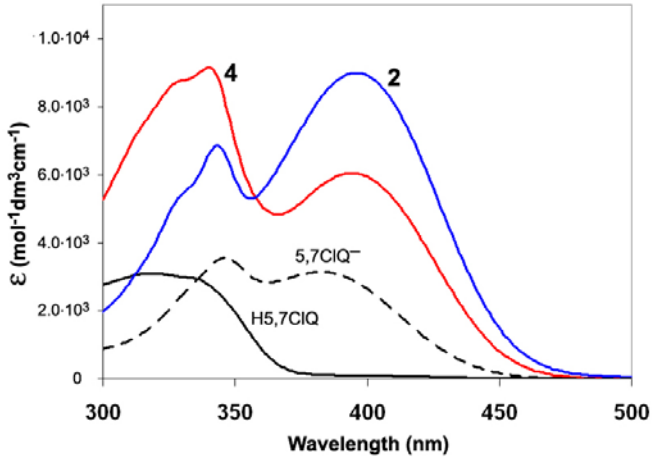

Fig. 3.13: UV-visible spectrum of **2** (blue line) and **4** (red line) in MeOH solution. The spectra of the ligand both in the neutral (continuous line) and in the anionic form (dashed line) are reported for comparison.

Approximate calculations based on semiempirical extended Hückel methods have been performed by using the CACAO program.[34]

In the ligands, as expected, the HOMO and LUMO are π orbitals. The phenoxidic ring gives a higher contribution to the HOMO and the pyridinic one to the LUMO.[33] As a consequence, the HOMO orbital of the anionic ligand is considerably raised in energy by the negative charge on the phenoxidic ring, therefore the lowest energy band of the anion, attributed to a π→π* transition, is red-shifted with respect to the neutral quinolinol.

The localisation of the frontier orbitals on different ligand moieties becomes more evident with the introduction of halogen atoms at the 5,7 positions of Q (Figure 3.14). This gives an increasing charge-transfer character to the HOMO-LUMO transition with a consequent increase in the absorptivities, as observed. Moreover, the strong antibonding character of the carbon-halogen bonds in the HOMO pushes up in energy this orbital as the population of the halogen atom increases (Br > Cl) but the antibonding character of the carbon-halogen bonds is weaker in the LUMO. This explains the observed red shift of the π→π* transition in the halo-substituted ligands.[33]

In the erbium complexes the frontier orbitals consist of set of closely spaced orbitals which preserve the electronic structure of the individual ligands with no significant contribution from the erbium ion. As an example, in **1** nine closely spaced HOMOs and nine LUMOs are found, and in Figure 3.15 the highest energy HOMO and the third LUMO are shown to compare with the frontier orbitals of the free ligand. These findings while based on

approximate calculations give a simplified description useful for a rough explanation of the observed spectral features.

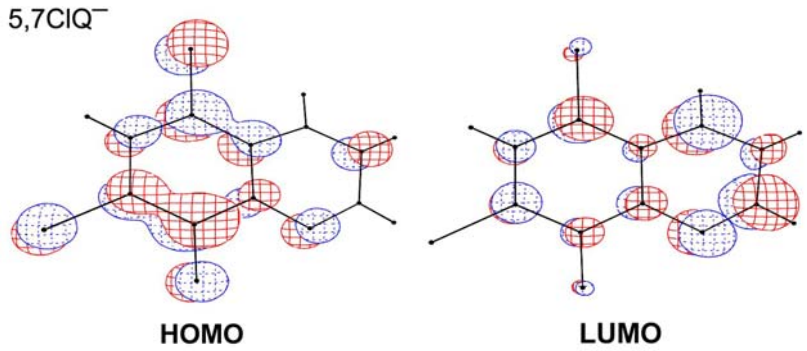

Fig. 3.14: *Frontier Molecular Orbitals in the free 5,7ClQ⁻ ligand, calculated by using semi-empirical extended Hückel methods through the CACAO program.*[31]

The negligible metal contribution to the frontier orbitals results in absorption spectra of the complexes that closely resemble those of the free ligand with molar extinction coefficient values that are roughly the sum of each ligand contribution. Furthermore, in the case of complexes with the dihalo-substituted quinolinols, electronic spectra may be effectively used as tools to recognise whether the product is a *tris* or *tetrakis* complex, since an inversion in intensity of the two lowest energy bands can be easily ascribed to the contributions of differently protonated forms of the ligand in the two types of complexes (Figure 3.13). This is confirmed by MO's calculations since each frontier orbital of compound **4**, depicted in Figure 3.16, arises from the contribution of both the anionic and the zwitterionic form of the quinoxaline ligand.

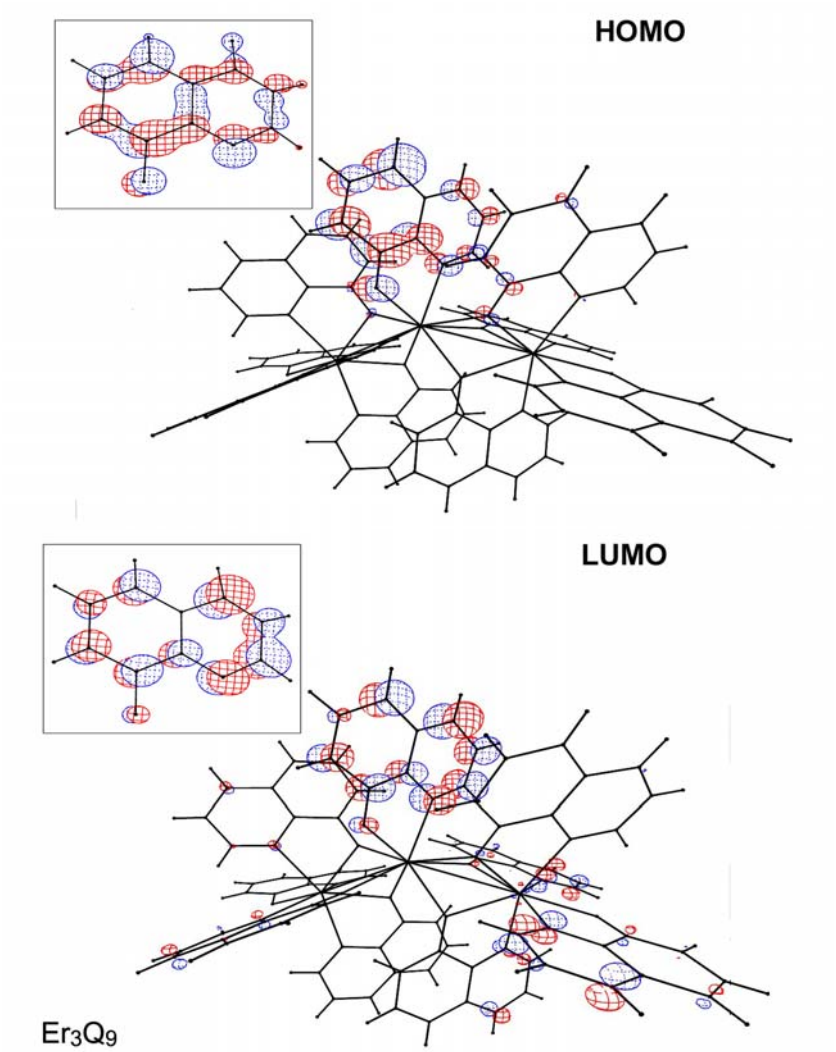

Fig. 3.15: *Frontier Molecular Orbitals in the free O^{-} ligand and in* **1**, *calculated by using semi-empirical extended Hückel methods through the CACAO program.*[34]

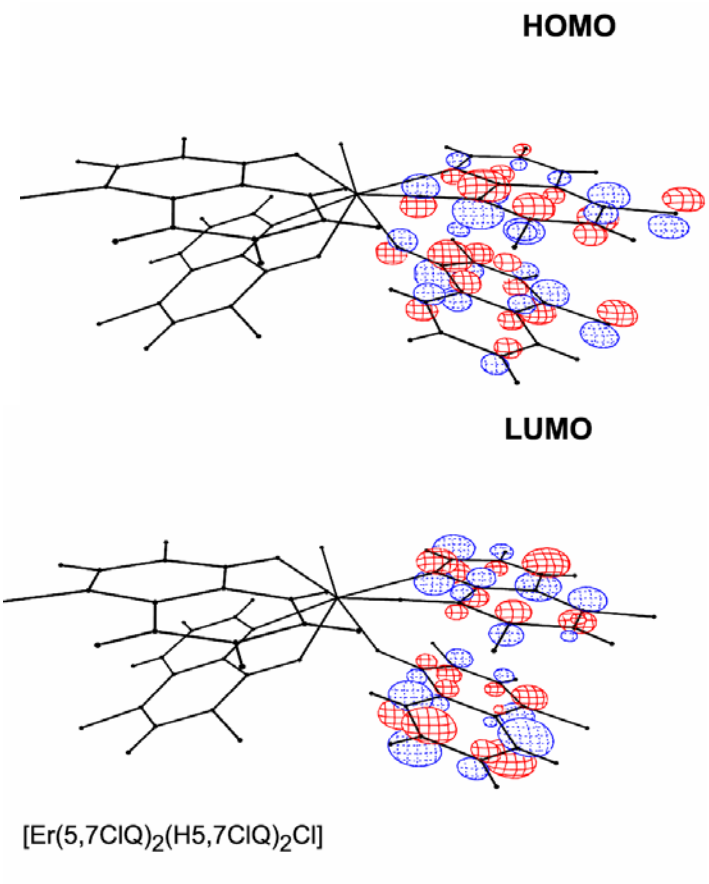

Fig. 3.16: Drawings of the last HOMO and the first LUMO in **4**, calculated by using semi-empirical extended Hückel methods through the CACAO program.[34]

The frontier orbitals of **2** and **5** are reported in the Appendix Section of this thesis (A.3).

3.3.2 Solid state electronic spectroscopy

The diffuse reflectance (DR) spectra allow to identify the ligand centered transitions as well as the sharp f→f erbium bands.

Although solid-state spectra in the UV-Vis spectral region of all the quinolinol complexes studied in this work show the same sequence of bands as solution spectra, the diffuse reflectance spectra of crystalline samples of *tetrakis* complexes (**4** and **5**) show the presence of an additional shoulder near 480 nm, which is absent in solution spectra (Figure 3.17). Moreover, this red-shifted band does not appear in the spectra of corresponding *tris* complexes with the same ligands (**2** and **3**) and therefore is attributable to solid-state effects due to the crystal packing arrangement.

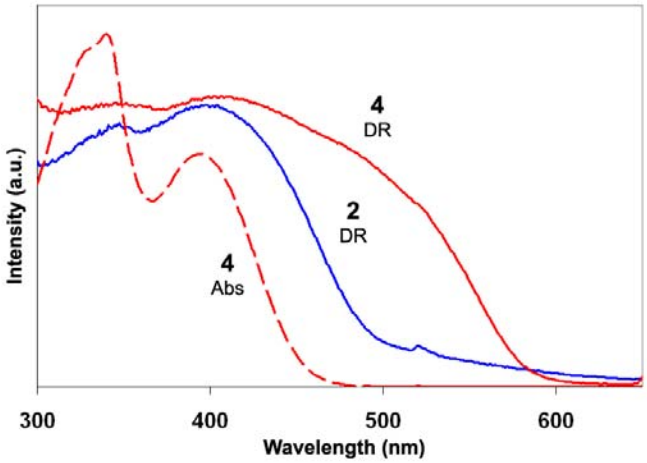

Fig. 3.17: *Diffuse reflectance spectra of* **2** *(blue line) and* **4** *(red line) in the 300-700 nm range. For comparison the MeOH solution spectrum of* **4** *(dashed line) is reported.*

According to Brinkmann et al.,[35-37] who correlated the spectral features of different crystalline phases of AlQ_3 and GaQ_3 to the density of the packing and particularly to the π-π orbital overlap between adjacent quinoxaline moieties, this red-shifted band could be assigned to a π-π* intermolecular transition due to the π-stacking, which is particularly effective in these complexes (short contacts between quinoxaline rings of adjacent molecules in the 3.4-3.8 Å range for **4** and **5**). A schematic illustration of the overlap between quinoxaline rings belonging to neighbouring molecules in the crystal packing of **2**, **4** and **5** is depicted in Fig. 3.18. As shown, significant π overlap exists between Q ligands in the crystal packing of *tetrakis* complexes (**4** and **5**, Figures 3.18a1, a2 and b), whereas only a poor superimposition is found for the *tris* complex **2** (Figure 3.18c).

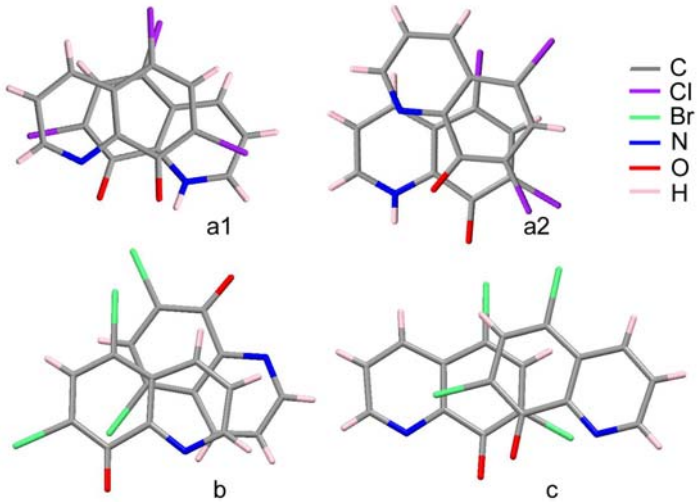

Fig. 3.18: *Schematic drawing of the relative stack between neighbouring quinolinol ligands in the crystal packing of* **4** (**a1** *intramolecular stacking between II and III Q rings;* **a2** *intermolecular stacking III-VIII Q),* **5** (**b** *I-IV'') and* **2** (**c** *I-II').*

The diffuse reflectance spectra in the Vis-NIR spectral region, performed on micro-crystalline powders dispersed on Teflon film of **1**, and of **2-4**, are reported in Figures 3.19 and 3.20, respectively.

All the spectra show the same sequence of sharp bands that are easily attributable to intra-atomic f→f transitions of the erbium ion and are assigned according to literature.[38-39]

The erbium f→f transition wavelengths and their labels are listed in Table 3.7.

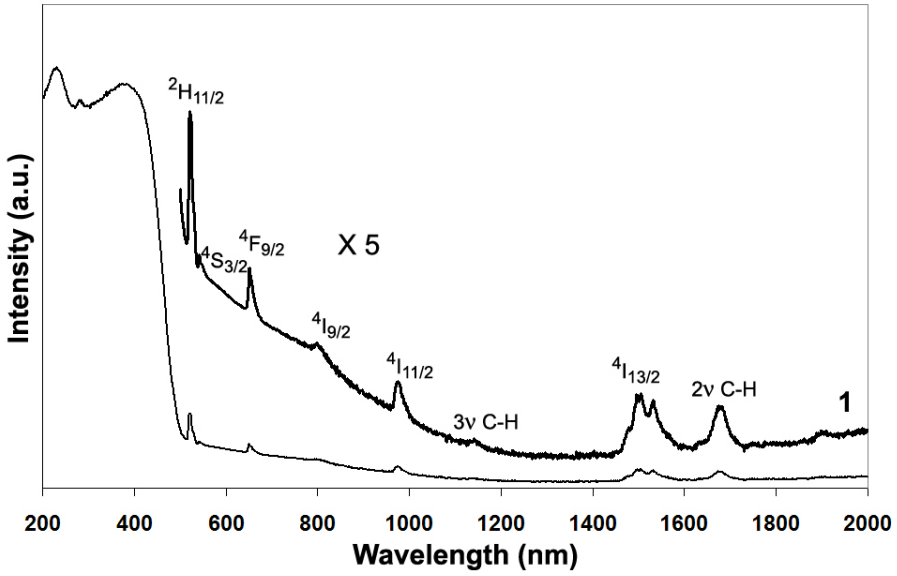

Fig. 3.19: *Diffuse reflectance spectrum of* **1**, *showing the f-f peaks and the overtones of CH stretchings.*

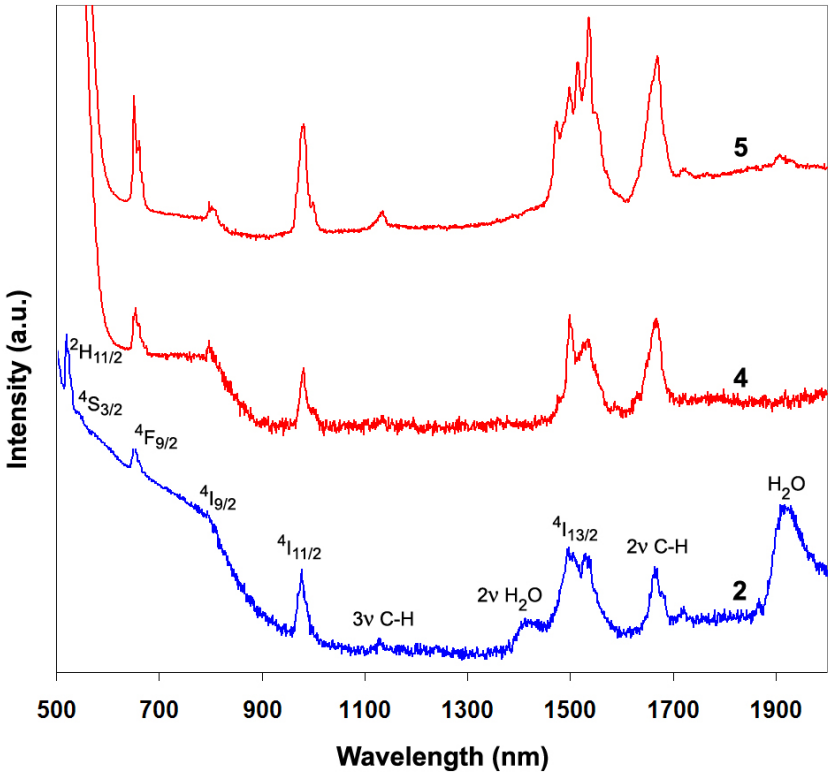

Fig. 3.20: *Diffuse reflectance spectra of* **2**, **4** *and* **5**, *showing the f-f peaks and the overtones of OH stretchings in* H_2O *(1920* $a\nu_1+\nu_2+b\nu_3$, ν_1 *symmetric,* ν_3 *antisymmetric stretching and* ν_2 *bending; 1420* $\nu_1+\nu_3$*).*

While most of these peaks are affected little by the coordination around the lanthanide ion, the peak near 520 nm shows different intensities in the different complexes. This peak is known as the hypersensitive band[40] and its

increase in intensity is related to the increase of the oscillator strength of the $^4I_{15/2}\rightarrow{}^4H_{11/2}$ pseudo-quadrupolar transition as a consequence of a lowering of the symmetry in the coordination sphere (see Chapter 2, Paragraph 2.1). For instance, in **1** the relative intensity of this peak, referred to the 975 nm one, is almost double than that found, as reference, in erbium chloride (whose structure is shown in the Appendix Section of this thesis (A.4)),[41] reflecting the lower symmetrical environment around the ion. In **2** and **3**, in the solid state, the peak at 521 nm is weaker than in **1**, while in **4** and **5** is covered by the additional shoulder near 480 nm.

Transition	Wavelength (nm)
$^2H_{11/2}\leftarrow{}^4I_{15/2}$	521
$^4S_{3/2}\leftarrow{}^4I_{15/2}$	535
$^4F_{9/2}\leftarrow{}^4I_{15/2}$	651
$^4I_{9/2}\leftarrow{}^4I_{15/2}$	795
$^4I_{11/2}\leftarrow{}^4I_{15/2}$	975
$^4I_{13/2}\leftarrow{}^4I_{15/2}$	1495-1530

Table 3.7: *Erbium intra-atomic f→f transitions in the Vis-NIR spectral region.*

Although the position of f→f transition peaks does not significantly change upon coordination, the band centred at 1500 nm is remarkably split in all the complexes. The splitting is relatable to a partial removal of the degeneration of the involved levels as a consequence of the asymmetry of the local field induced by the coordination (Stark splitting).[42-43] Therefore, the splitting

pattern of the erbium f→f bands, and in particular of the 1500 nm band, which is mostly affected by the ligand environment, is a peculiar characteristic of each complex and may be useful to distinguish between different molecular arrangements of complexes belonging to the same class. For instance, the absorption band of the highly dissymmetric *tetrakis* complex **5** displays an evident fine structure consisting of at least four distinct narrow peaks, while in the *tetrakis* complex **4** this band is much less split and only two main peaks are easily recognisable. Moreover, the 1500 nm band of the *tris* complexes **2** and **3**, reported in Figure 3.21, show a fine structure consisting of approximately the same sequence of peaks, and this further suggests that the two compounds possess similar structures.

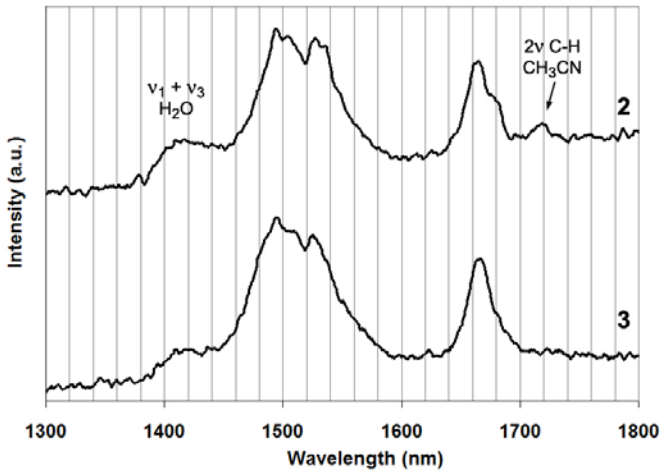

Fig. 3.21: Comparison of the diffuse reflectance spectra of **2** and **3** in the NIR spectral region, showing the fine structure of the 1500 nm band.

The near infrared region is relevant to find experimental evidence for the presence of IR quenchers responsible for the undesired shortening of the natural radiative lifetime of the Er^{III} $^4I_{13/2} \rightarrow {}^4I_{15/2}$ transition near 1500 nm.

In **1-5** the first and second overtones of the aromatic C–H stretching vibrations appear near 1675 nm (2ν C–H) and 1140 nm (3ν C–H) respectively, as indicated in Figures 3.19 and 3.20. In the spectra of crystalline sample of compounds **1**, **2** and **5**, which contain acetonitrile crystallisation molecules in the unit cell, a very small band at about 1710 nm, attributed to the second harmonic of the stretching vibration of aliphatic C–H groups, is found.

Moreover, the existence of water molecules in the first or second coordination sphere of the complexes is unambiguously identified in **2** and **3** through the peaks near 1920 and 1420 nm assigned to the combination bands $a\nu_1+\nu_2+b\nu_3$ and $\nu_1+\nu_3$, respectively (ν_1 and ν_3 = symmetrical and antisymmetrical stretching; ν_2 = bending of the HOH group).

The presence of the peaks near 1420 and 1675 nm, partially overlapping the emission peak, gives experimental evidence to take into account the quenching processes of the erbium emission. These data coupled with structural results have crucial importance for a quantitative study of the emission properties. Moreover, the identification of water through DR spectra on microcrystalline samples dispersed on a Teflon film has shown to be more reliable compared to the assignments through conventional infrared spectroscopy on samples dispersed as KBr pellets, being KBr easily contaminated by the ubiquitous presence of water.

3.3.3 Vibrational spectroscopy

The vibrational spectra of quinolinolato-metal complexes, including lanthanide derivatives, have been reported since long time.[14,43-46] More recently, more sophisticated theoretical studies, including *ab initio* calculations, have furnished reliable assignments on AlQ_3.[47] Based on these previous studies the FT-infrared and FT-Raman spectra of **1**, **2**, **3**, **4**, **5** are discussed.

The FT-IR spectra of the studied samples are shown in Figures 3.22a and b, where the spectra of compounds **1**, **2** and **4** and of ligands HQ and H5,7ClQ are reported for comparison. The spectra of compounds **3** and **5** are reported in the Appendix Section of this thesis (A.2).

All the spectra are mainly dominated by aromatic ring vibrations of the quinolinolate ligand with only slight modifications due to coordination. On the basis of the previous *ab initio studies* on AlQ_3[47] it is possible to assign the following common features: the aromatic CH vibrations near 3050 cm^{-1}, the ring stretching in the 1620-1300 cm^{-1} range, the CO stretching near 1100 cm^{-1}. Below 1000 cm^{-1} the CH wagging and ring deformation modes appear. A ring breathing mode and a ring deformation are found near 740 and 500 cm^{-1} respectively. In the spectra of **2** and **4** the two sharp bands at about 960 and 880 cm^{-1} are attributable to the C–Cl stretching vibration.[17]

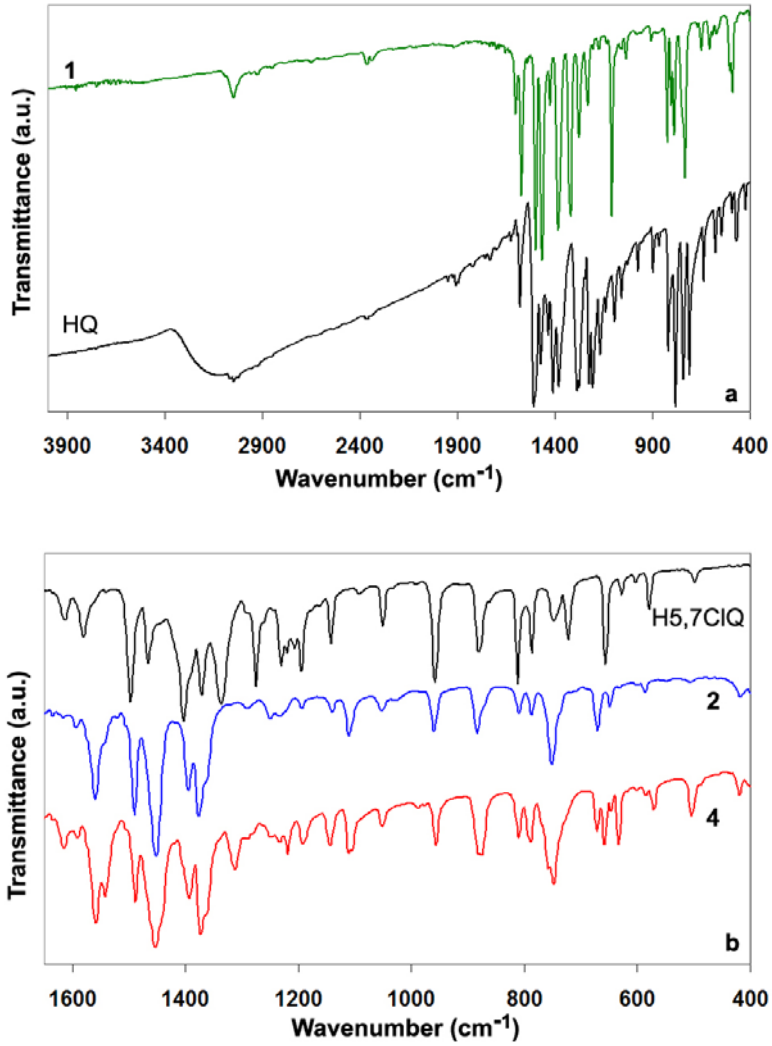

Figg. 3.22: a. Vibrational spectrum of Er_3Q_9 (**1**) and of the ligand HQ in the 3950-400 cm-1 spectral region. **b.** FT-IR spectra of **2** (*tris* complex), **4** (*tetrakis* complex) and of the ligand H5,7ClQ.

The bands at wavenumbers lower than 800 cm^{-1} seem to be somewhat influenced by coordination as they are slightly shifted with respect to those of the free ligand and of AlQ_3.[47] The band near 500 cm^{-1} may be attributable to the Ln–O vibration[14] or to a combination of ring vibrations and M–O stretching.[47]

The comparison of the infrared spectra of **2** and **4** (and similarly of **3** and **5**) allows to identify in **4**, additional peaks which are relatable to the ligand protonated as pyridinium (3200, 1620, 1311 cm^{-1}), see Figure 3.22b. The weak band at about 2115 cm^{-1} is attributable to the N^+–H stretching vibration. Furthermore, the band near 1100 cm^{-1}, due to CO stretching, as well as the peaks near 740 cm^{-1} (ring breathing) and near 586 cm^{-1}, results split as a consequence of the existence of two different forms of coordinated quinolinols in the complex. The sequence of bands between 672 and 634 cm^{-1} is very characteristic of this type of *tetrakis* lanthanide quinolinolates and is relatable to the presence of the zwitterionic ligand, along with the band at 1311 cm^{-1}. In the region between 3200 and 2600 cm^{-1} another peculiar sequence of weak peaks that most likely originates from combinations of the ring stretching modes, is found. This pattern is characteristic of lanthanide quinolinolates with extensive π-stacking.

Similar information are drawn by Raman spectra shown in Figures 3.23a and b, where the spectra of **1** and the ligand HQ, and of compounds **3** and **5** are depicted, while in Figure 3.24 a comparison of the FT-Raman and the FT-IR spectra of compounds **4** and **5** is reported. The spectrum of

compound **2** is qualitatively similar to that of **3** and is reported in the Appendix Section of this thesis (A.2).

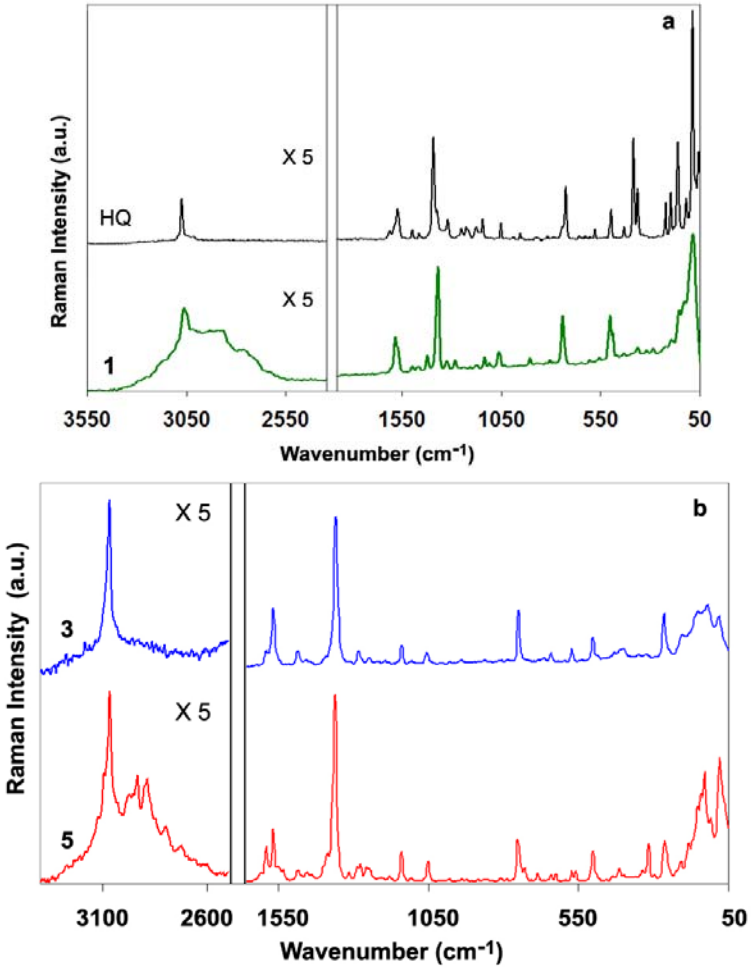

Figg. 3.23: a. FT-Raman spectrum of Er_3Q_9 (**1**) and of the ligand HQ. **b.** Comparison of the FT-Raman spectra of compounds **3** (*tris*) and **5** (*tetrakis*).

As expected, several additional peaks are found in the spectrum of **4** and **5** with respect to **2** and **3**. This clearly reflects the lower symmetry of the *tetrakis* complexes having two differently protonated forms of coordinated Q ligands. For instance, from the comparison of the FT-Raman spectra of **3** and **5** (see Figure 3.23b), it is possible to identify in **5** additional bands at 1315, 685 and 315 cm^{-1}, whereas in the 1610-1540 cm^{-1} region a complex sequence of peaks appears. Moreover, the bands near 1282, 1248, 750 and 641-572 cm^{-1} are split as a result of the presence of the zwitterionic ligands.

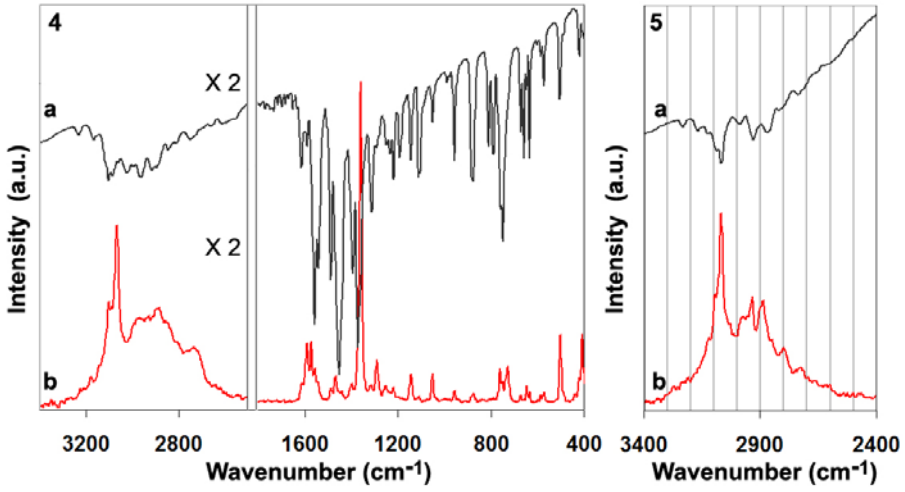

Figg. 3.24: *Comparison of the FT-IR (***a.** *grey line) and the FT-Raman (***b.** *red line) spectra of compound* **4**, *and, on the right, of compound* **5** *in the 3400-2400* cm^{-1} *range.*

The aromatic C–H stretching vibration falls at about 3068 cm^{-1} whereas an interesting sequence of combination bands of the ring vibrations is found in the 3000-2600 cm^{-1} region. These combination bands are more intense in **1**, **4** and **5** where several π-π intermolecular interactions are present with an overlapping of the rings more effective than in **2** where only a partial stacking and no combination bands are observed (see Figure 3.18). The same pattern is also found in the FT-IR spectra of compounds **1**, **4** and **5**, as shown in Figures 3.24.

3.4 Synthesis and characterisation of a series of lanthanide quinolinolates

With the aim to definitively assess the structure/property relationship of this class of compounds, our study has been extended to a series of analogous quinolinolates with other lanthanide ions. This study has allowed to identify unambiguously, by comparison of isostructural complexes, the spectroscopic markers useful to distinguish the different types of coordination modes. In particular, complexes of Nd^{III} and Yb^{III} have been investigated also in view of their potential NIR-emitting properties while gadolinium quinolinolates are useful as reference compounds for a deeper understanding of the photophysical properties of this class of complexes. In fact, the low-lying emissive level ($^6P_{7/2}$) of the Gd^{III} ion is much higher in energy than the singlet and triplet excited states of the Q ligand.[48-50] Therefore, no ligand to metal energy transfer can occur in gadolinium complexes and the donating luminescent levels of ligands can be determined. Moreover, the Gd^{III} ion, with a $^8S_{7/2}$ ground term, has, contrary to the other lanthanides, no orbital contribution to the magnetic moment and the Heisenberg-Dirac-Van Vleck Hamiltonian can be employed to quantify the magnetic exchange interaction in its compounds.[51] Moreover, it allows to evidence weak magnetic interactions that are usually hindered by the depopulation of the Stark sub-levels of the orbitally degenerated lanthanide ions (such as Er^{III}). Further interest to Gd^{III}-based compounds, given the high spin carried by this cation, arises from their potential biomedical applications, in particular as MRI

contrast agents.[50,52]

Yb^{III}, Nd^{III} and Gd^{III} quinolinolates have been prepared following the synthetic methods used for the erbium analogues. A summary of the obtained compounds is reported in table 3.9.

	Er	Yb	Nd	Gd
Trinuclear Ln_3Q_9	Er_3Q_9 Structurally characterised	$(YbQ_3)_n$#	$(NdQ_3)_n$ #	$(GdQ_3)_n$#
Tetrakis $[Ln(5,7XQ)_2(H5,7XQ)_2Cl]$ X = Cl, Br	$[Er(5,7ClQ)_2(H5,7ClQ)_2Cl]$ Structurally characterised	$[Yb(5,7ClQ)_2(H5,7ClQ)_2Cl]$ Structurally characterised	---	$[Gd(5,7ClQ)_2(H5,7ClQ)_2Cl]$ Structurally characterised
	$[Er(5,7BrQ)_2(H5,7BrQ)_2Cl]$ Structurally characterised	$[Yb(5,7BrQ)_2(H5,7BrQ)_2Cl]$ Structurally characterised*	---	---
Tris $[Ln(5,7XQ)_3(H_2O)_2]$ X = Cl, Br	$[Er(5,7ClQ)_3(H_2O)_2]$ Structurally characterised	$[Yb(5,7XQ)_3(H_2O)_2]$ X = Cl, Br	$[Nd(5,7XQ)_3(H_2O)_2]$ X = Cl, Br	$[Gd(5,7XQ)_3(H_2O)_2]$ X = Cl, Br
	$[Er(5,7BrQ)_3(H_2O)_2]$			

Table 3.9: Summary of lanthanide quinolinolates studied in this work.

Although X- ray evidence is missing, the *trinuclear* structure with n=3 seems to be the most likely. Analytical and spectroscopic results along with the comparison with already reported structures and ESI-Mass data support this assertion.[23,53]

* The structure has not been refined.

3.4.1 *Trinuclear* and *tris* complexes

The compounds obtained from syntheses in aqueous media, namely the *trinuclear* and the *tris* complexes, were easily isolated as pure products in high yields. CHN analysis and spectroscopic results are consistent with those found for the correspondent erbium complexes and are reported in the Experimental Section of this Chapter.

The FT-IR spectra of all the compounds belonging to the same class show similar patterns and, as an example, in Figure 3.25 a comparison of the spectra of E_3Q_9 (**1**) and the correspondent neodymium and gadolinium complexes is reported.

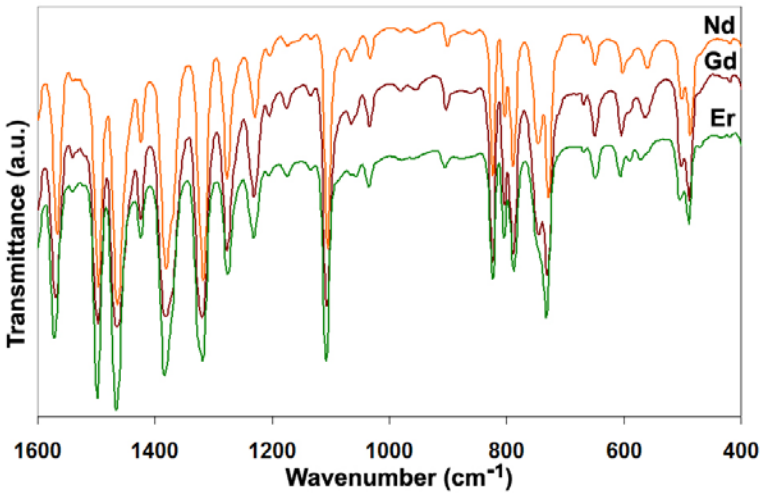

Figure 3.25: Comparison of the FT-IR spectra of neodymium, erbium and gadolinium Ln_3Q_9 *trinuclear* complexes in the 1600-400 cm^{-1} range.

As expected, the bands below 800 cm^{-1} seem to be somewhat sensitive to the metal. Actually, these low-frequency peaks are slightly shifted in the different complexes according to the different weights or the ionic potentials of the lanthanide cations.[14] Likewise, the C–O stretching band near 1100 cm^{-1} is affected to some extent by the weight of the coordinated lanthanide ion.

3.4.2 *Tetrakis* complexes

In contrast to the already mentioned classes of *trinuclear* and *tris* compounds, the preparation of the *tetrakis* complexes from organic media in certain cases has not been so straightforward.

In fact any attempt to isolate *tetrakis* complexes of neodymium, as well as other metals belonging to the first series of lanthanides (Ce-Eu) has so far been unsuccessful. On the other hand, obtaining such type of quinolinolates with the lanthanides of the second half of the series seems to become easier on going across the period from Gd to Yb. Actually, the mid-term of the series, the Gd^{III} ion, whose complexation behaviour places right on the border between the “light” and the “heavy” lanthanides,[54] seems to be the lowest limit for the formation of *tetrakis* complexes. This is not very surprising if the “lanthanide contraction” phenomenon across the period is taken into account, along with the fact that lanthanides coordination chemistry is mostly ruled by ionic bonding and steric effects. The coordination number 7 of this class of complexes, is probably inadequate for the lanthanide ions belonging

to the first half of the series, which have larger ionic radii and therefore tend to fill the coordination sphere by reaching very high C.N. (up to 12). In the *tetrakis* complexes two quinolinolate ligands are present in the zwitterionic form, therefore the N donor atoms on the pyridine rings are protonated and consequently they are no longer available for coordination to the metal ion. As a result, the ligands in the zwitterionic form cannot provide saturation of the lanthanide coordination sphere by acting as bidentate donors, and, at the same time, steric hindrance of the halogenides may prevent coordinating solvent molecules from getting in. This results in the unfavourable condition for the lightest lanthanide ions to satisfy the coordination requirements by forming *tetrakis* complexes under neutral conditions, with zwitterionic ligands.

Furthermore, the formation of the *tetrakis* complexes is probably driven by a delicate arrangement of the coordinated ligands around the lanthanide ion with stabilisation of the monodentate zwitterionic ligands occurring through hydrogen bonds. It descends that the size of the lanthanide ion plays an important role on complex formation which is mainly governed by stereochemistry. Also, according to Fajans' rule, the increased Lewis acid behaviour of the lanthanide ion and the increased covalent character of the metal-ligand bonding on going across the series may favour the complex formation and its stability.

The complexes $[Gd(5,7ClQ)_2(H5,7ClQ)_2Cl]$, $[Yb(5,7ClQ)_2(H5,7ClQ)_2Cl]$, $[Yb(5,7BrQ)_2(H5,7BrQ)_2Cl]$, have been characterised by single-crystal X-ray diffraction and the structural results are equivalent to those found for the erbium analogues.

4, $[Gd(5,7ClQ)_2(H5,7ClQ)_2Cl]$ and $[Yb(5,7ClQ)_2(H5,7ClQ)_2Cl]$, are isostructural and the most relevant difference is represented by the longer coordination bond distances (~0.1 Å) for the gadolinium complex when compared to both the erbium and ytterbium ones, in accordance with the greater ionic radii of Gd^{III} with respect to Er^{III} and Yb^{III}. In Figure 3.26 the molecular structure of the Gd complex is shown.

Due to the small crystal size, the crystal structure of $[Yb(5,7BrQ)_2(H5,7BrQ)_2Cl]$ could not be refined, however collected X-ray data are in agreement with those observed for the correspondent erbium compound **5**. Moreover CHN analysis matches well with the $C_{38}H_{21}Br_8ClErN_5O_4$ formula. Spectroscopic studies confirm these findings.

A summary of X-ray crystallographic data for $[Gd(5,7ClQ)_2(H5,7ClQ)_2Cl]$ and $[Yb(5,7ClQ)_2(H5,7ClQ)_2Cl]$ is reported in Table 3.10.

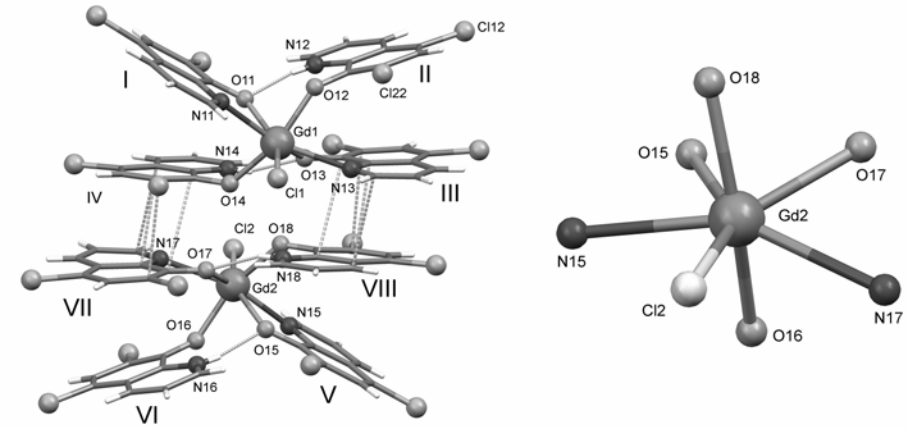

Figure 3.26: *(left) Molecular structure of the* $[Gd(5,7ClQ)_2(H5,7ClQ)_2Cl]_2$ *moiety. Dashed bonds represent inter-molecular* π *interactions and intra-molecular hydrogen bonds. (right) Coordination environment of the* Gd^{III} *ion.*

Crystallographic data for $[Gd(5,7ClQ)_2(H5,7ClQ)_2Cl]$ and $[Yb(5,7BrQ)_2(H5,7BrQ)_2Cl]$·		
Empirical formula	$C_{72}H_{36}Cl_{18}Gd_2N_8O_8$	$C_{72}H_{36}Cl_{18}Yb_2N_8O_8$
Formula weight	2093.69	2125.27
Colour, habit	Orange, prism	Orange, prism
Crystal system	Orthorhombic	Orthorhombic
Space group	*P*ca2$_1$	*P*ca2$_1$
a, b, c (Å)	25.678(2), 9.771(1), 29.367(2)	25.477(2), 9.7300(1), 29.439(2)
α, β, γ (deg.)	90, 90, 90	90, 90, 90
V (Å^3)	7368(1)	7297.7(11)
Z; ρ(calc) (Mg/m^3)	4; 1.887	4; 1.934
T (K)	293	293
μ (mm^{-1})	2.501	3.271
θ range (deg.)	1.59 to 27.99	0.69 to 26.01
No.of rflcn/obsv F>4σ(F)	83722/13821	72355/14340
GooF	1.011	0.616
R1 [a]	0.0390	0.0443
wR2 [b]	0.0749	0.0494

Table 3.10: Summary of X-ray crystallographic data.
[a] $R1 = \Sigma||F_O|-|F_C||/\Sigma|F_O|$; [b] $wR2 = [\Sigma[w(F_O^2-F_C^2)^2]/\Sigma[w(F_O^2)^2]]^{½}$, $w = 1/[\sigma^2(F_O^2) + (aP)^2 + bP]$, where $P = [max(F_O^2,0) + 2F_C^2]/3$

In the absorption spectrum of concentrated (10^{-3} M) DMSO solution of $[Gd(5,7ClQ)_2(H5,7ClQ)_2Cl]$, an additional weak shoulder ($\varepsilon \approx 84\ M^{-1}\ cm^{-1}$), at about 500 nm, becomes visible (see Figure 3.27). This band does not depend on concentration and does not appear in the spectra of analogous *tetrakis* erbium and ytterbium 5,7-dichloro-8-quinolinolate complexes. It might be tentatively ascribed to a forbidden $S_0 \rightarrow T_1$ ligand transition promoted by the presence of a heavy Gd^{III} ion with seven unpaired electrons or to a transition between levels originating from the mixing of opposite-parity wavefunctions.[43,55] However, these tentative assignments definitely deserve further studies.

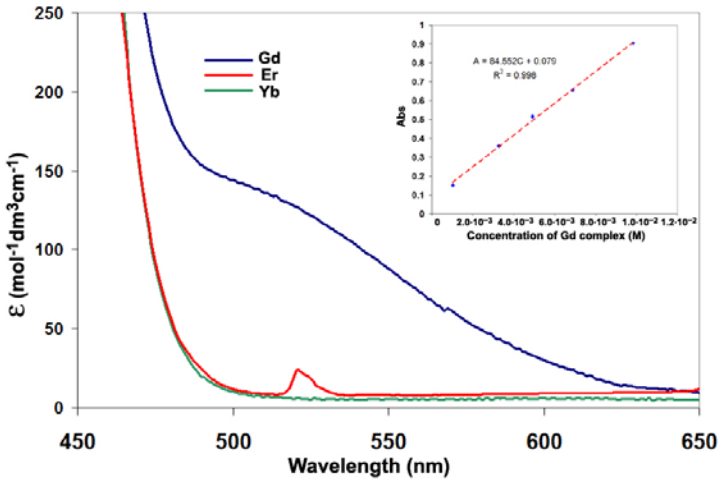

Figure 3.27: *Comparison of the Vis spectra in DMSO solution of ytterbium, erbium and gadolinium $[Ln(5,7ClQ)_2(H5,7ClQ)_2Cl]$ tetrakis complexes in the 450-650 nm range. In the insert the linear correlation between the absorbance at 510 nm and the concentration of the gadolinium complex, is shown.*

3.5 Conclusions

This work represents a significant progress with respect to the studies on this class of NIR-emitting lanthanide complexes available in the literature so far, since:

I. synthetic methods to obtain in high yields pure neutral lanthanide quinolinolate complexes have been optimised. It has been demonstrated that the assumed-to-be *tris*-chelated ErQ_3 is actually a water-free *trinuclear* complex Er_3Q_9 in which each erbium ion is octa-coordinated and has its coordination sphere fully saturated by the Q ligand. In addition, new neutral pure *tetrakis* complexes have been prepared and it has been confirmed[23] that the *tris* complexes are obtained in the halosubstituted case only;

II. structural data provide a detailed description of the molecules and of their different packing which involves well-defined short contacts between quinolinolate ligands, due to π-π orbital overlaps;

III. the investigation of the electronic and vibrational properties of the different complexes allows to select the most significant fingerprints to distinguish the different products, to identify the presence of water and to achieve a deep understanding of the obtained samples.

These results are crucial for a correct interpretation of the photophysical properties of this class of emitting molecules. This will be useful for

physicists who still prepare[5-6,56] erbium quinolinolate complexes following literature methods or a slight modification of these, which are wrongly expected to produce ErQ_3 mononuclear species with octahedral coordination geometry.

3.6 Experimental

3.6.1 Syntheses and analytical data

Chemicals. All the reagents and solvents were purchased from Aldrich and used without further purification.

$Er_3Q_9 \cdot CH_3CN$ (**1**): **Method A.** Few drops of NH_3 28% up to a final concentration of 2.0×10^{-2} mol dm^{-3} (pH ≅ 10) were added to a mixture of 8-hydroxy-quinoline (0.157 g, 1.08 mmol) in H_2O (100 mL) under mixing. (Caution must be taken in controlling the NH_3 amount in order to avoid its excess which can induce the precipitation of the very unsoluble erbium hydroxide). After 30 min a water solution of $Er(NO_3)_3 \cdot 5H_2O$ (0.160 g, 0.361 mmol) was added to the above mixture which is allowed to react for 2 days until the white solid due to the unreacted ligand disappears. A yellow precipitate is formed, collected by filtration, washed with water, NaOH 0.1 M (to improve the solubility of the free ligand eventually present), water, and dried in oven at 120°C (almost quantitative yield). Analytical results are in agreement with the $ErQ_3 \cdot H_2O$ formulation. CHN Found (Calculated) for $C_{27}H_{20}ErN_3O_4$: C% 52.31(52.50), H% 3.22(3.26), N% 6.96(6.80). The solid was then dissolved in warm CH_3CN, the solvent was roto-evaporated to incipient precipitation and after several days yellow crystals of pure $Er_3Q_9 \cdot CH_3CN$ were obtained (yield 46%). CHN Found (Calcd for $C_{83}H_{57}Er_3N_{10}O_9$): C% 53.75(54.07); H% 3.45(3.50); N% 7.07(7.01). **Method B.** $ErCl_3 \cdot 6H_2O$ (0. 159 g, 0.359 mmol) was dissolved in 30 mL of methanol (or ethanol) and the resulting solution was slowly added to 100 mL of a solution of 8-hydroxy-quinoline (0.156 g, 1.075 mmol) in the same solvent. Afterward, few drops of NH_3 28% were added to the reaction mixture and the resulting solution was maintained under stirring at room temperature for several days until a yellow solid precipitated.

The obtained product was washed with NaOH 0.1 M, water and dried in oven (almost quantitative yield). Analytical results are in agreement with the $ErQ_3{\cdot}2H_2O$ formulation. **CHN**: Found (Calculated) for $C_{27}H_{22}ErN_3O_5$: C% 51.12(51.01), H% 3.44(3.49), N% 6.82(6.61). The solid was then recrystallised from CH_3CN and the experimental data of the obtained crystals are in agreement with the $Er_3Q_9{\cdot}CH_3CN$ formulation. **ESI-Mass** (CH_3CN/CH_3OH 3/1): m/z 1654.98 [$Er_3Q_8^+$]. **FT-IR spectrum** (cm^{-1}): 3047 m, 2957 vw, 2928 vw (νC–H, CH_3CN), 2786 vw, 2697 vw, 2647 vw, 2562 vw, 1917 vw, 1601 m, 1571 s, 1498 vs, 1466 vs, 1424 mw, 1383 s, 1318 s, 1276 m, 1231 m, 1174 w, 1108 vs, 1035 w (δC–H), 905 w, 823 m, 804 m, 787 m, 732 s, 648 m, 606 m, 592 w; 571 w, 504 m, 489 m, 384 m, 361 m, 309 w, 210 s, 162 m, 144 w, 115 w, 70 w. **FT-Raman spectrum** (cm^{-1}): 3065 m, 2936 m, 2895 m, 2764 m, 1584 m, 1424 w, 1372 s, 1331 w, 1283 w, 1135 w, 1064 m, 905 w, 738 m, 504 m, 282 w, 140 m. **UV-Vis spectrum** (nm; [mol^{-1} dm^3 cm^{-1}]): 369[$(1.47\pm0.03)10^4$], 521[<17]. **DR spectrum** (nm): 227, 277 sh, 384; 521, 541, 652, 799, 977, 1501–1531 (f→f); 1679 (2νC−H).

[Er(5,7ClQ)$_3$(H$_2$O)$_2$]$_2$·3H$_2$O·CH$_3$CN (**2**): Few drops of NH_3 28% were added to a mixture of 5,7-dichloro-8-quinolinol (0.230 g, 1.075 mmol) in H_2O (150 mL) and the mixture was maintained under vigorous stirring at 35°C. After 60 min a water solution of $Er(NO_3)_3{\cdot}5H_2O$ (0.159 g, 0.359 mmol) was added and after few days of stirring at room temperature a dark-yellow precipitate was collected, washed with water, NaOH 0.1 M, water, and dried in oven at 120°C (yield 97%). **CHN**: Found (Calcd for $Er(5,7ClQ)_3{\cdot}3H_2O$ (**2**)): C% 37.54(37.69), H% 2.20(2.11), N% 5.02(4.88). The solid was dissolved in hot CH_3CN and the resulting solution was concentrated up to half volume and then left standing to the air. After several days dark-yellow crystals suitable for X-ray studies were collected (yield 30%). **CHN**: Found (Calcd for $C_{28}H_{20.50}Cl_6ErN_{3.50}O_{6.50}$ (**2**)) C% 37.88(37.79), H% 2.27(2.32), N% 5.47(5.51). **FT-IR spectrum** (cm^{-1}): 3074 w, 2928 w (νC–H, CH_3CN), 1594 w, 1560 s, 1491 s, 1452 vs, 1395 m, 1376 s, 1286 w, 1251 mw, 1234 mw, 1195 w, 1141 w, 1111 m, 1053 w (δC–

H), 1028 vw, 961 m (νC–Cl), 884 m (νC–Cl), 809 mw, 788 mw, 751 s, 671 m, 649 mw, 586 w, 507 vw, 418 mw. **FT-Raman spectrum** (cm^{-1}): 3071 m, 2936 mw, 2257 w, 1576 m, 1493 w 1457 vw, 1364 vs, 1290 w, 1140 w, 1054 w, 961 vw, 755 mw, 649 w, 590 w, 503 m, 412 m, 348 m, 246 m, 204 m, 177 m, 148 m. **UV-Vis spectrum** (nm; [mol^{-1} dm^3 cm^{-1}]): 343[(6.9±0.1)10^3], 396[(9.0±0.1)10^3], 521[<10]. **DR spectrum** (nm): 266, 348, 400; 520, 653, 803, 975, 1497-1527 (f→f); 1667 (2νC−H), 1917 (aν1+ν2+bν3 H_2O).

Er(5,7BrQ)$_3$(H$_2$O)$_2$ (**3**): The synthesis was carried out following the procedure described above, adding a water solution of $ErCl_3 \cdot 5H_2O$ (0.130 g, 0.340 mmol) to a mixture of 5,7-dibromo-8-quinolinol (0.309 g, 1.020 mmol) in H_2O (150 mL) made slightly basic by the addition of few drops of NH_3 28% (yield 97%). **CHN**: Found (Calcd for $Er(5,7BrQ)_3 \cdot 3H_2O$): C% 29.05(28.77), H% 1.20(1.61), N% 3.79(3.73). The solid was recrystallised in hot CH_3CN. After several days yellow crystals were collected (yield 30%). Experimental data are in agreement with the $Er(5,7BrQ)_3(H_2O)_2$ formulation. **CHN**: Found (Calcd for $C_{83}H_{39}Br_{18}Er_3N_{10}O_9$) C% 30.30(29.24), H% 1.17(1.45), N% 4.21(3.79). **FT-IR spectrum** (cm^{-1}): 3071 w, 1554 s, 1485 s, 1453 vs, 1391 s, 1372 s, 1274 w, 1248 mw, 1217 mw, 1202 w, 1138 mw, 1108 m, 1050 mw (δC–H), 938 m (νC–Br), 860 m (νC–Br), 809 m, 786 m, 744 s, 686 m, 667 m, 654 w, 641 mw; 625 vw, 595 w, 568 m, 503 vw, 419 mw, 414 s, 394 s, 361 m, 346 m, 243 s, 206 m, 164 m, 146 m, 115 w. **FT-Raman spectrum** (cm^{-1}): 3068 m, 1567 m, 1486 w 1457 vw, 1359 vs, 1282 w, 1138 w, 1054 w, 942 vw, 750 mw, 641 w, 572 mw, 501 m, 499 m, 348 m, 264 m, 203 m, 152 m, 119 m. **UV-Vis spectrum** (nm; [mol^{-1} dm^3 cm^{-1}]): 344[(7.6±0.1)10^3], 397[(9.1±0.1)10^3], 521[<10]. **DR spectrum** (nm): 228sh, 267, 348, 402; 521, 652, 803, 973, 1497–1531 (f → f); 1669 (2νC−H), 1917 (aν1+ν2+bν3 H_2O).

[Er(5,7ClQ)$_2$(H5,7ClQ)$_2$Cl] (**4**)*:* 0.442 g (2.064 mmol) of 5,7-dichloro-8-quinolinol were dissolved in 150 mL of CH_3CN/CH_3OH (4:1 v/v) at 35-40°C. $ErCl_3 \cdot 6H_2O$, (0.197 g, 0.516 mmol), dissolved in 10 mL of the same solvent mixture, (this salt is more soluble in organic solvent with respect to the nitrato one) was slowly added to the ligand solution and the reaction mixture turned suddenly yellow. After 24 hours the solution was roto-evaporated until it turned orange. After few days red crystals, suitable for X-ray studies, were collected and washed with diethyl ether (yield 61%). It is important to take good care in concentrating the mother liquor in order to avoid immediate precipitation of the rather insoluble 5,7-dichloro-8-quinolinol. The neutral ligand and the complex seem to have similar solubilities in organic solvents, thus working with a slight excess of the lanthanide ion may ensure that the crystallization of the complex takes place in advance, otherwise H5,7XQ will be subtracted from the equilibrium and no lanthanide complex can be obtained. Any residual of neutral quinolinol that may possibly precipitate after crystallization of the complex can be removed by washing with diethyl ether. **CHN**: Found (Calcd for $C_{36}H_{18}Cl_9ErN_4O_4$) C% 40.66(40.91), H% 1.70(1.72), N% 5.28(5.30). **FT-IR spectrum** (cm^{-1}): 3236 vw, 3171 vw, 3104 w, 3026 w, 2966 w, 2914 w, 2850 vw, 2752 vw, 2115 w(νN^+–H), 2013 w, 1616 m, 1592 w, 1559 s, 1542 m, 1489 m, 1454 vs, 1394 m, 1374 s, 1312 m, 1294 w, 1251 w, 1234 mw, 1220 m, 1193 m, 1144 m, 1112 m (split peak), 1051 mw (δC–H), 991 vw, 957 m (νC–Cl), 876 m (νC–Cl), 810 m, 789 m, 748 s (split peak), 672 m, 659 m, 646 w, 634 m, 586 w, 571 mw, 504 m, 420 mw. **FT-Raman spectrum** (cm^{-1}): 3068 m, 2887 m, 2730 m, 1592 m, 1574 m, 1555 mw, 1488 w, 1469 mw, 1455 w, 1405 w, 1360 vs, 1317 w, 1292 m, 1254 w, 1215 w, 1144 m, 1115 vw, 1051 m (δC–H), 956 w, 876 w, 761 m, 727 m, 680 w, 646 w, 572 w, 501 m, 407 m, 378 mw, 365 m, 348 mw, 275 w, 205 s, 170 s, 144 s. **UV-Vis spectrum** (nm; [mol^{-1} dm^3 cm^{-1}]): 340[$(9.17\pm0.05)10^3$], 394[$(6.05\pm0.03)10^3$], 521[<10]. **DR spectrum** (nm): 230, 267, 345sh, 405, 480sh; 521sh, 654, 799, 981, 1499–1536 (f → f); 1671 (2νC−H).

[Er(5,7BrQ)$_2$(H5,7BrQ)$_2$Cl]·CH$_3$CN (**5**): The synthesis was carried out following the procedure described for the analogous *tetrakis* complex with H5,7ClQ. A slight excess, in order to avoid the precipitation of the ligand, of $ErCl_3 \cdot 6H_2O$ (0.166 g, 0.434 mmol) dissolved in 10 mL of of CH_3CN/CH_3OH (4:1 v/v.) was slowly added to a solution of 5,7-dibromo-8-quinolinol (0.395 g, 1.304 mmol) in the same solvent mixture. After several days, red crystals, suitable for X-ray studies, were collected and washed with diethyl ether (yield 37%, calculated with respect to the ligand). **CHN**: Found (Calcd for $C_{38}H_{21}Br_8ClErN_5O_4$) C% 30.79(31.40), H% 1.42(1.46), N% 4.76(4.82). **FT-IR spectrum** (cm^{-1}): 3221 vw, 3143 vw, 3064 w, 2989 vw (νC–H, CH_3CN), 2928 vw, 2868 w, 2817 vw, 2734 vw, 2250 vw (νCN, CH_3CN), 2094 w(νN^+-H), 1609 m, 1594 m, 1552 vs, 1485 s, 1453 vs, 1389 s, 1368 vs, 1315 m, 1300 mw, 1242 mw, 1217 mw, 1196 mw, 1140 m, 1107 m, 1049 m (δC–H), 1005 vw, 986 vw, 939 m (νC–Br), 909 vw, 884 m, 860 m (νC–Br), 805 m, 789 m, 768 w, 743 s, 685 s, 668 m, 656 m, 641 mw, 625 m, 595 vw, 569 m, 507 m, 418 mw. **FT-Raman spectrum** (cm^{-1}): 3068 m, 2933 m, 2886 m, 2801 w, 2724 w, 2250 w, 1590 m, 1567 m, 1486 w, 1460 w, 1492 w, 1361 vs, 1315 w, 1285 w, 1276 w, 1257 w (split peak), 1179 vw, 1140 m, 1110 vw, 1050 m, 810 vw, 752 m, 731 m, 685 w, 640 w, 625 w, 572 w, 559 w, 501 m, 414 m, 338 w, 315 m, 263 m, 208 w, 185 m, 129 s, 108 m. **UV-Vis spectrum** (nm; [mol^{-1} dm^3 cm^{-1}]): 342[(8.21±0.10)10^3], 396[(6.17±0.09)10^3], 521[<10]. **DR spectrum** (nm): 271, 350, 406; 480sh; 652, 802, 982, 1472, 1498, 1514-1536 (f → f); 1669 (2νC−H).

NdQ$_3$, GdQ$_3$, YbQ$_3$: Syntheses were carried out following the procedure described for Er_3Q_9, adding a water solution of $LnCl_3 \cdot 5H_2O$ (Ln = Nd, Gd, Yb) to a mixture of 8-hydroxy-quinoline (ratio 1:3) in H_2O (150 mL) made slightly basic by the addition of few drops of NH_3 28% (yield 95%). All the compounds precipitate as yellow micro-crystalline solids. **CHN**: *NdQ$_3$.* Found (Calcd for $NdQ_3 \cdot H_2O$): C% 53.64(54.07), H% 3.80(3.39), N% 7.88(7.07). *GdQ$_3$.* Found (Calcd for $GdQ_3 \cdot H_2O$):

C% 51.38(51.83), H% 3.39(3.54), N% 6.95(6.72). *YbQ_3.* Found (Calcd for $YbQ_3 \cdot H_2O$): C% 52.18(52.01), H% 3.35(3.23), N% 6.82(6.74). **FT-IR spectra** (cm^{-1}): *NdQ_3.* 3045 m,br, 1598 w, 1566 s, 1496 vs, 1463 vs, 1423 m, 1379 s, 1317 s, 1276 m, 1228 m, 1105 s, 1031 m, 898 m, 823 s, 802 m, 786 s, 744 m, 727 s, 646 w, 599 w, 555 w, 491 m, 484 s. *GdQ_3.* 3045 m,br, 1598 w, 1568 s, 1496 vs, 1462 vs, 1425 m, 1379 s, 1317 s, 1276 m, 1228 m, 1106 s, 1033 m, 900 m, 823 s, 802 m, 786 s, 741 m, 727 s, 648 w, 603 w, 557 w, 491 m, 487 s. *YbQ_3.* 3047 m, 1601 m, 1571 s, 1498 vs, 1466 vs, 1424 mw, 1383 s, 1318 s, 1276 m, 1231 m, 1174 w, 1109 vs, 1035 w, 907 w, 823 m, 804 m, 788 m, 732 s, 648 m, 607 m, 592 w; 571 w, 504 m, 490 m. **UV-Vis spectrum** (nm, [mol^{-1} dm^3 cm^{-1}]): *GdQ_3.* (DMSO) 340[$(1.53\pm0.03)10^4$], 383[$(1.94\pm0.03)10^4$]. **DR spectra** (nm): *NdQ_3.* 264, 342(sh), 386; 529 ($^4I_{9/2} \rightarrow {}^4G_{7/2}+{}^2G_{9/2}$), 582($^4I_{9/2} \rightarrow {}^4G_{7/2}+{}^2G_{7/2}$, hypersensitive transition), 749($^4I_{9/2} \rightarrow {}^4F_{7/2}+{}^4S_{3/2}$), 802($^4I_{9/2} \rightarrow {}^4F_{5/2}+{}^2H_{9/2}$), 877($^4I_{9/2} \rightarrow {}^4F_{3/2}$);[17,57] 1683 (2νC−H). *GdQ_3.* 263, 343(sh), 382, 1683 (2νC−H). *YbQ_3.* 262, 344, 385; 928, 952, 979 (split, $^2F_{7/2} \rightarrow {}^2F_{5/2}$);[10] 1683 (2νC−H).

$Nd(5,7XQ)_3(H_2O)_2$, *$Gd(5,7XQ)_3(H_2O)_2$*, *$Yb(5,7XQ)_3(H_2O)_2$ (X=Cl,Br)*: Syntheses were carried out following the procedure described for Er_3Q_9, adding a water solution of $LnCl_3 \cdot 5H_2O$ (Ln = Nd, Gd, Yb) to a mixture of 5,7 – dihalo – 8 – quinolinol (ratio 1:3) in H_2O (150 mL) made slightly basic by the addition of few drops of NH_3 28% (yield 95%). All the compounds precipitate as yellow micro-crystalline solids. **CHN**: *$Nd(5,7ClQ)_3(H_2O)_2$*. Found (Calcd for $Nd(5,7ClQ)_3 \cdot 3H_2O$): C% 38.64 (38.73), H% 2.40 (2.17), N% 4.99 (5.02). *$Nd(5,7BrQ)_3(H_2O)_2$*. Found (Calcd for $Nd(5,7BrQ)_3 \cdot 3H_2O$): C% 29.54 (29.37), H% 1.80(1.64), N% 3.93(3.81). *$Gd(5,7ClQ)_3(H_2O)_2$*. Found (Calcd for $Gd(5,7ClQ)_3 \cdot 3H_2O$): C% 38.27(38.13), H% 2.31(2.13), N% 4.97(4.94). *$Gd(5,7BrQ)_3(H_2O)_2$*. Found (Calcd for $Gd(5,7BrQ)_3 \cdot 3H_2O$): C% 29.17(29.03), H% 1.91(1.62), N% 3.87(3.76). *$Yb(5,7ClQ)_3(H_2O)_2$*. Found (Calcd for $Yb(5,7ClQ)_3 \cdot 3H_2O$): C% 37.66(37.44), H% 2.22(2.09), N% 4.90(4.85).

Yb(5,7BrQ)$_3$(H$_2$O)$_2$. Found (Calcd for Yb(5,7BrQ)$_3$·3H$_2$O): C% 29.00(28.62), H% 1.82(1.60), N% 3.80(3.71). **FT-IR spectra** (cm^{-1}): *Nd(5,7ClQ)$_3$(H$_2$O)$_2$*. 3074 w, 2928 w (νCH, CH$_3$CN), 1594 w, 1557 s, 1489 s, 1447 vs, 1393 m, 1373 s, 1360 m, 1285 w, 1246 mw, 1229 mw, 1192 w, 1140 w, 1107 m, 1051 w (δC–H), 1028 vw, 957 m (νC–Cl), 882 m (νC–Cl), 808 mw, 787 mw, 750 s, 671 m, 644 mw, 583 w, 502 vw. *Nd(5,7BrQ)$_3$(H$_2$O)$_2$*. 3071 w, 1551 s, 1483 s, 1449 vs, 1389 s, 1369 s, 1271 w, 1246 mw, 1213 mw, 1202 w, 1138 mw, 1105 m, 1047 mw (δC-H), 935 m (νC-Br), 858 m (νC-Br), 808 m, 785 m, 741 s, 685 m, 667 m, 652 w, 637 mw; 621 vw, 594 w, 565 m, 499 vw, 419 mw, 414 s. *Gd(5,7ClQ)$_3$(H$_2$O)$_2$*. 3074 w, 2928 w (νCH, CH$_3$CN), 1594 w, 1557 s, 1489 s, 1449 vs, 1394 m, 1375 s, 1361 m, 1285 w, 1246 mw, 1231 mw, 1193 w, 1140 w, 1109 m, 1051 w (δC–H), 1028 vw, 957 m (νC–Cl), 882 m (νC–Cl), 809 mw, 789 mw, 752 s, 672 m, 646 mw, 586 w, 502 vw. *Gd(5,7BrQ)$_3$(H$_2$O)$_2$*. 3071 w, 1551 s, 1483 s, 1449 vs, 1392 s, 1371 s, 1271 w, 1246 mw, 1213 mw, 1204 w, 1138 mw, 1107 m, 1047 mw (δC–H), 935 m (νC–Br), 858 m (νC–Br), 809 m, 787 m, 743 s, 685 m, 669 m, 653 w, 637 mw; 621 vw, 594 w, 567 m, 499 vw, 421 mw, 414 s. *Yb(5,7ClQ)$_3$(H$_2$O)$_2$*. 3074 w, 2928 w (νC–H, CH$_3$CN), 1594 w, 1560 s, 1491 s, 1452 vs, 1396 m, 1376 s, 1286 w, 1251 mw, 1234 mw, 1196 w, 1141 w, 1112 m, 1053 w (δC–H), 1028 vw, 961 m (νC–Cl), 884 m (νC–Cl), 809 mw, 788 mw, 751 s, 672 m, 649 mw, 586 w, 507 vw, 418 mw. *Yb(5,7BrQ)$_3$(H$_2$O)$_2$*. 3071 w, 1554 s, 1485 s, 1453 vs, 1391 s, 1372 s, 1274 w, 1248 mw, 1217 mw, 1202 w, 1138 mw, 1108 m, 1050 mw (δC-H), 938 m (νC–Br), 860 m (νC–Br), 809 m, 786 m, 744 s, 686 m, 667 m, 654 w, 641 mw; 625 vw, 595 w, 568 m, 503 vw, 421 mw, 414 s, 394 s, 361 m, 346 m, 243 s, 206 m, 164 m, 146 m, 115 w.

[Gd(5,7ClQ)$_2$(H5,7ClQ)$_2$Cl]: 0.202 g (0.543 mmol) of 5,7-dichloro-8-quinolinol were dissolved in 100 mL of CH$_3$CN/CH$_3$OH (4:1 v/v) at 50-60°C. A slight excess of GdCl$_3$·6H$_2$O, (0.197 g, 1.625 mmol), dissolved in 10 mL of the same solvent mixture, was slowly added to the ligand solution and the reaction mixture turned suddenly

yellow. After 24 hours the solution was roto-evaporated until it turned orange and left standing to the air. After few days red crystals, suitable for X-ray studies, were collected and washed with diethyl ether (yield 45%). **CHN**: Found (Calcd for $C_{36}H_{18}Cl_9GdN_4O_4$) C% 41.37(41.30), H% 1.70(1.73), N% 5.18(5.35). **FT-IR spectrum** (cm^{-1}): 3236 vw, 3171 vw, 3102 w, 3026 w, 2966 w, 2914 w, 2850 vw, 2752 vw, 2110 w(νN^+–H), 2013 w, 1616 m, 1592 w, 1558 s, 1541 m, 1489 m, 1452 vs, 1393 m, 1373 s, 1310 m, 1292 w, 1250 w, 1232 mw, 1219 m, 1192 m, 1144 m, 1111 m (split peak), 1051 mw (δC–H), 991 vw, 957 m (νC–Cl), 876 m (νC–Cl), 809 m, 789 m, 747 s (split peak), 672 m, 658 m, 645 w, 634 m, 585 w, 572 mw, 503 m, 417 mw. **FT-Raman spectrum** (cm^{-1}): 3068 s, 2887 m, 1592 s, 1574 s, 1552 m, 1469 m, 1360 vs, 1291 mw, 1145 m, 1051 m (δC–H), 761 m, 727 m, 500 m, 404 m, 357 m, 203 m, 168 m, 142 m. **UV-Vis spectrum** (nm; [mol^{-1} dm^3 cm^{-1}]): 340[(10.07±0.03)10^3], 395[(7.01±0.02)10^3. **DR spectrum** (nm): 272, 358sh, 410, 480sh, 1667 (2νC-H).

[Yb(5,7ClQ)$_2$(H5,7ClQ)$_2$Cl]: The synthesis was carried out following the procedure described for the analogous Er, Gd *tetrakis* complexes with H5,7ClQ. $YbCl_3 \cdot 6H_2O$ dissolved in 10 mL of of CH_3CN/CH_3OH (4:1 v/v.) was slowly added to a solution of 5,7-dichloro-8-quinolinol (1:4 ratio) in the same solvent mixture. After several days, red crystals, suitable for X-ray studies, were collected and washed with diethyl ether (yield 53%). **CHN**: Found (Calcd for $C_{36}H_{18}Cl_9YbN_4O_4$) C% 40.95(40.69), H% 1.63(1.71), N% 5.43(5.27). **FT-IR spectrum** (cm^{-1}): 3236 vw, 3171 vw, 3102 w, 3026 w, 2966 w, 2914 w, 2850 vw, 2752 vw, 2116 w(νN^+–H), 2013 w, 1616 m, 1592 w, 1560 s, 1544 m, 1489 m, 1455 vs, 1394 m, 1364 s, 1314 m, 1292 w, 1250 w, 1232 mw, 1220 m, 1194 m, 1144 m, 1106 m (split peak), 1051 mw (δC–H), 991 vw, 957 m (νC–Cl), 876 m (νC–Cl), 810 m, 789 m, 749 s (split peak), 672 m, 659 m, 646 w, 634 m, 585 w, 571 mw, 505 m, 422 mw. **FT-Raman spectrum** (cm^{-1}): 3106 m, 3068 s, 2887 m, 1591 s, 1572 s, 1561 m, 1470 m, 1360 vs, 1294 mw, 1145 m, 1051 m (δC–H), 799 m, 763 m, 668 m, 570 m, 504 m, 407 w. **UV-Vis spectrum** (nm; [mol^{-1} dm^3

cm^{-1}]): 340[(8.63±0.03)10^3], 394[(6.55±0.02)10^3. **DR spectrum** (nm): 268, 351sh, 405, 480sh; 928, 952, 979 (split, $^2F_{7/2} \rightarrow {}^2F_{5/2}$);[10] 1667 (2νC–H).

[Yb(5,7BrQ)$_2$(H5,7BrQ)$_2$Cl]·CH$_3$CN: The synthesis was carried out following the procedure described for the analogous Er *tetrakis* complex with H5,7BrQ. $YbCl_3 \cdot 6H_2O$ dissolved in 10 mL of of CH_3CN/CH_3OH (4:1 v/v.) was slowly added to a solution of 5,7-dibromo-8-quinolinol (1:4 ratio) in the same solvent mixture. After several days, red crystals, suitable for X-ray studies, were collected and washed with diethyl ether (yield 38%). **CHN**: Found (Calcd for $C_{38}H_{21}Br_8ClYbN_5O_4$) C% 30.54(30.49), H% 1.13(1.28), N% 4.02(3.95). **FT-IR spectrum** (cm^{-1}): 3221 vw, 3143 vw, 3064 w, 2989 vw (νC–H, CH_3CN), 2928 vw, 2868 w, 2817 vw, 2734 vw, 2250 vw (νC–N, CH_3CN), 2094 w(νN$^+$-H), 1615 m, 1590 m, 1553 vs, 1484 s, 1452 vs, 1388 s, 1370 vs, 1310 m, 1300 mw, 1247 mw, 1208 mw, 1193 mw, 1141 m, 1106 m, 1048 m (δC–H), 1005 vw, 986 vw, 936 m (νC–Br), 909 vw, 876 m, 853 m (νC–Br), 808 m, 787 m, 768 w, 740 s, 687 s, 668 m, 653 m, 638 mw, 624 m, 595 vw, 568 m, 502 m, 411 mw. **UV-Vis spectrum** (nm; [mol^{-1} dm^3 cm^{-1}]): 341[(12.6±0.1)10^3], 394[(8.59±0.09)10^3. **DR spectrum** (nm): 271, 350, 406; 480sh; 928, 952, 979 ($^2F_{7/2} \rightarrow {}^2F_{5/2}$);[10] 1669 (2νC–H).

3.6.2 Measurements

CHN analysis:

Data were collected with a Carlo Erba mod.EA1108 CHNS analyzer.

Spectroscopy and spectrometry

UV-Vis-NIR. Diffuse reflectance (DR) and absorption spectra in CH_3OH solution (10^{-4} mol/L) were collected with a Varian Cary 5 spectrophotometer. Crystalline samples for DR spectra were dispersed on a Teflon film. ***IR.*** FT-IR spectra on KBr pellets were collected with a Bruker Equinox 55 spectrophotometer. ***RAMAN.*** FT-Raman spectra of crystalline samples were collected with a Bruker RFS/100S spectrometer operating in a back-scattering geometry with a Nd:YAG (1064 nm) laser source. **ESI-Mass.** Mass spectra were obtained with a Micromass ZMD spectrometer operating in *positive ionization* mode.

Data Collection and Structure Determination

$Er_3Q_9 \cdot CH_3CN$ (**1**). Data collection was performed on a Bruker AXS Smart 1000 area detector diffractometer (Mo Kα, λ = 0.71073 Å). Structure solution was by direct methods and refined on F^2. Crystal data follow: formula $C_{83}H_{57}Er_3N_{10}O_9$, crystal size 0.15×0.10×0.10 mm^3, triclinic $P\bar{1}$, a = 12.352(1) Å, b = 16.775(1) Å, c = 18.199(1) Å, α = 83.488(1)°, β = 79.302(1)°, γ = 83.831(1)°, V = 3667.0(4) Å^3, Z = 2, F(000) = 1802, μ(Mo Kα) = 3.468 mm^{-1}. Least-squares refinement based on 8675 reflections with $I > 2\sigma(I)$ gave final R = 0.0390 and R_w = 0.0487. Acetonitrile solvent molecules were severely disordered and were treated using the SQUEEZE PLATON program.

2, **4**, **5**, **[Gd(5,7ClQ)$_2$(H5,7ClQ)$_2$Cl]**, **[Yb(5,7ClQ)$_2$(H5,7ClQ)$_2$Cl]**. Single crystal data were collected with a *Bruker AXS Smart 1000* area detector diffractometer (Mo Kα, λ = 0.71073 Å) and with a Philips PW 1100 diffractometer (Mo Kα, λ = 0.71073 Å) for **5**. Cell constants were obtained from a least-square refinement of selected

strong reflections distributed over a hemisphere of the reciprocal space[58] and by a least-square refinement of the setting angles of 24 randomly distributed and carefully centered reflections ($6.14 < 2\theta < 16.00$) for **5**. No crystal decay was observed for all the compounds. Absorption correction using the program SADABS[59] was applied for all the compounds except **5** (min. and max. transmission factors: 0.822-1.000 for **2**, 0.735 and 1.000 for **4**, 0.722 and 1.000 for $[Gd(5,7ClQ)_2(H5,7ClQ)_2Cl]$). An absorption correction using the method of Walker & Stuart[60] was applied for **5** giving transmission factors of 0.873-1.000. The structures were solved by direct methods (SIR97)[61] and refined with full-matrix least squares (SHELXL-97),[62] using the Wingx software package.[63] All non-hydrogen atoms were refined anisotropically. The H atoms were placed at their calculated positions. The twin law 100, 010, 00–1 was applied for the refinement of **4**. In the crystal structure of 2, acetonitrile and water were found disordered with site occupancy factor of 0.5 and 1.5, respectively. The maximum and minimum peaks of the final difference Fourier maps corresponded to 0.986 and –0.352(2), 2.873 and –2.205(4) and 1.228 and –1.217 (5) $eÅ^{-3}$. Graphical material was prepared with the ORTEP3 for Windows program.[64] §

§ ESI-Mass spectra and crystal structure determinations were performed by Dr. Luciano Marchiò, University of Parma, Italy.

References

[1] R.J. Curry, W.P. Gillin, *Appl. Phys. Lett.* **1999,** *75,* 1380.

[2] W.P. Gillin, R.J. Curry, *Appl. Phys. Lett.* **1999**, *74,* 798.

[3] R. J. Curry, W. P. Gillin, *Synth. Met.* **2000**, *111–112*, 35.

[4] R.J. Curry, W.P. Gillin, A.P. Knights, R. Gwilliam, *Opt. Mater.* **2001**, *17*, 161.

[5] J. Thompson, R.I.R. Blyth, G. Gigli, R. Cingolani, *Adv. Funct. Mater.* **2004**, *14*, 979.

[6] S. Penna, A. Reale, R. Pizzoferrato, G. M. Tosi Beleffi, D. Musella, W. P. Gillin, *Appl. Phys. Lett.* **2007**, *91*, 021106.

[7] S. W. Magennis, A. J. Ferguson, T. Bryden, T. S. Jones, A.Beeby, I. D. W. Samuel, *Synth. Met.* **2003**, *138*, 463.

[8] O.M. Khreis, R.J. Curry, M. Somerton, W.P. Gillin, *J. Appl. Phys.* **2000**, *88*, 777;

[9] Y. Kawamura, Y. Wada, Y. Hasegawa, M. Iwamuro, T. Kitamura, S. Yanagida, *Appl. Phys. Lett.* **1999**, *74*, 3245,

[10] O. Khreis, W. Gillin, M. Summerton, R. Curry, *Org. Electron.* **2001**, *2*, 45.

[11] R. I. R. Blyth, J. Thompson, Y. Zou, R. Fink, E. Umbach, G. Gigli, R. Cingolani, *Synth. Met.* **2003**, *139*, 207.

[12] W.W. Wendlandnt, *Anal. Chim. Acta* **1956**, *15*, 109.

[13] W.W. Wendlandnt, *Anal. Chim. Acta* **1957**, *17*, 428.

[14] H. F. Aly, F. M. Abdel Kerim, A. T. Kandil, *J. Inorg. Nucl. Chem.* **1971**, *33*, 4340.

[15] D. Czakis-Sulikowska, N. Pustelnik, A. Malinowska, B. Kuźnik, *Chem. Anal.* (Warsaw) **1997**, *42*, 23, D. Czakis-Sulikowska, N. Pustelnik, B. Kuźnik, A. Malinowska, *J. All. Compd.* **2000**, *300-301*, 234-235 and references therein.

[16] M. Iwamuro, T. Adachi, Y. Wada, T. Kitamura, S. Yanagida, *Chem. Lett.* **1999**, 539.

[17] M. Iwamuro, T. Adachi, Y. Wada, T. Kitamura, N. Nakashima, S. Yanagida, *Bull. Chem. Soc. Jpn.* **2000**, *73*, 1359-1363.

[18] R. Van Deun, P. Fias, K. Driesen, K. Binnemans, C. Görller-Walrand, *Phys. Chem. Chem. Phys.* **2003**, *5*, 2754.

[19] T. Pirtea, *Z. Anal. Chem.* **1936**, *107*, 191.

[20] R. Berg, *Z. Anal. Chem.* **1927,** 70, 341.

[21] O. Tochiyama, H. Frieser, *Anal. Chem.* **1981**, *53*, 874.

[22] T. Moeller, D. Jackson, *Anal. Chem.* **1950**, 22, 1393.

[23] R. Van Deun, P. Fias, P. Nockemann, A. Schepers, T. N. Parac-Vogt, K. Van Hecke, L. Van Meervelt, K. Binnemans, *Inorg. Chem.* **2004,** *43*, 8461.

[24] F.Artizzu *"Complessi di erbio chinolinolati come materiali luminescenti per applicazioni in fotonica"*, Master Degree thesis, University of Cagliari, **2004**.

[25] F. Artizzu, P. Deplano, L. Marchiò, M. L. Mercuri, L. Pilia, A. Serpe, F. Quochi, R. Orrù, F. Cordella, F. Meinardi, R. Tubino, A. Mura, G. Bongiovanni, *Inorg. Chem.* **2005,** *44* , 840-842.

[26] F. Artizzu, P. Deplano, L. Marchiò, M. L. Mercuri, L. Pilia, A. Serpe, F. Quochi, R. Orrù, F. Cordella, M. Saba, A. Mura, G. Bongiovanni, *Adv. Funct. Mater.* **2007,** *17*, 2365-2376.

[27] H. Gershon, M. W. McNeil, S. G. Shulman, J. W. Parkes, *Anal. Chim. Acta*, **1972**, *62*, 43-47; R. E. Ballard, J. W. Edwards, *J. Chem. Soc.* **1964**, 4868-4874.

[28] F. Goldman, E. L. Wehry, *Anal. Chem.* **1970**, *42*, 1178.

[29] D. D. Perrin, *IUPAC Chemical Data Series, Stability Constant of Metal – Ion Complexes, Part B, Organic Ligands,* **1983**, *22*, 649-685.

[30] T. Moeller, N. Fogel, *J. Am. Chem. Soc.*, **1951**, *73*, 4481.

[31] S. G. Leary, G. B. Deacon, P. C. Junk, *Z. Anorg. Allg. Chem.* **2005**, *631*, 2647.

[32] R. Ballardini, G. Varani, M. T. Indelli, F. Scandola, *Inorg. Chem.***1986**, *25*, 3858.

[33] C. H. Chen, J. Shi, *Coord. Chem. Rev.* **1998**, *171*, 161.

[34] C. Mealli, D. Proserpio, *J. Chem. Ed.* **1990**, *67*, 39.

[35] M. Brinkmann, G. Gadret, M. Muccini, C. Taliani, N. Masciocchi, A. Sironi, *J. Am. Chem. Soc.* **2000**, *122,* 5147.

[36] M. Brinkmann, B. Fite, S. Pratontep, C. Chaumont, *Chem. Mater.* **2004**, *16*, 4627-4633.

[37] H. Kaji, Y. Kusaka, G. Onoyama, F. Horii, *J. Am. Chem. Soc.* **2006**, *128*, 4292.

[38] K. Kuriki, Y. Koike, Y. Okamoto, *Chem. Rev.* **2002**, 102, 2347.

[39] L.H. Slooff, A. Van Blaaderen, A. Polman, G. A. Hebbink, S. I. Klink, F. C. J. M. Van Veggel, D. N. Reinhoudt, J. W. Hofstraat, *Appl. Phys. Lett.* **2002**, *91*, 7, 3955.

[40] S. A. Davis, F. S. Richardson, *Inorg. Chem.* **1984**, *23*, 184.

[41] R. D. Rogers, L. K. Kurihara, *Lanthanide and Actinide Research* **1986**, 296.

[42] J. Kido, Y.Okamoto*, Chem. Rev.* **2002**, *102*, 2357.

[43] J.-C.G. Bunzli, *Electronic Levels and Spectroscopy of 4f Elements*, Lecture, Summer School 2005 on *"Advanced Luminescent Materials Based on Lanthanide Organic/Inorganic Complexes"*, Krutyn, Poland, 2005.

[44] A. A. Shabaka, M. Fadly, M.A. El Ghandoor, F. M. Abdel Kerim, *J. Mater. Sci.* **1990**, *25*, 2193.

[45] A. T. Rane, V. V. Ravi, *Spectrochim. Acta* **1982**, *38A*, *8*, 937.

[46] B. Marchon, L. Bokobza, G. Cote, *Spectrochim. Acta* **1986**, *42A*, *4*, 537.

[47] M. D. Halls, R. Aroca, *Can. J. Chem.* **1998**, *76*, 1726.

[48] G. A. Crosby, R. E. Whan, R. M. Alire, *J. Chem. Phys.* **1961**, *34*, 743.

[49] M. L. Bhaumik, M. A. El-Sayed, *J. Phys. Chem.* **1965**, *69*, 275.

[50] P. Caravan, J. J. Ellison, T. J. McMurry, R. B. Lauffer, *Chem. Rev.* **1999,** *99,* 2293-2352 and references therein.

[51] O. Kahn, *Molecular Magnetism*, VCH : Weinhem, **1993**.

[52] V.W.-W. Yam, K.K.-W. Lo, *Coord. Chem. Rev.* **1999**, *184*, 157–240.

[53] E. Silina, Yu. Bankovsky, V. Belsky, J. Lejejs, L. Pech, *Latvijas Kimijas Zurnals* **1997**, *4*, 89.

[54] R. H. Byrne, B. Li, *Geochim. Cosmochim. Acta* **1995**, *22*, 4575-4589.

[55] J.-C.G. Bunzli, C. Piguet *Chem. Soc. Rev.* **2005** *34*, 1048-1077.

[56] Y. Li, H. Yang, Z. He, L. Liu, W. Wang, F. Li, L. Xu, *J. Mater. Res.* **2005**, *20,* 2940.

[57] E. M. Stephens, K. Schoene, F. S. Richardson, *Inorg. Chem.* **1984**, *23*, 1641-1648.

[58] SMART (control) and SAINT (integration) software for CCD systems, Bruker AXS, Madison, WI, USA, **1994**.

[59] Area-Detector Absorption Correction, Siemens Industrial Automation, Inc.: Madison, WI, **1996**.

[60] N. Walker, D. Stuart, *Acta Cryst.* **1983**, *A39*, 158.

[61] A. Altomare, M. C. Burla, M. Camalli, G. L. Cascarano, C. Giacovazzo, A. Guagliardi, A. G. G. Moliterni, G. Polidori, R. Spagna, *J. Appl. Cryst.* **1999**. *32,* 115.

[62] G.M. Sheldrick, SHELX97. Programs for Crystal Structure Analysis **1997**, (Release 97-2). University of Göttingen, Germany.

[63] L. J. Farrugia, *J. Appl. Cryst.* **1999**, *32*, 837.

[64] L. J. Farrugia, *J. Appl. Crystallogr.* **1997**, *30*, 565.

Chapter 4

Photoluminescence Studies on Erbium Quinolinolates

The excited-state dynamics and light emission properties of Er-complexes are discussed. Experimental evidence confirms that the most important quenchers for the erbium emission are the coordinated water molecules and shows that the ligand emission is significantly affected by the π-π interactions.

*Photophysical studies have been carried out in cooperation with the Prof. Bongiovanni's group, Physics Department, University of Cagliari, which have also performed all the photoluminescence measurements.

4.1 Introduction

A simplified energy level scheme of the luminescent organo-erbium complexes is reported in Figure 4.1. As explained in detail in Chapter 2, the lanthanide emission is sensitised by energy transfer from the coordinated antenna ligand.[1-3] After optical excitation, ligand singlet states S_1 can either decay to the ground state S_0, or to triplet states T_1. These latter excitations can subsequently transfer to the metal. Following a fast excited-state ion relaxation, the radiative decay $^4I_{13/2} \rightarrow {}^4I_{15/2}$ yields the NIR emission of Er(III) at 1.54 μm.

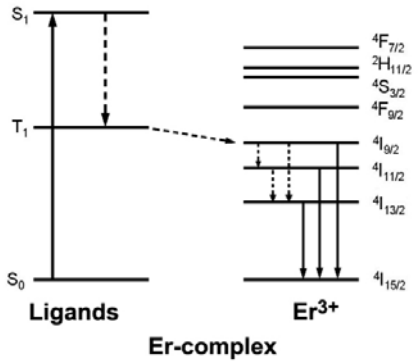

Figure 4.1: *Jablonski diagram depicting excited-state relaxation and NIR emission in Er-complexes. The singlet states S_1 are excited through the absorption of one photon. Downward arrows show relaxation channels, including radiative (continuous lines) and nonradiative (dashed lines) decay pathways. The long-dashed arrow indicates energy transfer from the ligand to the Er-ion.*

It is well known that quinolinol ligands show good photosensitizing properties toward the NIR emissive lanthanide ions, since they possess triplet state energies (around 17100 cm^{-1}) which overlap well with the accepting energy levels of the 4f orbitals ($^4F_{9/2}$, $^4I_{9/2}$ for Er^{3+}; $^4G_{5/2}$, $^2G_{7/2}$ for Nd^{3+}).[4-6]

4.2 Photoluminescence

4.2.1 Visible luminescence

Figure 4.2 shows the luminescence spectra in the visible spectral region of **1**, **2**, **4** and of AlQ_3 excited at 390 nm. Emission bands are assigned to the $S_1 \rightarrow S_0$ transitions of the ligand. The spectra of the *trinuclear* species **1**, and of the *tetrakis* complex **4** in solution are similar, featuring an unstructured band peaked at 520 nm. The large Stokes-shift from the absorption maximum at 370-400 nm arises from the fast geometrical relaxation following excitation of the S_1 state.[7]

The luminescence spectrum in the solid state of the *tetrakis* complex **5** is very similar to that of **4** shown in Figure 4.2. In crystals with *tetrakis* molecular arrangement, the emission is significantly shifted to longer (~100 nm) wavelength (λ_{max} = 620 nm) with respect to the emission of the same complex in DMSO solution or to that of *tris* complexes with the same ligand, both in the solid state and solution. The influence of the isomeric states and

of the crystal packing on the fluorescence wavelengths of AlQ_3 and GaQ_3 compounds has been also investigated.[9-11] It has therefore been observed that the maximum of fluorescence is red-shifted with increasing density of the crystal packing (i.e. length of interligand contacts between neighbouring molecules) or the overlap between adjacent quinoline moieties. This is in agreement with our findings, given that the *tetrakis* complexes show extensive π-stacking in the crystal packing (see Chapter 3, Paragraph 3.3.2). Also, these peculiar π-π intermolecular interactions of the *tetrakis* crystal structure, may account for the additional broad band in the visible region, observed in the diffuse reflectance (DR) spectra.[8]

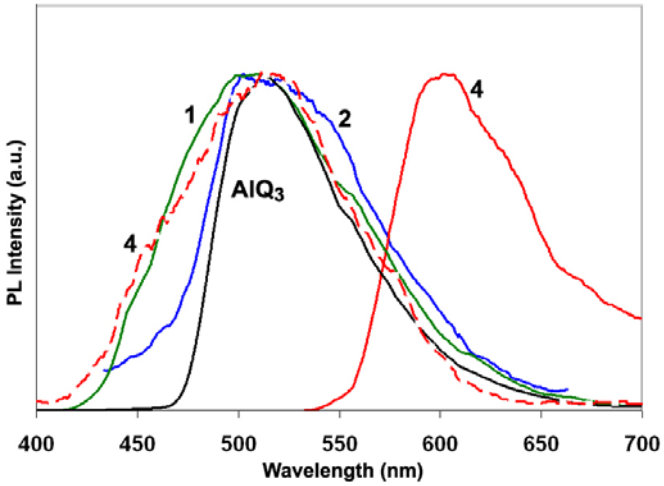

Figure 4.2: Photoluminescence spectra of the *trinuclear* complex **1** (green line), *tris* complex **2** (blue line) and of the *tetrakis* complex **4** in the solid state (solid red line) and in DMSO solution (dashed red line) compared to that of AlQ_3 (black line).

Visible emission is detected by a 2D-streak-camera with a rise-time of 10 ps.

Figure 4.3 shows that the intensity of the singlet luminescence of the quinoline ligands in Er-complexes decays with characteristic times ranging from 10 to 40 ps both in crystals and in solution. This fast radiative relaxation should be compared with that observed in complexes with lighter ions, as AlQ_3, which are characterised by a nanosecond decay time. The short singlet lifetime in erbium complexes is thus ascribed to the very efficient spin-triplet conversion due to the presence of the lanthanide ion, which enhances the spin-orbit coupling (heavy-atom effect). At later delays, the excitation energy of triplet states in the ligand can transfer to the erbium ion.

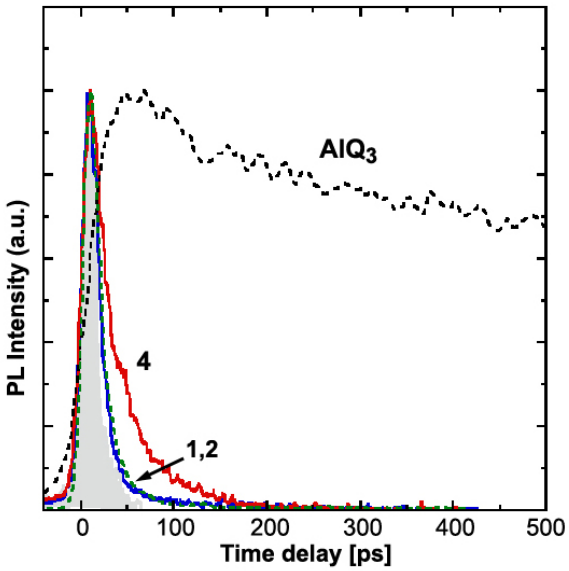

Figure 4.3: *Spectral integrated vis-photoluminescence decay traces of trinuclear complex* **1** (dotted green line), *tris-complexes* **2** (blue line) and AlQ_3 (dotted black line), *tetrakis* complex **4** (red line). The shaded gray curve represents the temporal response of the streak camera to fs-pulses.

4.2.2 NIR luminescence

Representative photoluminescence (PL) spectra in the NIR of **1**, **4**, **5** and **3** are depicted in Figures 4.4, 4.5a,b and 4.6, respectively. The peaks in the 1.4-1.5 μm range are typical of Er^{3+} radiative decay from the first excited state $^4I_{13/2}$ to the fundamental state $^4I_{15/2}$ manifold. The spontaneous emission reveals the same Stark-split transitions (due to the local Crystal Field affecting the erbium ions) reported in the DR optical response. The relative line intensities differ slightly: the lower energy transitions of the photoluminescence spectra are more intense due to efficient electron thermalisation, which favours the occupation of the lower energy states of the $^4I_{13/2}$ manifold.

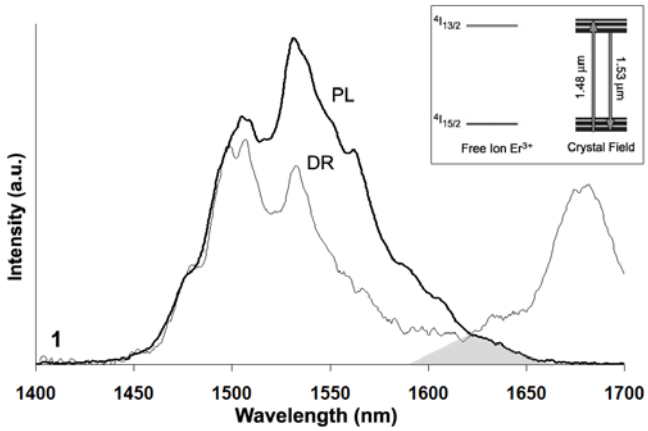

Figure 4.4: *Continuous wave (CW) photoluminescence (PL, thick line) and diffuse reflectance (DR, thin line) spectra of Er_3O_9 (**1**) in the 1400-1700 nm region. The shaded grey area represents the overlap between the emission spectrum of Er^{III} and the absorption spectrum of the oscillating C-H groups. In the insert a scheme of the energy levels of Er^{III} in a local Crystal Field, is shown.*

The full width at half maximum of the PL spectra of all the studied compounds exceeds 80 nm, one of largest values ever observed in this class of complexes. The wideness of these spectra could, in principle, allow to obtain high gain bandwidth for optical amplification in laser systems.

In addition to Crystal Field effects, room temperature lattice vibrations which interact with the emitting ion are also responsible for the broadening of the lanthanide emission lines (*vibrational coupling*). In the *trinuclear* Er_3Q_9 complex, an additional contribution to spectral breadth is given by the simultaneous vibrations of neighbouring lanthanide ions, which act as oscillating dipoles and produce a transient Crystal Field around each ion. This effect is different for the central erbium ion with respect to the outer ones, reflecting the unequivalence of the coordination configurations and therefore leading to line broadening. Hence, the existence of two distinct coordination sites in the molecule may result, in principle, in a slight difference in the emission wavelengths of the central erbium ion with respect to the external ones which therefore may be distinguishable.

The shaded grey areas in Figures 4.4 and 4.6 represent the spectral overlap (*resonance condition*) between the emission spectrum of the donor, the emitting Er^{III} acting as oscillating dipole, and the absorption spectrum of the acceptor (aromatic C–H groups or water molecules) which interacts with this oscillating field and is therefore responsible for the quenching effects (see Chapter 2, Paragraph 2.3). From these spectra it is possible to retrieve the experimental data useful to assess the entity of the Förster's non-radiative decay in this class of NIR-emitting molecules.[12,13]

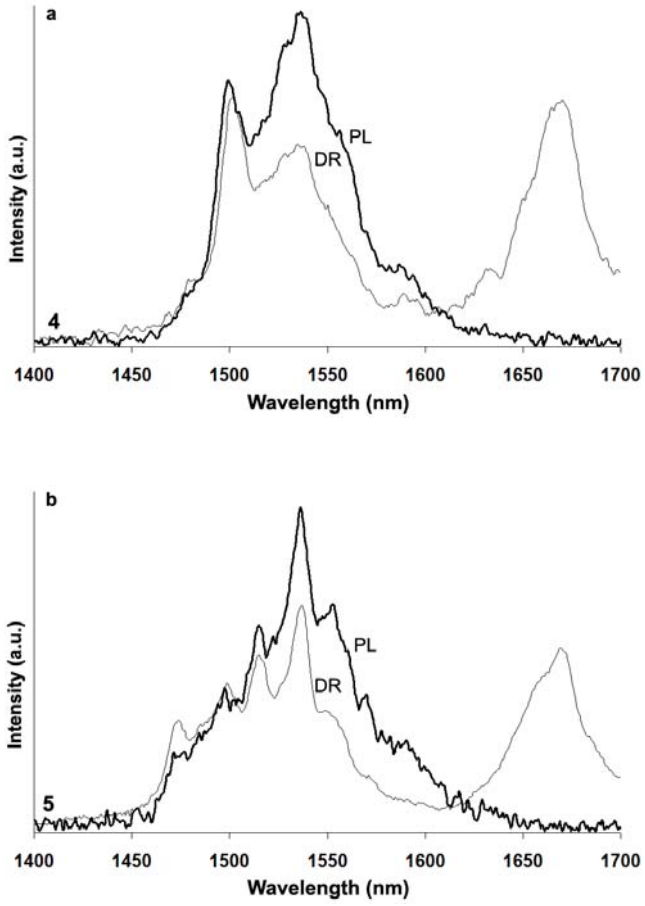

Figure 4.5: *Continuous wave (CW) photoluminescence (PL, thick line) and diffuse reflectance (DR, thin line) spectra of* **4** *and* **5** *in the 1400-1700 nm region.*

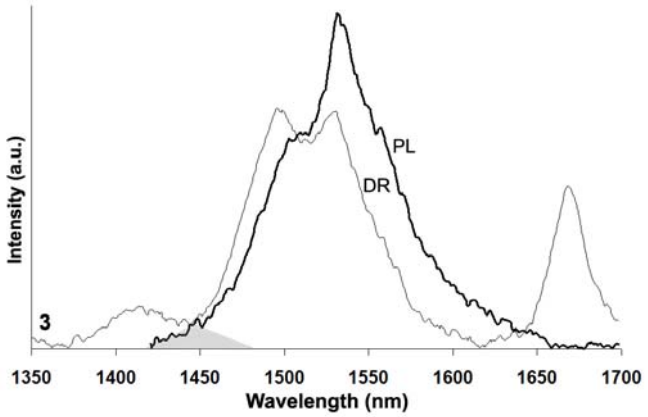

Figure 4.6: *Continuous wave (CW) photoluminescence (PL, thick line) and diffuse reflectance (DR, thin line) spectra of* $[Er(5,7BrQ)_3(H_2O)_2]$ (**3**) *in the 1400-1700 nm region. The shaded grey area represents the overlap between the emission spectrum of* Er^{III} *and the absorption spectrum of the coordinated water molecules (1420 nm, combination band symmetrical-antisymmetrical stretchings HOH,* $\nu_1+\nu_3$*).*

Excited-state relaxation dynamics has been investigated by looking at the time evolution of the luminescence of the ligand and the phosphorescence of the Er^{III} ions. Complexes are excited by 200-fs-long-pulses at 390 nm. Spectrally integrated NIR emission has been selected by low energy band-pass filters and detected by an amplified photodiode with 2 ns resolution. The energy transfer process from the ligand triplet state is monitored by studying the build up of the NIR emission from the lanthanide ion. Experimental results are reported in Figures 4.7a,b, and 4.8a,b. The signal risetime is limited by the time resolution of the experimental apparatus,

which fixes an upper limit of ~2 ns to the energy transfer time to the lanthanide ion. Since the characteristic triplet lifetime of the ligand is much longer, these data indicate that most of the triplet population is transferred to the metal.

The erbium emission dynamics for Er_3Q_9 (**1**), following ultrafast photoexcitation of the quinolinolate ligands, is shown in Figures 4.7a,b. The emission build-up occurs in the time scale of a few nanoseconds. Although there are two unequivalent coordination sites in the *trinuclear* complex, nearly single-component decay is observed within the available dynamic range. This nearly single-exponential behaviour can be explained considering that Er-Er energy migration within an Er_3Q_9 molecule occurs in the 10-ns time scale according to Förster's theory,[12-13] much faster than the Er non-radiative decay time; as a result, Er excitations are effectively delocalised over the three metal ions and experience only a coordination configuration average.

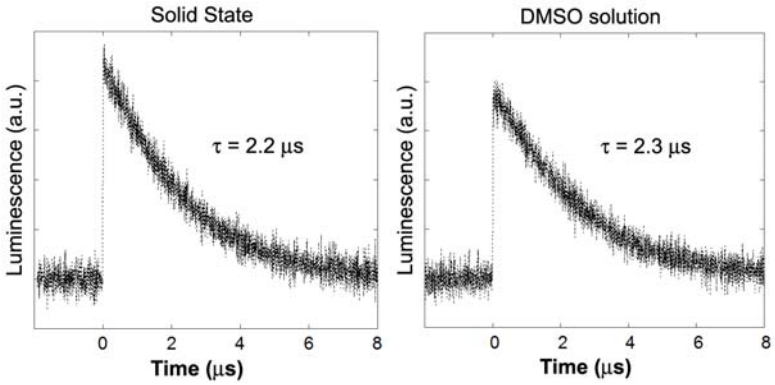

Figures 4.7: *Photoluminescence exponential decay for* **1** *in the solid state (left) and in DMSO solution (right).*

Er intrinsic deactivation occurs with a time constant of 2.2 μs, at least 3 orders of magnitude faster than the natural radiative lifetime of this emission (14 ms), in agreement with previous reports.[14-15] The combined structural and spectroscopic results allow to ascribe the erbium luminescence quenching in water-free Er_3Q_9 uniquely to the aromatic C–H vibrations of the ligand. This effect shortens the erbium population lifetime from milliseconds to microseconds.

Moreover, measurements made in non-deuterated DMSO degassed solutions of Er_3Q_9 ($1.0 \cdot 10^{-3}$ M) show very similar results with nearly the same PL lifetime. This suggests that the Q ligands, which saturate the erbium coordination sphere, effectively shield the central ion from the environment thus preventing further coordination to solvent molecules.

NIR-photoluminescence decay curves for **2**, **3**, **4** and **5** are reported in Figures 4.8a,b. The transient phosphorescence signal reveals a fast peak-response at time equal to zero, followed by a slower decay. A spectral analysis shows that the former signal arises from the radiative decay at 980 nm from the $^4I_{11/2}$ level, which is transiently populated during energy relaxation. The slower signal stems from the radiative decay at 1540 nm of the $^4I_{13/2}$ state.

The luminescence lifetimes for the erbium quinolinolates studied in this work are reported in Table 4.1.

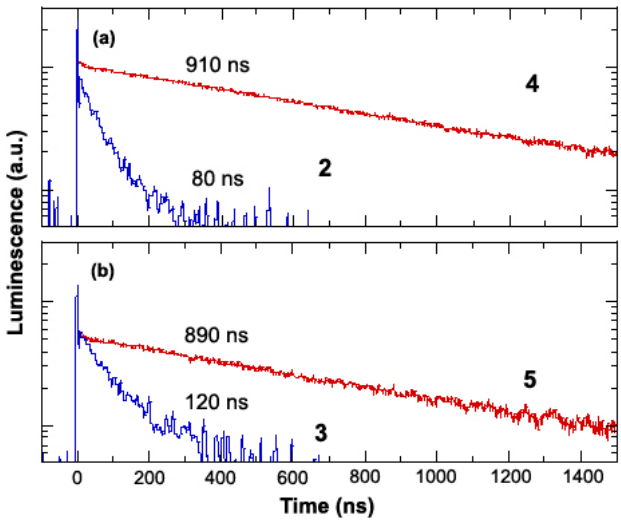

Figures 4.8: *NIR-photoluminescence decay traces of* **4** *and* **2** (**a**), **5** *and* **3** (**b**) *crystals. The peak at time equal to zero arises from the radiative decay at 980 nm of the* $^4I_{11/2}$ *state, which is transiently populated during energy relaxation in the lanthanide ion. Such peak is not visible in the traces of* **4** *and* **5,** *for which the detection bandwidth was reduced from 1GHz to 20MHz. The slower signal stems from the radiative decay at 1540 nm of the* $^4I_{13/2}$ *state.*

Complex	τ (solid state)
Er_3Q_9 (1)	2.2 μs
$Er(5,7ClQ)_2(H_2O)_2$ (2)	~ 0.1 μs
$Er(5,7BrQ)_2(H_2O)_2$ (3)	~ 0.1 μs
$[Er(5,7ClQ)_2(H5,7ClQ)_2Cl]$ (4)	~ 1 μs
$Er(5,7BrQ)_2(H5,7BrQ)_2Cl]$ (5)	~ 1 μs

Table 4.1: *Decay constants for 1.5 μm emission of erbium quinolinolates.*

The analysis of the time-resolved photoluminescence signal supports the conclusion that the two-step process $S_1 \rightarrow T_1 \rightarrow Er^{III}$ is the dominant excited-state relaxation pathway of the lanthanide complexes. The low quantum yield of the NIR emission is primarily caused by the non-radiative decay of the ion excitation. Both CH groups and water are responsible for the NIR emission quenching. Water molecules in the first coordination sphere of the Ln^{III}-ion lead to a much faster nonradiative decay rate as illustrated in Figure 4.8, where the emission decay is reported for complexes with (**2** and **3**) and without (**4** and **5**) water molecules. In water-free compounds, the nonradiative lifetime falls in the μs time-scale, in agreement with literature data.[6,16-18] In hydrated complexes, interaction with the vibrations of water shortens the excited-state lifetime down to ~80-120 ns.

4.3 Quenching effects: Förster's model

The experimental decay time (~2.3 μs) of Er_3Q_9 is consistent with the transfer time (~2.8 μs) from the Er ions to the aromatic C–H groups of the ligand calculated in the framework of the Förster's resonance energy transfer (RET) theory[12,13] applied to the trinuclear molecular structure.[18]

Experimental data obtained from the combined structural/spectroscopic investigation on Er_3Q_9 allows to calculate the non-radiative decay constant k_{nr}, describing the rate of the Förster's vibrational deactivation of lanthanide luminescence through oscillating C–H groups at a distance **r** from the emitting ion, through the following equation (See also Chapter 2, Eq. 4 and 5).[18]

$$k_{nr}(r) = k_r \sum_j \left(\frac{R_j}{r_j}\right)^6 ; R_j^6 = \left(\frac{9\kappa^2}{128\pi^5 n^4}\right) \int F_D(\lambda)\sigma_A(\lambda)\lambda^4 d\lambda; \qquad \text{Eq. 8}^{\clubsuit}$$

This equation depends on two spectroscopic quantities: the radiative NIR-emission rate constant k_r and the overlap integral between the emission spectrum of the donor (the 1.5 μm band of Er^{III}) and the absorption spectrum of the acceptor (the 2nd vibrational harmonic of the oscillating C–H dipoles near 1670 nm). In a simplified model, the latter can be replaced by $\lambda^4 \cdot \langle \alpha_A \rangle_{Er}$, where $\langle \alpha_A \rangle_{Er}$ represents the absorption of the vibrating C–H groups averaged over the erbium emission spectral window, peaked at λ_{em} = 1530

♣ R is the Förster's distance (see Chapter 2); n is the refractive index of the medium. The value n = 1.479 was taken for crystalline samples.

nm (see Figure 4.4). $\langle \alpha_A \rangle_{Er}$ has been evaluated taking into account the diffuse reflectance spectra of the analogous neodymium compound, for which no resonant absorption at 1.5 μm is found. Moreover, being $\alpha_A=\sigma_A\rho_A$, where σ_A is the acceptor absorption cross section, and ρ_A is the acceptor density, $\langle \alpha_A \rangle_{Er}$ depends on the real C–H group density of the specific molecular structure (in Er_3Q_9 there exist 54 C–H groups per 3 erbium ions).§ For Er_3Q_9 $\langle \alpha_A \rangle_{Er}$ = 1.0±0.3 cm^{-1}. This value is obtained from the fitting of absorption and emission spectra by considering the structural parameters.

The radiative decay constant k_r (= $1/\tau_r$) for erbium emission has been calculated from the measurements of the Er emission cross-section (σ_{Er} = $0.7236 \cdot 10^{-20}$ cm^2)*, through the Strickler-Berg equation[20] (Eq. 6, Chapter 2) resulting in the experimental value of τ_r = 5.0 ± 0.1 ms.[19]

Moreover, structural data (i.e. distances and angles between the emitting metal ion and each C–H bond) have been used to evaluate (Eq. 7, Chapter 2) the κ^2 parameter, which represents the relative orientation of donor and acceptor transition dipole moments, for the real molecular structure of Er_3Q_9. This parameter has been measured and indexed for each C–H oscillator sitting in the surrounding of the emitting erbium ion (C–H groups of the nearest neighbouring molecules in the crystal packing have been taken into

§ The relative absorption cross-section of the single CH group is calculated through: $\sigma_{CH}(\lambda)/\sigma_{Er}(\lambda) = (3/54)I_{rel}$, where I_{rel} (= 0.92) is the relative intensity of the absorption bands of Er (λ=1530 nm) and of CH groups (λ = 1670 nm).

* Since the absorption and emission spectral shapes for erbium at 1.5 μm, are almost coincident, it has been assumed that $\sigma_{Em} = \sigma_{Abs}$.

account as well) to estimate the overall non-radiative decay constant k_{nr} (k_{obs}) through the summation over each *j*-term of k_{nr} referring to the single CH quenching dipole (Eq. 8).

These calculations gave $\tau_{nr} = 2.863 \cdot 10^{-6}$ s as the predicted non-radiative decay time for Er_3Q_9. The obtained value is therefore close to the measured experimental lifetime of 2.3 μs, thus proving the general validity of the model.[19]

Furthermore, for comparison, the model has been implemented by assuming, instead of a discrete distribution of C–H oscillators, a continuous medium approximation, in which κ^2 is averaged over all the possible orientations of the oscillating dipoles, and thus takes the value $\kappa^2 = 2/3$.

In this approximation, Equation 8 can be rewritten as:[21]

$$k_{nr} \cong \frac{\lambda_{em}^4}{(2\pi n)^4} \frac{k_r \langle \alpha_A \rangle_{Er}}{R_{\min}^3}; \qquad \text{Eq. } \mathbf{9}$$

Where R_{min} represents the minimum distance between the erbium ion and the nearest neighbouring C–H group. The radiative decay time obtained in this approximation ($\tau_{nr} = 2.941 \cdot 10^{-6}$ s) is again similar to the experimental value and is almost the same of that estimated by considering all the geometrical parameters of the molecule. Only R_{min} should be enclosed in the continuous model equation. The reason why this approximation works so well in this case, ultimately stems from the relatively large value of R_{min} (≅ 3.4 Å), which permits to consider a continuous-like packing of hydrogen atoms for Er_3Q_9. The application of the Förster's model for **4** and **5** gave similar results.

For **2** and **3**, the efficient quenching induced by water molecules can be quantitatively accounted for by assuming a dipolar coupling between the excited states of the Ln^{III} ion and the high frequency water vibration at 1420 nm. It must be remarked that this vibration is a combination of the symmetrical and antisymmetrical stretchings of O–H groups in water, thus it will be absent in compounds containing isolated O–H groups.

In the framework of the Förster's energy transfer resonant theory,[12,13,19] a theoretical non-radiative lifetime of ~100 ns is estimated using the spectroscopic and structural data of the hydrated complexes. The fast decay induced by water molecules results from: (i) the shorter Er^{3+}–OH_2 distance, (ii) the larger transition dipole of the HOH combination overtone, and (iii) the better fulfilment of the resonance condition between the Er and OH vibrational dipoles.[22]

The described model definitively demonstrates that the non-radiative lifetime of excited Er ions falls in the microsecond timescale if coupled to CH or HOH vibrations. For achieving more efficient near infrared emission ($k_{nr} \leq k_r$), which means that CH coupling would not affect the lanthanide emission at all, R_{min} should be larger than 30 Å assuming $\langle \alpha_A \rangle_{Er}$ = 1 cm^{-1}.[19] However, since the decrease of k_{nr} with increasing R_{min} becomes remarkably smoother above ~6 Å, according to the power-law dependence of Eq.8, it descends that even a distance of at least 7-8 Å between the emitting ion and the nearest neighbouring C–H groups should be effective for significantly improving the NIR-luminescence lifetime (decay about two orders of magnitude slower) of this class of lanthanide-based complexes.[8,19,22-24]

4.4 Conclusions

In the light of the results obtained from the photoluminescence studies on fully-characterised erbium complexes it then possible to draw the following conclusions:

I. Visible emission in the solid state is significantly affected by the supra-molecular arrangement of the quinolinolate complex. In particular, extensive π-π stacking between close-contact quinoline moieties of neighbouring molecules in the crystal packing results in a remarkable red-shift (100 nm) of the ligand emission wavelength. As a consequence, the energy transfer process from the excited donor states of the ligand to the 4f levels of the lanthanide ion should be influenced as well.

Although electroluminescence and photoluminescence devices are mostly based on amorphous films, the use of solid state characterisation can provide a helpful guide to the knowledge of the molecular packing preferences of the corresponding molecular materials which can effectively influence their optical properties.

II. The erbium quinolinolates studied in this work show NIR-luminescence efficiencies which are consistent with those previously reported for this class of emitting molecules,[4-6,16-17] with radiative lifetimes that fall in the microsecond timescale. This rather low efficiency is relatable to the presence of deactivating groups in the

molecule. In particular, it has been confirmed that water molecules directly bounded to the emitting lanthanide ion definitely represent the most effective quenchers for the erbium luminescence at 1.5 μm. Additionally, the combined optical and structural investigation of water-free Er-quinolinolate complexes, allows to conclude that the C–H groups sitting in the Er inner coordination sphere represent a very severe limit to the near-infrared emission yield.

III. Implementation of structural/spectroscopic data into a theoretical model based on Förster's energy transfer resonant theory provides a comprehensive analysis of the near infrared emission quenching in erbium complexes useful to predict the quenching effects in luminescent organo-lanthanides from the measurements of the vibrational absorption spectrum of the complex, the lanthanide radiative lifetime, and the minimum distance between the emitting ion and the quenchers.

In summary, photo-physical properties of the erbium compounds investigated in this work have been interpreted on the basis of their structure/properties relationship. The knowledge of the molecular structure allows to understand the spectral features of this class of emitting molecules both in the visible and in the near-infrared spectral regions and to assess unambiguously the quenching effects affecting the NIR-luminescence. These results are helpful to draw up the guidelines for the design of new complexes with improved efficiency. A further support to this is provided by the results obtained on the basis of the Förster's theory suggesting the use

of other suitable ligands which do not bear CH or OH groups at a distance shorter than 7-8 Å from the emitting ion to prepare complexes with enhanced emission efficiency.

4.5 Experimental

Photoluminescence measurements.

Photoluminescence spectra and transients were excited by 1-kHz train of 200-fs-long-pulses at 390 nm. Visible emission was spectrally and temporally dispersed by an imaging polychromator coupled to a 2D-streak camera. At low repetition rate, the signal rise-time is 10 ps. NIR emission was detected using an amplified InGaAs photodiode with a 2-ns response time, and averaged using a digitizing scope with either 20MHz or 1GHz detection bandwidth. The laser and visible frequencies were cut using color-glass filters. The NIR emission spectra were recorded using a monochromator coupled to an amplified low-noise InGaAs photodiode.

Diffuse reflectance spectroscopy.

DR spectra in the near-infrared were recorded on crystalline samples dispersed on Teflon film using a Varian Cary 5 spectrophotometer equipped with a diffuse reflectance accessory.

References

[1] J. Kido, Y. Okamoto *Chem. Rev.* **2002**, *102,* 2357-2368.

[2] G. A. Crosby, R. E. Whan, R. M. Alire, *J. Chem. Phys.* **1961**, *34*, 743.

[3] M. L. Bhaumik, M. A. El-Sayed, *J. Phys. Chem.*, **1965**, *69*, 275.

[4] W.P. Gillin, R.J. Curry, *Appl. Phys. Lett.* **1999**, *74,* 798.

[5] M. Iwamuro, T. Adachi, Y. Wada, T. Kitamura, N. Nakashima, S. Yanagida, *Bull. Chem. Soc. Jpn.* **2000**, *73*, 1359-1363.

[6] J. Thompson, R.I.R. Blyth, G. Gigli, R. Cingolani, *Adv. Funct. Mater.* **2004**, *14*, 979.

[7] M. Ottonelli, G. Izzo, F. Rizzo, G. Musso, G. Dellepiane, R. Tubino, *J. Phys. Chem. B* **2005**, *109,* 19249.

[8] F. Artizzu, P. Deplano, L. Marchiò, M. L. Mercuri, L. Pilia, A. Serpe, F. Quochi, R. Orrù, F. Cordella, M. Saba, A. Mura, G. Bongiovanni, *Adv. Funct. Mater.* **2007,** *17*, 2365-2376**.**

[9] M. Brinkmann, G. Gadret, M. Muccini, C. Taliani, N. Masciocchi, A. Sironi, *J. Am. Chem. Soc.* **2000**, *122,* 5147.

[10] M. Brinkmann, B. Fite, S. Pratontep, C. Chaumont, *Chem. Mater.* **2004**, *16*, 4627-4633.

[11] H. Kaji, Y. Kusaka, G. Onoyama, F. Horii, *J. Am. Chem. Soc.* **2006**, *128*, 4292.

[12] T. Förster, *Discuss. Faraday Soc.* **1959**, *27*, 7.

[13] T. Förster, *Annalen der Physik* **1948**, *2*, 55-75; english translation (1993).

[14] K. Kuriki, Y. Koike, Y. Okamoto, *Chem. Rev*. **2002**, *102*, 2347-2356.

[15] L. H. Slooff, A. van Blaaderen, A. Polman, G. A. Hebbink, S. I. Klink, F. C. J. M. Van Veggel, D. N. Reinhoudt, J. W. Hofstraat, *J. Appl. Phys.* **2002**, *91*, 3955-3979.

[16] R. Van Deun, P. Fias, K. Driesen, K. Binnemans, C. Görller-Walrand, *Phys. Chem. Chem. Phys.* **2003**, *5*, 2754.

[17] R. Van Deun, P. Fias, P. Nockemann, A. Schepers, T. N. Parac-Vogt, K. Van Hecke, L. Van Meervelt, K. Binnemans, *Inorg. Chem.* **2004,** *43*, 8461.

[18] F. Artizzu, P. Deplano, L. Marchiò, M. L. Mercuri, L. Pilia, A. Serpe, F. Quochi, R. Orrù, F. Cordella, F. Meinardi, R. Tubino, A. Mura, G. Bongiovanni, *Inorg. Chem.* **2005,** *44* , 840-842.

[19] F. Quochi, R. Orrù, F. Cordella, A. Mura, G. Bongiovanni, F. Artizzu, P. Deplano, M. L. Mercuri, L. Pilia, A. Serpe, *J. Appl. Phys.* **2006**, *99*, 053520.

[20] S. J. Strickler, R. A. Berg, *J. Chem. Phys.* **1962**, *37*, 814.

[21] M. D. Galanin, I. M. Frank, Zh. Eksp. Teor. Fiz. **1951**, *21*, 114.

[22] L. Ning, M. I. Trioni, G. P. Brivio, *J. Mater. Chem.*, **2007**, *17*, 4464 – 4470.

[23] L. Winkless, R. H. C. Tan, Y. Zheng, M. Motevalli, P. B. Wyatt, W. P. Gillin, *Appl. Phys. Lett.* **2006**, *89*, 111115.

[24] S. W. Magennis, A. J. Ferguson, T. Bryden, T. S. Jones, A.Beeby, I. D. W. Samuel, *Synth. Met.* **2003**, *138*, 463.

Chapter 5

Magnetic Properties

The magnetic properties of erbium quinolinolates are presented here. This study points out the importance of studying a gadolinium analogue to evidence small magnetic interaction, due to supramolecular arrangement, relevant in the optical behavior of optically active Er^{III} derivatives.

*Magnetic measurements have been performed by Prof. Andrea Caneschi and Dr. Kevin Bernot, LAboratory of Molecular Magnetism, Dipartimento di Chimica e UdR INSTM di Firenze

5.1 Introduction

The magnetic properties of lanthanide trications, which possess large orbital angular momenta and orbitally degenerate ground states (with the exception of Gd^{III} having the $^8S_{7/2}$ ground term), are influenced by strong spin-orbit coupling and large magneto-crystalline anisotropy compared to transition metal ions. Crystal Field effects in lanthanide compounds are so small (of the order of 100 cm^{-1}) that the magnetic susceptibility at room temperature is very close to that of the free ion and may differ from that only at very low temperature. In particular, the Crystal Field splits the ground state in close-energy Stark sublevels.[1-3] Consequently, when the temperature decreases, the depopulation of these sub-levels leads to a deviation from the Curie law and to a consequent variation of the $\chi_M T$ product even in the absence of any exchange interaction. Furthermore, core f electrons give rise to intrinsic weak magnetic interactions.

For these reasons, no simple models can be developed for a rational analysis of the magnetic exchange interactions in such coumpounds.[1]

Hovewer, since the Gd^{III} ion, has, contrary to the other lanthanides, no orbital contribution to the magnetic moment (S=0), it can be used as reference for evidencing weak magnetic interactions that are usually hindered by the depopulation of the Stark sub-levels of the orbitally degenerated lanthanide ions (such as the Er^{III}) derivatives. In fact, in gadolinium-based compounds, the Heisenberg-Dirac-Van Vleck

Hamiltonian[4-6] can be employed to quantify the magnetic exchange interaction.[1]

5.2 Magnetic measurements

The erbium quinolinolates (compounds **1**, **2**, **4**, and **5**) display the typical magnetic behaviour of isolated paramagnetic ions with no exchange interactions. As an example, the $\chi_M T$ *vs* T and the M *vs* H curves for the *trinuclear* Er_3Q_9 (**1**) are reported in Figures 5.1 and 5.2. The $\chi_M T$ *vs* T curves of **2** and **5** are reported in the Appendix Section (A.5).

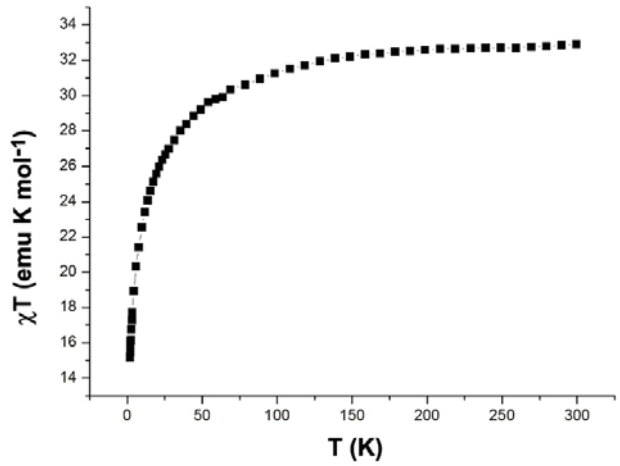

Fig. 5.1: Temperature dependence of the $\chi_M T$ product in the temperature range 2-300 K for Er_3Q_9 (**1**).

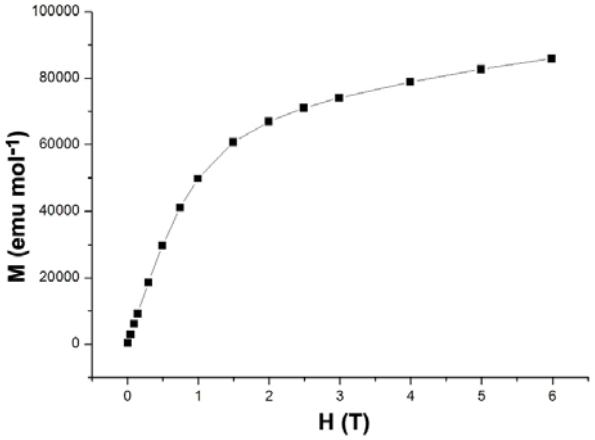

Fig. 5.2: Field dependence of the magnetisation M for **1**.

In Table 5.1 the experimental and theoretical values of $\chi_M T$ at room temperature for the studied complexes, are listed.

Compound	$\chi_M T$ *theo.* (emu K mol^{-1})	$\chi_M T$ *exp.* (emu K mol^{-1})
1	34.44	32.90
2	11.48	10.68
4	11.48	11.46
5	11.48	11.75
[Gd(5,7ClQ)$_2$(H5,7ClQ)$_2$Cl]	7.88	7.85

Table 5.1: $\chi_M T$ values at room temperature for **1**, **2**, **4**, **5** and [Gd(5,7ClQ)$_2$(H5,7ClQ)$_2$Cl].

The experimental $\chi_M T$ value at room temperature for Er_3Q_9 is close to the sum for three isolated Er^{III} ions (for a single Er^{III}: $\chi_M T_{(RT)}$= 11.48 emu K mol^{-1}; $^4I_{15/2}$, g_J = 6/5, J = 15/2).

In **1**, the Er···Er distance is 3.488 Å for Er(1)-Er(2) and 3.495 for Er(2)-Er(3). Studies on the magnetic coupling of some oxo-bridged dinuclear gadolinium compounds,[7] have shown that the ferromagnetic interaction between the lanthanide cores is favoured by the asymmetry of the metal coordination environment (i.e. differences in Ln–O bond lengths) and by large Ln–O–Ln angles. In Er_3Q_9, all the Er–O_{bridge} bond lengths are very similar from each other and the Er–O–Er angles (93.57°, 95.76°, 97.77° for Er(1) ···Er(2)) are quite small if compared with those for Gd^{III} and Er^{III} complexes displaying ferromagnetic coupling (Figure 5.3).[7-8]

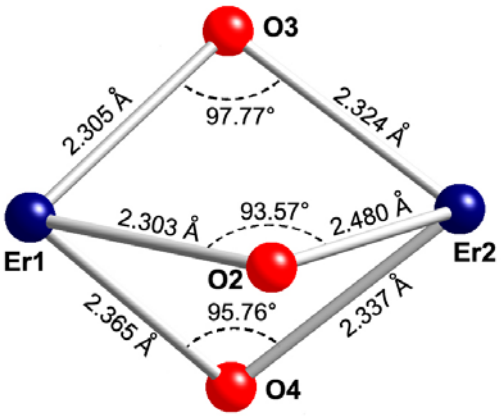

Fig. 5.3: *Sketch of the Er(1)Er(2)O_3 core in Er_3Q_9 (1) reporting Er–O bond lengths and Er(1)–O–Er(2) angles.*

For the *tetrakis* [Gd(5,7ClQ)$_2$(H5,7ClQ)$_2$Cl], stacking interactions through the quinoline molecules (see Chapter 3), although not providing direct magnetic exchange interaction, give rise to ferromagnetic interaction relatable to a dipolar interaction between the Gd^{III} ions.

The thermal variation of the $\chi_M T$ product for [Gd(5,7ClQ)$_2$(H5,7ClQ)$_2$Cl], is shown in Figure 5.4. The value of $\chi_M T$ at room temperature is close to the expected value of 7.88 emu K mol^{-1} for one isolated Gd^{III} (S = 7/2, g = 2.00).[9] $\chi_M T$ takes a constant value equal to 7.8 emu K mol^{-1} from 300 to 15 K. Below 15 K, the $\chi_M T$ product increases abruptly to reach a value of 8.11 emu K mol^{-1} at 2 K.

The experimental magnetisation from 0 to 60 kOe is shown in Figure 5.5. The value of the magnetization at 60 kOe is 38883 emu mol^{-1} (6.96 μ_B), close to the expected saturated value of 7 μ_B.

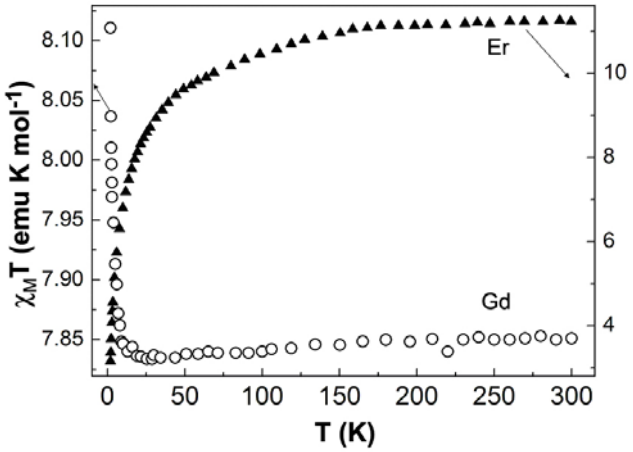

Fig. 5.4 *Temperature dependence of the $\chi_M T$ product in the temperature range 2-300 K for [Gd(5,7ClQ)$_2$(H5,7ClQ)$_2$Cl] (circles, left axis and ticks) and the Er^{III} derivative* **4** *(triangles, right axis and ticks).*

The magnetic measurements for [Gd(5,7ClQ)$_2$(H5,7ClQ)$_2$Cl] can be compared with those for the isostructural *tetrakis* erbium complex, **4**, whose

$\chi_M T$ *vs* T curve is also reported in figure 5.4. At room temperature the $\chi_M T$ value (11.46 emu K mol^{-1}) is in agreement with the theoretically expected one ($\chi_M T_{(RT)}$= 11.48 emu K mol^{-1}) for a Er^{III} ion ($^4I_{15/2}$, g_J = 6/5, J = 15/2). The $\chi_M T$ product takes a constant value from 300 K to 150 K, and then continuously decrease when lowering the temperature to reach the value of 3.16 emu K mol^{-1} at 2 K. As expected for this type of compound, the *M vs H* curve does not show any saturation and the magnetisation at 60 kOe (27812 emu mol^{-1}) is lower than the saturated value (50265 emu mol^{-1}).

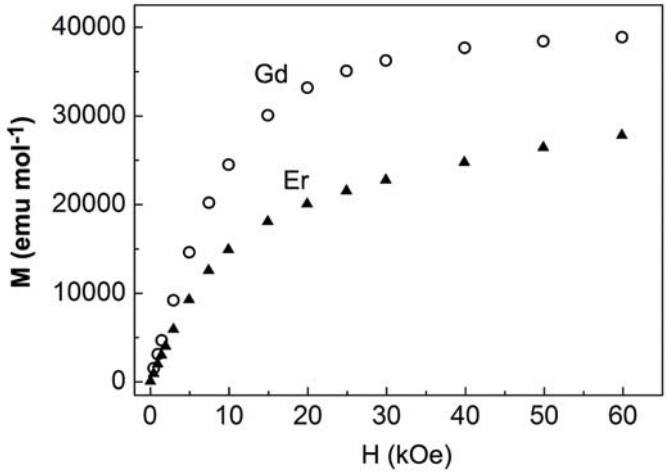

Fig. 5.5 *Field dependence of the magnetisation M for the Gd^{III} derivative (circles) and the Er^{III} derivative (triangles).*

Although these $\chi_M T$ *vs* T curves seem to be different they are the consequence of the same magnetic behaviour. In fact, the Gd^{III} derivative show an increase of the $\chi_M T$ product at low temperature that is characteristic

of a small ferromagnetic interaction between two Gd^{III} centres. Taking into account the arrangement of the $[Gd(5,7ClQ)_2(H5,7ClQ)_2Cl]$ moieties in the crystal structure, this small magnetic interaction is likely to be mediated by the stacking interaction through the quinoline molecules.

From the magnetic point of view, such stacking interactions are not expected to provide direct magnetic exchange interaction, and in that case it is reasonable to consider the small ferromagnetic interaction as a consequence of a dipolar interaction between the Gd^{III} ions. Since the stacking interactions are very numerous in the crystal structure, it is almost impossible to assign which pathways is responsible for the ferromagnetic interaction visible in the $\chi_M T$ *vs* T curve. As the Gd^{III} is non-orbitally degenerated, a Curie-Weiss fit is usually performed in order to quantify this interaction. In this case, this procedure was affected by the noise of the measurement and consequently is not reported here. This further supports the attribution of the rising of the $\chi_M T$ product at low temperature to a low dipolar interaction between the Gd^{III} ions and not to a magnetic exchange interaction (expected to be more significant).

The Er^{III} derivative is also expected to behave in the same way, as seen on numerous comparative studies along the lanthanides series.[1] The Er^{III} ion is a Kramer ion with a $^4I_{15/2}$ ground state[3] and is affected, like all the lanthanide ions that are orbitally degenerated, by a strong spin-orbit coupling. Below 150 K, the decrease of the $\chi_M T$ product for this compound is therefore only attributed to the depopulation of the Stark sub-levels of the Er^{III} ions. Hence, the small interaction seen on the Gd^{III} derivative is expected to be

present on the Er^{III} one since this interaction is of dipolar origin and the two compounds are isostructural. However the depopulation of the Stark sub-levels hampers its observation here.

Even if not surprising these magnetic measurements have confirmed the presence of significant stacking interactions through the quinoline moieties in both the Gd^{III} and Er^{III} *tetrakis* complexes with the H5,7ClQ ligand, which are responsible for the additional band in the visible region of diffuse reflectance spectrum (see Chapter 3, Paragraph 3.3.2).

5.3 Conclusions

All the erbium quinolinolates show magnetic properties that can be ascribed to isolated paramagnetic Er^{III} ions. In the case of the *trinuclear* complex Er_3Q_9, the geometric parameters of the oxo-bridged Er_2O_3 cores, do not seem to favour the ferromagnetic interaction between the lanthanide ions.

The magnetic behaviour of $[Gd(5,7ClQ)_2(H5,7ClQ)_2Cl]$ has been investigated and explained by taking into account that the π-stacking interactions give rise to a crystal structure in which the gadolinium centres interact in a dipolar way. In a more general picture, the use of Gd^{III} derivatives seems to be a quite efficient strategy to magnetically evidence the presence of stacking interaction, usually undetectable, in optically active

Er^{III} complexes. The presence of structural interactions that are responsible for solid state effects that influences the optical properties of the investigated compounds are thus confirmed by this study. In fact, the presence of significant stacking interactions through the quinoline molecules has been evidenced to be at the origin of the additional band in the diffuse reflectance spectrum, and also in the red-shift of the ligand emission.

5.4 Experimental

Magnetic Measurements.[§] All magnetic measurements were performed on pellets. The *dc*-magnetic susceptibility measurements were performed with a Cryogenic S600 SQUID magnetometer between 2 and 300 K in an applied magnetic field of 1000 Oe for temperatures in the range 2-100 K and 10000 Oe for temperatures between 100 and 300 K. These measurements were all corrected for the diamagnetic contribution as calculated with Pascal's constants.

[§] Magnetic measurements were performed by Dr. Kevin Bernot, University of Florence

References

[1] C. Benelli, D. Gatteschi, *Chem. Rev.* **2002**, *102*, 2369.

[2] F. A. Hart, "Scandium, Yttrium and the Lanthanides", *Comprehensive Coordination Chemistry*, chap.39.

[3] R. L. Carlin, *Magnetochemistry*, Springer, Berlin, **1986**, 228.

[4] Heisenberg, W., *Z. Phys.* **1928**, *49*, 619.

[5] Dirac, P. A. M. *Proc. R. Soc. (London)* **1929**, *A123*, 714.

[6] Van Vleck, J. H. *The Theory of Electric and Magnetic Susceptibilities*, The Clarendon, Oxford, **1932**.

[7] L. E. Roy, T. Hughbanks, *J. Am. Chem. Soc.* **2006**, *128*, 568-575.

[8] J.-P. Costes, J. M. C. Juan, F. Dahan, F. Nicodème, M. Verelst, *Angew. Chem. Int. Ed.* **2002**, *41*, 323.

[9] O. Kahn, *Molecular Magnetism*, Wiley-VCH, Weinheim, **1993**.

Chapter 6

Lanthanide-doped Sol-gel Glasses

Several lanthanide quinolinolates have been incorporated into sol-gel glasses with the aim to investigate the processing potential of this class of emitting molecules. The sol-gel method used to prepare doped silica glasses, as promising low-cost materials for optical applications, is described.

*This work has been carried out at the Coordination Chemistry Department of the Catholic University of Leuven (Belgium). Dr. Rik Van Deun and his coworkers, suggested this research and performed the photoluminescence measurements.

6.1 Introduction

With the aim to investigate the processing potential of lanthanide (Er, Nd, Yb) quinolinolates emitting in the NIR, experiments on incorporation of these luminescent compounds into sol-gel glasses have been carried out.

Silica glasses doped with luminescent lanthanide inorganic salts are suitable materials to be used for the fabrication of several optical devices, such as Nd lasers and optical fibres,[1-4] since they are highly transparent and homogeneous and feature good mechanical properties. Moreover, the silica matrix hardly influences the energy levels of the lanthanide ions and has also a negligible absorption coefficient at the excitation or emission wavelengths used in photoluminescence experiments.

Lanthanide-doped silica glasses can be prepared through the convenient sol-gel process, which offers several advantages over the traditional melt preparation. The most important one arise from the fact that sol-gel glasses, being prepared through a solution process, can hold a higher concentration of dopants than melt glasses, without losing their amorphous character. Moreover, they are generally of better purity and can be fabricated at much lower temperatures. In addition, synthetic conditions, such as composition and pH, can be more easily changed and optimised.

Optical properties achievable in sol-gel materials include graded refractive indexes, waveguiding, chemical sensing, optical amplification, frequency doubling, and lasing.[5]

However, the low luminescence quantum yield of Ln-doped sol-gel glasses developed so far, has limited their success as viable industrial alternatives. This is due to the presence of OH quenching groups which favour non-radiative de-excitation pathways in these materials, and to the weak absorption cross-section of the lanthanide ion, which severely limits the pumping efficiency. A promising way to improve the luminescence properties of these materials is to replace the traditional inorganic pigments with suitable lanthanide-based complexes with light-harvesting (antenna) ligands enhancing the optical pumping efficiency. In addition, the cage formed by organic ligands around the lanthanide ion shields the metal from quenching groups present in the host matrix.

The incorporation of lanthanide complexes into a silica host material increases their stability while their luminescence properties remain unchanged with respect to the same complexes in solution. In principle, the emission efficiency may be even improved as the complex is immobilised in a rigid medium that reduces the number of vibrational degrees of freedom, therefore lowering the non-radiative deactivation due to the ligand and enhancing the ligand-to-metal energy transfer as well.[6] In addition, the good solubility of lanthanide complexes into organically modified sol-gel matrices allows to obtain a homogeneous final material without the presence of molecular aggregates and clusters, which may drop the luminescence quantum yield through self-extinction processes (*concentration effect*).[7]

Moreover, among the several advantages of sol-gel glasses, the most valuable is that the sol-gel process can be carried out at room temperature.

Therefore, with this processing technique, dissociation or degradation of the lanthanide complex can be avoided. This is of great importance since most of the commonly used methods to process luminescent organo-lanthanides, such as vacuum deposition, require very high thermal stability of the compound to be processed, which is not always ensured.[8]

6.1.1 Sol-gel process

The *sol-gel method* is a synthetic procedure to obtain ceramic materials of high purity and homogeneity, which consists of different sequential steps, namely the preparation of the *sol*, its gelation and subsequent treatment of the *gel* to obtain the desired product.[9]

The process is usually carried out in alcoholic or hydro-alcoholic solution, starting from precursors such as inorganic salts (e.g. sodium silicate Na_2SiO_3)[10] or, more commonly, metallic alkoxides. In the case of silica-based sol-gel glasses, these precursors consist of alkoxy-silanes which may bear a variety of alkoxydic or alkyl chains (ORMOSILs=organically modified silicon alkoxides).

The reactions involved in this process are the hydrolysis and the condensation of the precursors to form a tri-dimensional silica network, as shown in Scheme 6.1.

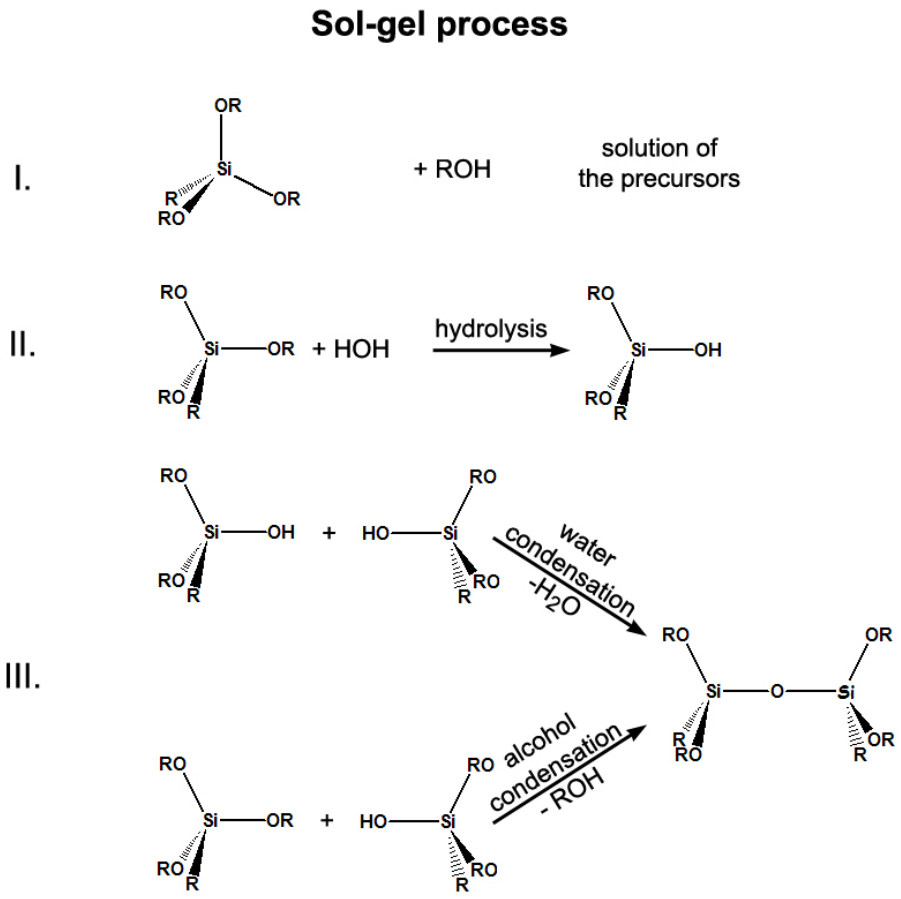

Scheme 6.1: Sol-gel process.

These are nucleophilic substitution reactions which, in the first step, involve the replacement of alkoxide groups, –OR, by hydroxyl groups, –OH,

with alcohol release (*hydrolysis reaction*). Condensation reactions then follow, leading to the formation of Si–O–Si bridges with water release (*water condensation*) or alcohol release (*alcohol condensation*). Generally, hydrolysis can be catalysed by acids whereas basic conditions speed up the condensation process. Moreover, the choice of the catalyst influences the structure of the matrix.

It must be remarked that the described reactions, once started, do not occur in sequence but involve simultaneous equilibria.

The colloidal solution obtained as a result of the initial formation of the siloxanes Si–O–Si bridges as a consequence of the condensation of the monomers, is defined as *sol*. As the reactions go on, a continuous silica-network begins to form until the *gelation point* is reached. The *gelation point* corresponds to the reaction time in which the *sol*-to-*gel* transition occurs. A *gel* is defined as a colloidal system of solid character in which the dispersed substance forms a continuous, coherent framework that is interpenetrated by a liquid system consisting of units smaller than colloidal entities. The silica network can assume several possible polymeric structures depending on numerous parameters such as composition, pH, temperature, water content, etc… *Gel aging* allows the tri-dimensional network to strengthen. When the *sol* becomes a *gel*, the tri-dimensional silica network retains most of the by-products of the sol-gel process, namely H_2O and ROH (*wet gel*), which should be removed to obtain a dry gel. Solvent removal by slow evaporation at ambient pressure, leads to a dense ceramic material, which can undergo a glass transition thus originating a sol-gel glass.

6.1.2 ORMOSILs

Organically modified silicon alkoxide precursors (ORMOSILs) are constituted by a silicate backbone in which alkoxidic –OR groups are replaced by organic –R groups.[11-12] ORMOSILs have some significant advantages over the commonly used tetra-alkoxy-silanes, such as TMOS (tetra-methoxy-silane) and TEOS (tetra-ethoxy-silane), for the preparation of doped sol-gel glasses.[6-7,13-17] In particular, these advantages are:

- more efficient control of the optical properties (i.e. refractive index);
- higher thermal stability and damage threshold upon lasing in photoluminescence experiments.[15]
- improvement of the mechanical properties of the sol-gel glass;
- lower shrinkage due to the filling of the pores by organic bulky groups;
- better transparency of the glass without thermal treatment;
- better control of the thickness of the thin film obtained through spincoating techniques.[6]
- opportunity to adjust the chemical composition depending on the interaction/affinity of the matrix with the dopant.[16] ORMOSILs also allow chemical binding between the dopant and the host matrix, which improves the stability and the homogeneity of the sample.[7,17]
- opportunity to control the size of the pores depending on the size of the dopant;[16]

- introduction of hydrophobic organic chains which lowers the polarity of the material. It descends that water molecules potentially entrapped in the matrix are expected to be expelled. Also, the presence of hydrophobic groups on the surface of the material should hamper the diffusion of water molecules from the environment into the porous glass. Moreover the number of residual Si–OH groups in the silica host is reduced.[6,13-18]

The last point is particularly advantageous for the fabrication of sol-gel glasses doped with NIR-emitting lanthanide complexes, since quenching effects induced by resonant coupling with water molecules or hydroxy-groups can be reduced.

6.2 Incorporation of lanthanide quinolinolates into sol-gel glasses

6.2.1 Lanthanide quinolinolates as dopants

Among the available quinolinolates, *tetrakis*-type complexes of Nd, Er and Yb, with dihalo-substituted quinolinol ligands, which give the best results in terms of emission efficiency,[19] have been selected to be incorporated into sol-gel glasses. In addition, samples containing analogous Gd complexes have been prepared to be used as references. These complexes have been

prepared following either a slight modification of the synthetic procedure described in reference 19 (method A), which yields charged complexes, and also according to the method reported herein (method B, see Chapter 3) with which neutral compounds are obtained. 5,7-dichloro-8-quinolinol and 5,7-dibromo-8-quinolinol have been used as ligands and, in the first case, tetraethylammonium hydroxide has been used as base to deprotonate the ligand in order to obtain *tetrakis* complexes as tetraethylammonium salts. This countercation is supposed to make the saline compounds more soluble in organic solvents (used in the sol-gel method) than sodium salts. The complexes which have been incorporated into sol-gel glasses are listed in Table 6.1.

	Method A[19]	Method B
Nd	o $[Nd(5,7ClQ)_4]NEt_4$ o $[Nd(5,7BrQ)_4]NEt_4$	--*
Er	o $[Er(5,7ClQ)_4]NEt_4$ o $[Er(5,7BrQ)_4]NEt_4$	o $[Er(5,7ClQ)_2(H5,7ClQ_2)Cl]$ o $[Er(5,7BrQ)_2(H5,7BrQ_2)Cl]$
Yb	o $[Yb(5,7ClQ)_4]NEt_4$ o $[Yb(5,7BrQ)_4]NEt_4$	o $[Yb(5,7ClQ)_2(H5,7ClQ_2)Cl]$ o $[Yb(5,7BrQ)_2(H5,7BrQ_2)Cl]$
Gd	o $[Gd(5,7ClQ)_4]NEt_4$ o $[Gd(5,7BrQ)_4]NEt_4$	o $[Gd(5,7ClQ)_2(H5,7ClQ_2)Cl]$*

Table 6.1: Lanthanide quinolinolates incorporated into sol-gel glasses.
*Neither neutral neodymium *tetrakis* complexes nor $[Gd(5,7BrQ)_2(H5,7BrQ_2)Cl]$ could be obtained with the synthetic method described in this thesis (see Chapter 3).

6.2.2 Preparation of doped sol-gel glasses

The preparation is performed with a one-step process in which a solution of the lanthanide complex is mixed with the sol matrix at low temperature (~ 50°C) and at neutral pH.

Hydrolysis and condensation reactions in the sol-gel process are carried out without acid or basic catalysis in order to avoid either the protonation of the quinolinolate ligand or the dissociation of the complex as well as the formation of insoluble lanthanide hydroxides.[7] Furthermore, the slowness of the process in the absence of a catalyst, should lead to the best results in terms of transparency, homogeneity and mechanical resistance of the doped glass.

The sol solution is prepared using ORMOSILs as precursors and ethanol as solvent. In particular, three different mixtures of ORMOSILs components, depicted in Scheme 6.2, have been used. Each mixture contains 50% in volume of TMOS (tetra-methoxy-silane) and one or two more components to form binary or ternary systems. Compositions of the precursor mixtures are reported in Table 6.2.

Mixture	Ratio (V/V)
TMOS/GLYMO	1:1
TMOS/GLYMO/DEDMS	1:0.5:0.5
TMOS/ITMS	1:1

Table 6.2: *Composition of the ORMOSILs mixtures.*

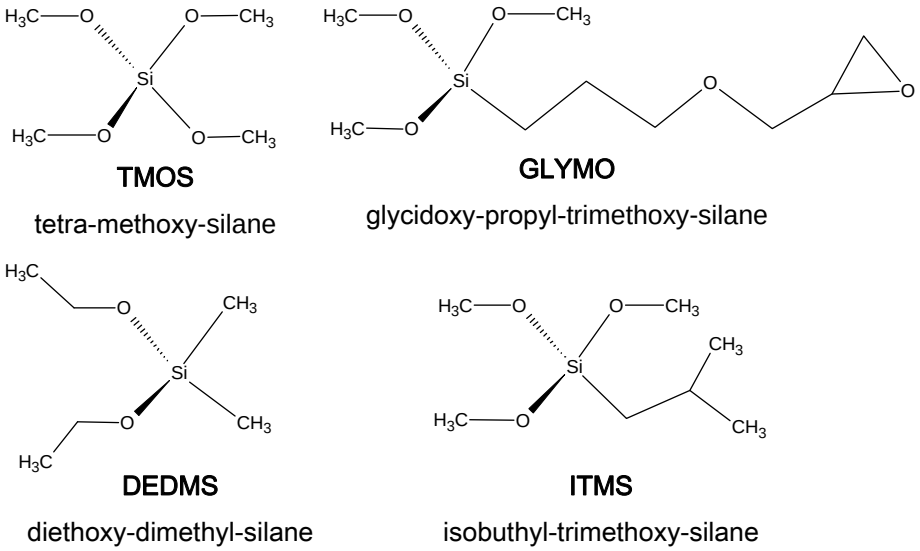

Scheme 6.2: *ORMOSILs used as precursors for the preparation of doped sol-gel glasses.*

TMOS has been preferred to TEOS given its higher facility to hydrolyse under neutral conditions while DEDMS has been chosen because of its tendency to form linear chains upon condensation, which is expected to improve the mechanical resistance and flexibility of the glass.[7,17]

Among the precursors reported in Scheme 6.2, GLYMO has been selected with the perspective to obtain a lanthanide doped glass with good luminescence efficiency.[6,17] In fact, the epoxy group may easily react with water molecules lowering the water content in the sol-gel material and thus reducing the quenching phenomena affecting NIR luminescence.

The preparation of lanthanide quinolinolates doped sol-gel glasses can be summarised as follows (Scheme 6.3):

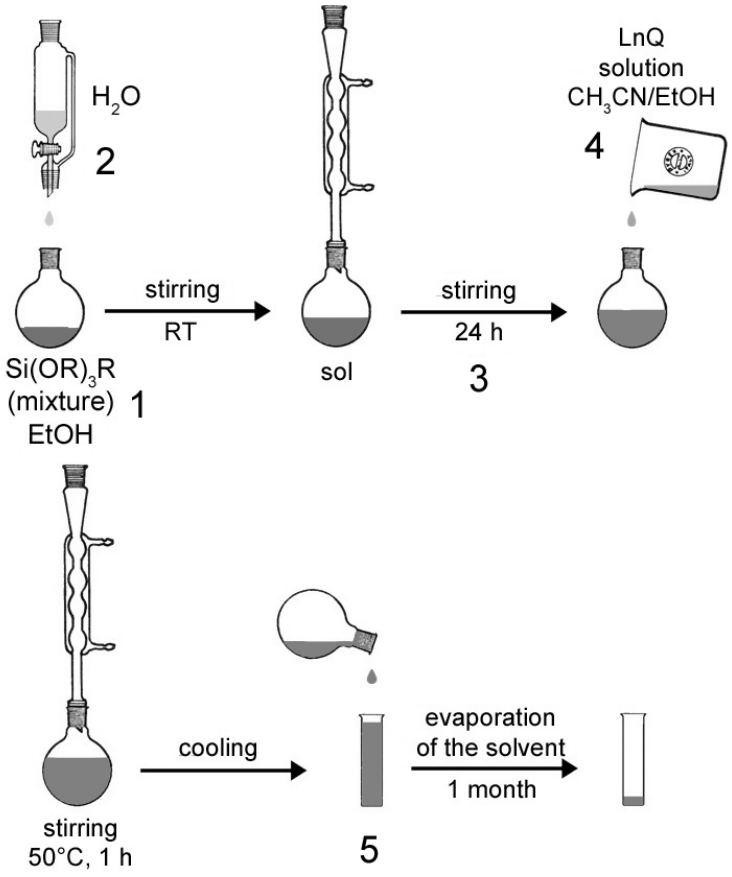

Scheme 6.3: *Preparation of sol-gel glasses doped with lanthanide quinolinolates.*

1. Preparation of the precursor solution in ethanol;
2. Addition of a small amount of water that starts the hydrolysis reaction;
3. 1 day stirring at room temperature in order to let the silica network grow as a result of condensation reactions;
4. Addition of the lanthanide quinolinolate solution to the sol matrix; 1 h stirring at 50°C;
5. Aging of the doped sol gel in a vial for approximately 1 month at room temperature and slow solvent evaporation which leads to the formation of the glass;
6. Annealing of the doped sol-gel glasses in order to remove residual solvent molecules.

Several experiments have been performed in order to find the best conditions to obtain homogeneous and transparent doped sol-gel glass which do not exhibit tendency to fracture.

Samples based on TMOS/GLYMO and TMOS/GLYMO/DEDMS have given good results in terms of homogeneity, transparency and mechanical resistance whereas most of the samples obtained from the TMOS/ITMS mixture of precursors cracked when the glass transition took place.

It has been observed that dopant concentration has some influence on the formation of the glass. In fact, it seems that lanthanide complexes act as catalysts for the gelation process, therefore the higher the concentration, the more the gelation process is speeded up.[17] As a consequence, samples

prepared with dopant concentrations of about $8 \cdot 10^{-4}$ mol L^{-1} (in the sol solution), have shown a short gelification time (only few days) and a strong tendency to crack. Instead homogeneous doped sol-gel glasses have been obtained on halving that concentration at which both the saline and the neutral *tetrakis* complexes disperse well in each matrix.

6.3 Conclusions

The conditions to obtain transparent and homogeneous sol-gel glasses doped with NIR-emitting *tetrakis* quinolinolates have been optimised. Several samples suitable for photoluminescence measurements have been obtained.

Preliminary photoluminescence studies on these samples have shown that only those doped with Yb^{III}-based quinolinolates give rise to detectable emission outputs. Since Yb^{III} emission at about 980 nm is not highly resonant with vibrating –OH or –CH groups, the low luminescence efficiency displayed by Er^{III} and Nd^{III} samples is relatable to a relatively high content of these quenchers into the sol-gel material.

These preliminary results suggests that the NIR-luminescence efficiency of lanthanide doped sol-gel glasses may be improved by changing their composition, for instance by using different ORMOSILs precursors bearing highly hydrophobic chains.

6.4 Experimental

6.4.1 Synthesis of the complexes

Two types of *tetrakis* complexes with 5,7-dichloro-8-quinolinol (H5,7ClQ) and 5,7-dibromo-8-quinolinol (H5,7BrQ) ligands have been synthesised to be used as dopants into sol-gel glasses, according to two synthetic procedures (methods A and B). Method A, reported in reference 20, yields negatively charged *tetrakis* complexes of general formula $[Ln(5,7XQ)_4]NEt_4$ while neutral complexes $[Ln(5,7XQ)_2(H5,7Q)_2Cl]$ are obtained with method B, already described in the third chapter of this thesis.

Method A. $[Ln(5,7XQ)_4]NEt_4$ (Ln=Nd, Er, Yb, Gd; X=Cl, Br). To 30 ml of absolute ethanol, 0.75 mmol of the ligand (previously purified by recrystallisation in CH_3CN/CH_3OH 1:1 solvent mixture) and 0.75 mmol of tetraethylammonium hydroxide are added. The mixture is heated to 60-70°C and stirred until all the reactants are dissolved. In some cases this requires up to 20 ml of extra solvent. 0.15 mmol of hydrated lanthanide chloride salt are dissolved in 10 ml of absolute ethanol, and added slowly over 10 minutes. After one extra hour of stirring the reaction mixture is cooled down. The precipitate is filtered of and washed with small amounts of water and ethanol/water mixture 1:1. Products were characterised by CHN analysis.

Method B. $[Ln(5,7XQ)_2(H5,7Q)_2Cl]$ (Ln=Er, Yb, Gd; X=Cl, Br). A brief summary of the procedure described in the Experimental Section of Chapter 3 follows: a solution of the lanthanide chloride salt in CH_3CN/CH_3OH 4:1 is slowly added to a solution of the ligand (ratio 1:4) dissolved in the same solvent mixture, under gentle heating. The mixture is stirred for approximately 1 day at room temperature and is then roto-

evaporated up to half volume. After few days red crystals of $[Ln(5,7XQ)_2(H5,7Q)_2Cl]$ are obtained.

6.5.2 Preparation of doped sol-gel glasses

Chemicals. All solvents and reactants were used without further purification.

Preparation of precursor solutions. **TMOS/GLYMO**: 8 mL of absolute ethanol, 8 mL of TMOS, 8 mL of GLYMO and 4 mL H_2O are mixed in a round-bottom flask. This mixture is maintained 1 day under stirring at room temperature (~22°C). **TMOS/GLYMO/DEDMS**: this mixture is obtained following the procedure described above, by adding 8 mL of TMOS, 4 mL of GLYMO, 4 mL of DEDMS and 4 mL of water to 8 mL of absolute ethanol. **TMOS/ITMS**: this mixture is obtained following the procedure described above, by mixing 8 mL of absolute ethanol, 8 mL of TMOS, 8 mL of ITMS and 4 mL of water.

Preparation of doped sol-gel glasses. 2 mL of a $1 \cdot 10^{-3}$ M solution of the lanthanide quinolinolate in CH_3CN/EtOH 1:1 are added to 3 mL of the sol solution and the mixture is maintained under stirring at 50°C for 1 h. The mixture is then transferred into a cylindrical glass vial and let cool down at room temperature. Afterward, the vial is covered with Parafilm pierced with a needle to let the solvent evaporate slowly. After few days, depending on the viscosity of the sol-gel, 2 or 3 more holes are made into the Parafilm and the sample is allowed to stand at room temperature (~22°C) until the glass is formed (> 1 month).

References

[1] F. Wu, D. Machewirth, E. Snitzer, G. H. Sigel, *J. Mater. Res.* **1994**, *9*, (10) 2703-2705

[2] F. Wu, G. Puc, P. Foy, E. Snitzer, G. H. Sigel Jr., *Mat. Res. Buill.* **1993**, *28*, 637-644

[3] A. Polman, D. C. Jacobson, D. J. Eaglesham, R. C. Kistler, J. M. Poate, *J. Appl. Phys.* **1991**, *70*, 3778.

[4] M.J. Weber, *J. Non-Cryst. Solids* **1990**, *123*, 208.

[5] V. C. Costa, M. J. Lochhead, K. L. Bray, *Chem. Mater.* **1996,** *8,* 783-790.

[6] R. Reisfeld, T. Saraidarov, M. Pietraszkiewicz, S. Lis, *Chem. Phys.Lett.* **2001**, *349*, 266.

[7] K. Binnemans, P. Lenaerts, K. Driesen, C. Görller-Walrand, *J. Mater Chem.* **2004**, *14*, 191.

[8] J. Kido, Y.Okamoto*, Chem. Rev.* **2002**, *102*, 2357.

[9] C. J. Brinker, G. W. Scherer, *Sol-gel Science*; Academic Press, San Diego, **1990**.

[10] S. S. Kistler, *Nature* **1931**, *127*, 741.

[11] P. Judeistein, C. Sanchez, *J. Mater. Chem.* **1996**, *6* , 511–525.

[12] J. Portier, J.-H. Choy, M. A. Subramanian*, Int. J. of Inorg. Mater.* **2001**, *3*, 581–592.

[13] H. Li, S. Inoue, K. Machida, G. Adachi, *Chem. Mater.* **1999**, *11,* 3171-3176.

[14] K. Machida, H. Li, D. Ueda, S. Inoue, G. Adachi, *J. Lumin.* **2000**, *87-89*, 1257-1259.

[15] M. Lal, S. Pakatchi, G. S. He, K. S. Kim, P. N. Prasad, *Chem. Mater.* **1999**, *11,* 3012-3014.

[16] M. Zayat, R. Pardo, D. Levy, *J. Mater. Chem.*, **2003**, *13*, 2899–2903.

[17] P. Lenaerts, A. Storms, J. Mullens, J. D'Haen, C. Görller-Walrand, K. Binnemans, K. Driesen, *Chem. Mater.* **2005**, *17,* 5194-5201.

[18] A. P. Otto, K. S. Brewer, A. J. Silversmith, *J. Non-Cryst. Solids*, **2000**, *265*, 176-180.

[19] R. Van Deun, P. Fias, P. Nockemann, A. Schepers, T. N. Parac-Vogt, K. Van Hecke, L. Van Meervelt, K. Binnemans, *Inorg. Chem.* **2004**, *43*, 8461.

[20] P. Fias, "Lanthanide(III) quinolinolates and phenalenolates: a structural and spectroscopic investigation", PhD Thesis, University of Leuven, **2005**.

Chapter 7

Conclusions and Perspectives

7.1 Conclusions

This research has allowed a revision of the literature data on erbium complexes with 8-hydroxy-quinoline and its derivatives, a class of complexes proposed as near-infrared emitters for several applications (e.g. optical fibers amplifiers…), providing a satisfactory structure/property relationship, valuable for the interpretation of their photo-physical properties previously based on unreliable assumptions.[1-9]

This work has been addressed to a detailed investigation on the proper synthetic procedures useful to prepare pure products suitable for structural, spectroscopic and photo-physical studies. Three types of erbium quinolinolates have been identified and characterised depending on reaction' conditions and on the nature of the ligand (i.e. 8-hydroxy-quinoline HQ or its 5,7-dihalo-derivatives H5,7XQ; X=Cl,Br): i) the homoleptic *trinuclear* complex Er_3Q_9, whose characterisation definitively rules out the possibility of an unsaturated tris-chelated structure for the erbium(III) quinolinolato complex (ErQ_3); ii) the *tris* hydrated complexes $[Er(5,7XQ)_3(H_2O)_2]$ in which the erbium coordination sphere is filled by two additional water molecules; iii) the epta-coordinated *tetrakis* complexes $[Er(5,7XQ)_2(H5,7XQ)_2Cl]$ where two ligands are in the zwitterionic form. These *tetrakis* complexes show extensive π-π stacking in the crystal packing which results in interesting solid-state optical properties.

Difficulties in obtaining pure products, have been overcome by this study, which provides experimental conditions to obtain in high yields well defined neutral compounds. This is of great importance since impure products are detrimental for applications in optical devices, and neutral compounds are preferable with respect to ionic ones for processing purposes.

The spectroscopic studies have allowed to provide suitable markers to distinguish the different types of complexes and to identify the presence of the most important quenchers as well as of solid-state interactions which affect the deactivation processes.

Gd^{III}, Nd^{III}, and Yb^{III} analogues have then been synthesised and characterised with the aim to assess unequivocally the spectroscopic features of this class of compounds by comparisons of isostructural complexes. Moreover, it has been confirmed that the "light" (Nd^{III}) and the "heavy" (Er^{III}, Yb^{III}) lanthanides feature slightly different chemical behaviour while gadolinium displays borderline properties.[10]

The comparison of the magnetic properties of isostructural *tetrakis* complexes of Er^{III} and Gd^{III} has allowed to evidence the presence of π-stacking interactions, usually undetectable, in these compounds. In fact, $[Gd(5,7ClQ)_2(H5,7ClQ)_2Cl]$ shows low-temperature ferromagnetic coupling between the lanthanide centres due to dipolar interaction through π-stacking.

Photoluminescence studies have shown that the radiative lifetimes of the erbium complexes, which fall in the microsecond timescale, are consistent with those commonly reported for analogous compounds.[1-9,11-13] In the light

of the structural and spectroscopic characterisation of the *trinuclear* Er_3Q_9, the quenching effects affecting the erbium luminescence have been ascribed only to ligand oscillating C–H groups which couple with ion emission through the Förster's resonant energy transfer mechanism. Similar conclusions are drawn for the water-free *tetrakis* complexes, whereas the emission lifetime of the *tris* complexes is considerably shortened (decay ten-times faster with respect to water-free quinolinolates) by the presence of directly bounded water molecules whose $\nu_1+\nu_3$* combination band is highly resonant with the erbium emission. Structural and spectroscopic data have been valuable to calculate the non-radiative decay constant through a theoretical model based on the Förster's theory. A distance of 7-8 Å between the emitting ion and the nearest neighbouring C–H groups should be effective for significantly enhancing the NIR-emission efficiency in this kind of compounds.[14-16] This model is of general application providing the guidelines to design new complexes with improved luminescence properties.

The experiments addressed to evaluate the processing potential for optical applications as sol-gel glasses of this class of complexes, have shown to be promising for the Yb-containing glasses. For the other cases, further research to optimise the composition of the sol-gel material to lower the content of quencher groups, is required.

* ν_1=symmetric, ν_3=antisymmetric stretching vibration.

7.2 Perspectives

The progress of this work is addressed to find new routes to optimise the luminescent properties of lanthanide complexes on the basis of the obtained experimental and theoretical results. Experiments in course involve: **i)** the use of antenna ligand which do not contain quenching groups, and **ii)** d-complexes to be used as ligands toward the lanthanide.

i) The ligand, which should not contain quenching groups, must satisfy additional requirements:

- efficient energy transfer to the lanthanide ion;
- suitable coordinating properties with a good “shielding” on the lanthanide ion to protect it from the surrounding (solvent,..) in order to avoid non-radiative processes and to form complexes with high thermal stability, capability to form uniform thin films and high electron transport ability for EL applications.

Perfluorinated systems have been proposed to increase the NIR emission lifetime of erbium. Decay times as long as 50 μs have been observed in a partially fluorinated system, namely, 1,1,1-tris(4-trifluorovinyloxy)phenylethane (TVE)-based polymer doped with Er^{III} (TVE-Er).[17-18] In a fully fluorinated imidodiphosphinate Er complex, $Er(F\text{-}tpip)_3$, in the solid state, an increase in luminescence decay time up to 220 μs has been observed.[19] However, this value is still much shorter than the radiative

Er lifetime and this may be due to excited-state energy transfer toward residual quenching centres containing hydrogen or deuterium atoms. Moreover, perfluorinated ligands usually have absorption bands that fall in the UV region, thus optical pumping is still rather inconvenient in these systems.

In Scheme 7.1, some examples of the ligands under investigation are shown.

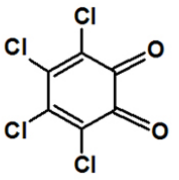

Tetrachloro-1,4-benzoquinone

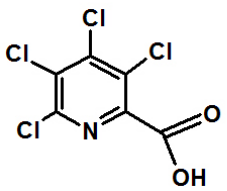

Tetrachloro-pyridine-carboxylic acid

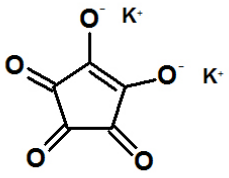

Croconate
Dianion of 4,5-dihydroxycyclopent-4-ene-1,2,3-trion

Scheme 7.1.i: *Selected Examples of Organic ligands Non-Containing CH or OH quenchers.*

Some lanthanide complexes of these ligands currently under investigation have been obtained. Among these, the erbium croconates seem to be promising since the highly aromatic croconato ligand has high

absorptivity in the Visible region and therefore may act as efficient light harvester for the erbium ion.

With the aim to synthesise a heterobimetallic Er^{III}-Cr^{III} complex, of potential interest for both optical and magnetic properties, the $ErCl_3$ salt has been reacted with the chrome alum salt and the croconato ligand. However, attempts to prepare an Er-Cr croconato-bridged complex have led to the isolation of an erbium homo-dinuclear complex $K_2[Er(C_5O_5)(\mu_2\text{-}SO_4)(OH_2)_4]_2$. This is the first example of complex in which the croconato ligand chelates a "yttrium group" Ln^{III} ion* in a bidentate fashion.[20] In the molecular structure, shown in figure 7.1.i, the SO_4^{2-} groups bridge two octa-coordinated Er^{III} ions. The erbium coordination sphere is filled by four additional water molecules.

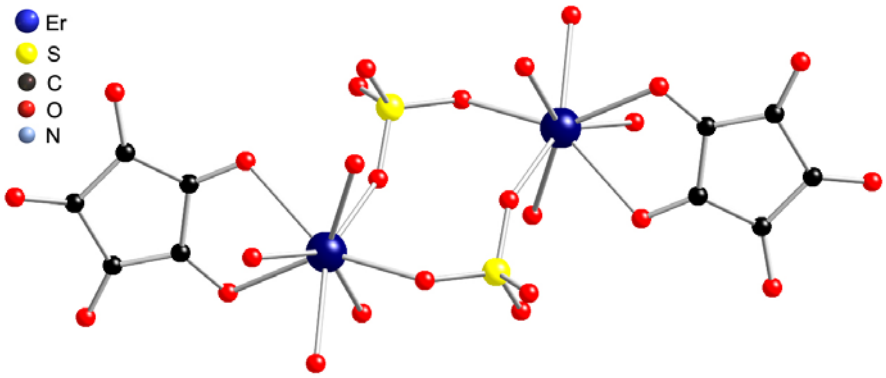

Fig. 7.1.i: *Structure of $[Er(C_5O_5)(\mu_2\text{-}SO_4)(OH_2)_4]_2^{2-}$. Hydrogen atoms and K^+ ions were removed for clarity.*

Unfortunately, due to the strong affinity of this ligand for water, it is difficult to avoid its presence in the reaction mixture.

* The "yttrium group" corresponds to the second half of the lanthanide series from Gd to Lu.

ii) The other strategy we are following to obtain organo-lanthanide systems with improved luminescence properties involves the use of metal-d complexes-as-ligands which can transfer absorbed energy to the lanthanide ion thus enhancing its emission.[21-28] This study opens new perspectives into the investigation of the magnetic properties of these systems and into their potential influence on the optical properties.[29-33]

It has been established that transition metal complexes can act as efficient sensitizers toward NIR-emitting lanthanide ions (see Chapter 2, Paragraph 2.23), provided that they have intense absorption bands in the visible region which allow to maximise the spectral overlap with the acceptor (the Ln ion) receiving levels.[21,23,25-26] The electronic properties of d-metal complexes can be easily tuned by varying the metal centre or the coordinated ligands.[27] Moreover, d-f systems can be prepared trough convenient synthetic procedures since metal complexes having vacant coordination sites or ligands which can act as bridges, can provide saturation of the coordination sphere of lanthanide ions. This should prevent further coordination of the lanthanide ion to water molecules. In addition, sensitisation through energy transfer from a long-lived excited state of a transition metal ion such as chromium, may remarkably extend the lanthanide luminescence lifetime.[27-28]

For fast and efficient energy transfer in d-f systems, it is desirable to have a short d-metal-f-metal separation occurring through unsaturated bridging groups (in order to allow inter-metallic communication), such as, for instance, cyanide groups.[25] Moreover, inter-metallic d–f communication allows

potential interesting magnetic properties,[29-35] such as, for instance, spin-crossover[30] or Single Molecule Magnet (SMM) behaviour.[29,32-33]

The dicyano-bis-1,10-phenantroline iron(II), $[Fe(phen)_2(CN)_2]$§ has been selected to prepare a mixed d-f complex with the Er^{III} ion. This complex has two cyanide groups which can act as bridging ligands toward the erbium ion and, due to its neutrality, it allows to synthesise a neutral heterobimetallic complex by reacting with an uncharged erbium complex. Furthermore, it has intense absorption in the visible region (λ_{max}=593 nm).

By reacting $[Fe(phen)_2(CN)_2]$ with $Er(NO_3)_3 \cdot 5H_2O$ (1:1 molar ratio) in $CHCl_3/CH_3CN$ solvent mixture, crystals suitable for X-ray structural studies of the heterobimetallic neutral complex $[Fe(phen)_2(\mu\text{-}CN)_2Er(NO_3)_3(H_2O)]_2$ (**Fe_2Er_2**) have been obtained (Figure 7.2.ii).

In the molecular structure the asymmetric unit is dinuclear and the Fe^{II} and Er^{III} metal centres are bridged by μ-CN groups with inter-metallic distances of about 5.4 Å (Figure 7.2.ii). The local coordination geometry of Fe^{II} is octahedral while each erbium ion is nine-coordinated by two bridging cyanides (Fe–CN–Er), three bidentate nitrato groups and a water molecule (Figure 6.2). The coordination geometry of Er^{III} is tricapped trigonal prismatic distorted by the effect of the low bite angle (~50°) of the chelating nitrato groups.

§ $[Fe(phen)_2(CN)_2]\cdot 2H_2O$ (phen = 1,10-phenantroline) has been prepared according to a slight modification of the synthetic procedure reported by Shilt.[36] The molecular structure and crystallographic details are reported in the Appendix Section (A.7).

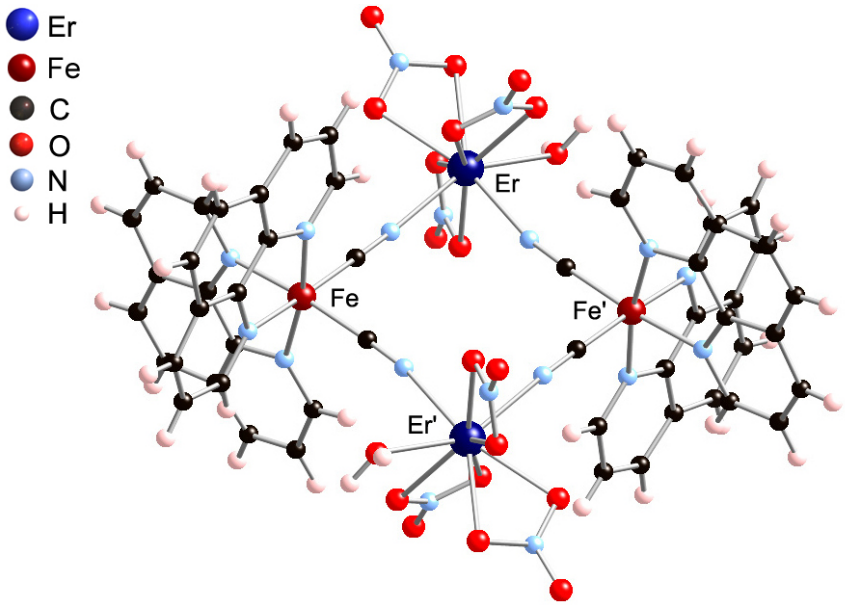

Figure 7.2.ii: *Molecular structure of* **Fe_2Er_2**. *Acetonitrile molecules were removed for clarity. '=-x; -y; 1-z.*

In this complex, no organic ligands bearing C–H groups are directly coordinated to the erbium ion, and the minimum distance from the nearest C–H group of a phenantroline ligand is 4.848 Å, whereas distances from the other C–H groups are above 5.7 Å. However, due to the low hindrance of the chelating nitrato ligands, a water molecule is directly bounded to the lanthanide center, providing nine-coordination.

Crystallographic data for $K_2[Er(C_5O_5)(\mu_2\text{-}SO_4)(OH_2)_4]_2$, $[Fe(phen)_2(CN)_2]\cdot 2H_2O$ and $[Fe(phen)_2(\mu\text{-}CN)_2Er(NO_3)_3(H_2O)]_2\cdot 2CH_3CN$ are reported in the Appendix Section (A.6, A.7).

These preliminary results are only partially satisfactory since both of the obtained class of complexes still contain coordinated water molecules. The next step will be addressed to find suitable synthetic strategies to eliminate the presence of water molecules. Suitable ways to achieve this goal are: i) to further react these complexes with additional chelating ligands which can displace coordinated water molecules; ii) to carry out the syntheses under strictly anhydrous conditions in a vacuum chamber; iii) hydrothermal synthesis;[37] iv) to react the lanthanide metal in the presence of oxidizing reagents.[38-39] Finally, vapor phase deposition may be a suitable technique to remove water molecules as well.

References

[1] R.J. Curry, W.P. Gillin, *Appl. Phys. Lett.* **1999,** *75,* 1380.

[2] W.P. Gillin, R.J. Curry, *Appl. Phys. Lett.* **1999**, *74,* 798.

[3] R. J. Curry, W. P. Gillin, *Synth. Met.* **2000**, *111–112*, 35.

[4] R.J. Curry, W.P. Gillin, A.P. Knights, R. Gwilliam, *Opt. Mater.* **2001**, *17*, 161.

[5] J. Thompson, R.I.R. Blyth, G. Gigli, R. Cingolani, *Adv. Funct. Mater.* **2004**, *14*, 979.

[6] S. Penna, A. Reale, R. Pizzoferrato, G. M. Tosi Beleffi, D. Musella, W. P. Gillin, *Appl. Phys. Lett.* **2007**, *91*, 021106.

[7] S. W. Magennis, A. J. Ferguson, T. Bryden, T. S. Jones, A.Beeby, I. D. W. Samuel, *Synth. Met.* **2003**, *138*, 463.

[8] R. I. R. Blyth, J. Thompson, Y. Zou, R. Fink, E. Umbach, G. Gigli, R. Cingolani, *Synth. Met.* **2003**, *139*, 207.

[9] Y. Li, H. Yang, Z. He, L. Liu, W. Wang, F. Li, L. Xu, *J. Mater. Res.* **2005**, *20,* 2940.

[10] R. H. Byrne, B. Li, *Geochim. Cosmochim. Acta* **1995**, *22*, 4575-4589.

[11] M. Iwamuro, T. Adachi, Y. Wada, T. Kitamura, N. Nakashima, S. Yanagida, *Bull. Chem. Soc. Jpn.* **2000**, *73*, 1359-1363.

[12] R. Van Deun, P. Fias, K. Driesen, K. Binnemans, C. Görller-Walrand, *Phys. Chem. Chem. Phys*. **2003**, *5*, 2754.

[13] R. Van Deun, P. Fias, P. Nockemann, A. Schepers, T. N. Parac-Vogt, K. Van Hecke, L. Van Meervelt, K. Binnemans, *Inorg. Chem.* **2004,** *43*, 8461.

[14] F. Quochi, R. Orrù, F. Cordella, A. Mura, G. Bongiovanni, F. Artizzu, P. Deplano, M. L. Mercuri, L. Pilia, A. Serpe, *J. Appl. Phys.* **2006**, *99*, 053520.

[15] L. Ning, M. I. Trioni, G. P. Brivio, *J. Mater. Chem.*, **2007**, *17*, 4464-4470.

[16] L. Winkless, R. H. C. Tan, Y. Zheng, M. Motevalli, P. B. Wyatt, W. P. Gillin, *Appl. Phys. Lett.* **2006**, *89*, 111115.

[17] J. Gordon, J. Ballato, D. W. Smith Jr., J. Jin, *J. Opt. Soc. Am.* B **2005**, *22*, 1654.

[18] J. Ballato, S. H. Foulger, D. W. Smith Jr., *J. Opt. Soc. Am. B* **2004**, *21*, 958.

[19] G. Mancino, A. J. Ferguson, A. Beeby, N. J. Long, and T. S. Jones, *J. Am. Chem. Soc.* **2005**, *127*, 524.

[20] C. Brouca-Cabarreq, J.-C. Trombe, *Inorg. Chim. Acta* **1992**, *191*, 227-240.

[21] M. D. Ward, *Coord. Chem. Rev.* **2007**, *251*, 1663-1677.

[22] M. D. Seltzer, *J. Chem. Educ.* **1995**, *72*, 886.

[23] N. M. Shavaleev, G. Accorsi, D. Virgili, Z. R. Bell, T. Lazarides, G. Calogero, N. Armaroli, M. D. Ward, *Inorg. Chem.* **2004**, *44*, 61.

[24] D. Imbert, M. Cantuel, J.C. G. Bünzli, G. Bernardinelli, C. Piguet, *J. Am. Chem. Soc.* **2003**, *125*, 15698.

[25] G. M. Davis, S. J. A. Pope, H. Adams, S. Faulkner, M. D. Ward, *Inorg. Chem.* **2005**, *44*, 4656-4665.

[26] J.-C.G. Bunzli, C. Piguet *Chem. Soc. Rev.* **2005** *34*, 1048-1077.

[27] C. Piguet, C. Edder, S. Rigault, G. Bernardinelli, J.-C. G. Bünzli, G. Hopfgartner, *J. Chem. Soc.*, *Dalton Trans.*, **2000**, 3999–4006.

[28] D. Imbert, M. Cantuel, J.-C. G. Bünzli, G. Bernardinelli, C. Piguet, *J. Am. Chem. Soc.* **2003**, *125*, 15698-15699.

[29] M. Ferbinteanu, T. Kajiwara, K.-Y. Choi, H. Nojiri, A. Nakamoto, N. Kojima, F. Cimpoesu, Y. Fujimura, S. Takaishi, M. Yamashita, *J. Am. Chem. Soc.* **2006**, *128*, 9008-9009.

[30] C. Edder, C. Piguet, G. Bernardinelli, J. Mareda, C. G. Bochet, J.-C. G. Bünzli, G. Hopfgartner, *Inorg. Chem.* **2000**, *39,* 5059-5073.

[31] T. Sanada, T. Suzuki, T. Yoshida, S. Kaizaki, *Inorg. Chem.* **1998,** *37,* 4712-4717.

[32] J.-P. Costes, F. Dahan, W. Wernsdorfer, *Inorg. Chem.* **2006**, *45*, 5-7.

[33] V. Chandrasekhar, B. M. Pandian, R. Azhakar, J. J. Vittal, R. Clérac, Inorg. Chem, 2007, 46, 5140-5142.

[34] S. Tanase, J. Reedijk, *Coord. Chem. Rev.* **2006**, *250*, 2501–2510.

[35] T. Shiga, N. Ito, A. Hidaka, H. Okawa, S. Kitagawa, M. Ohba, *Inorg. Chem.* **2007**, *46*, 3492- 3501.

[36] A. A. Schilt, *J. Am. Chem. Soc.* **1960**, *82*, 3000-3005.

[37] B. Li, W. Gu, L.-Z Zhang, J. Qu, Z.-P. Ma, X. Liu, D.-Z. Liao, *Inorg. Chem.*, **2006**, *45*, 10425.

[38] L. E. Sweet, T. Hughbanks, *Inorg. Chem.*, **2006**, *45*, 9696.

[39] S. G. Leary, G. B. Deacon, P. C. Junk, *Z. Anorg. Allg. Chem.* **2005**, *631*, 2647.

Appendixes

A.1 Applications of luminescent lanthanide complexes

Due to their luminescent properties, with emission wavelengths ranging from UV to near-infrared (NIR), lanthanides are currently finding many applications in several different fields ranging from optoelectronics to biology. A full description of all the possible applications of these lanthanide-based materials is certainly unfeasible and beyond the scope of this thesis, mainly focused on NIR-emitting complexes to be used in telecommunication technology. Therefore, only a brief overview on new-generation OLED devices and on optical fibres and amplifiers will be given in the following paragraphs.

A.1.1 OLED devices

Organic Light Emitting Diodes (OLED) are multi-layer diodes for electroluminescence (EL) based on organic electroluminescent materials. The EL method of excitation is based on the direct conversion of electricity in molecular excited states in order to afford light emission. In the so-called *Low Molecular Weight Molecule*-OLEDs the emitting centre is a small organic dye or a metal-containing molecule possessing electro-luminescence properties. The first example of a luminescent metal complex used as emitter in OLED devices is the *tris*(8-quinolinolate) aluminium(III) (AlQ_3), which displays efficient green emission upon electro-excitation.[1-5]

Emission arises from a ligand-centred $\pi \rightarrow \pi^*$ transition remarkably enhanced by the presence of the metal ion. In addition, the metal centre increases the thermal and photo-stability of the molecule as well as the rigidity of the system leading to a more efficient radiative quantum yield with respect to free organic dyes.

In Figure A.1.i a sketch of a typical multi-layer OLED is depicted. This device consists of a series of three organic semiconducting layers embedded between two electrodes injecting charge carriers into the diode when a small voltage is applied. The diode is deposited over a thin, flexible glass support, transparent to the light output.

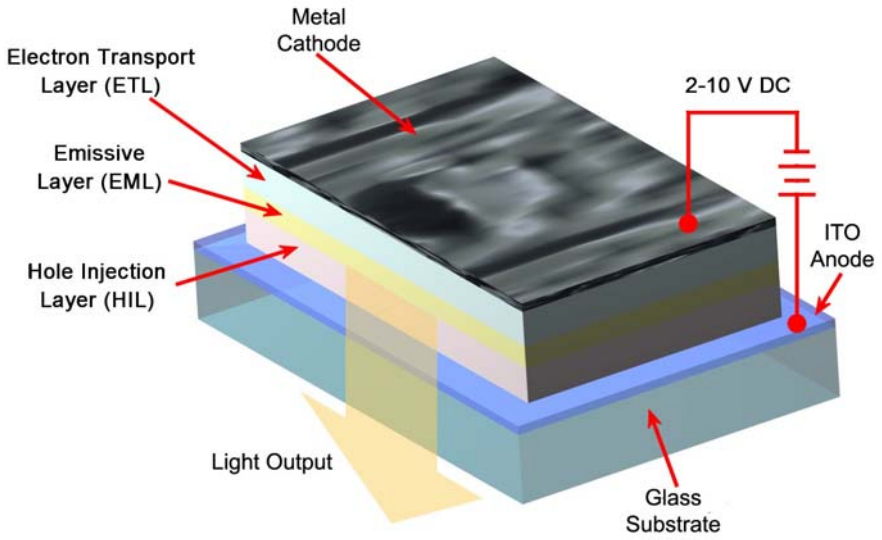

Fig. A.1.i: Draw of a typical multi-layer OLED device.

In the AlQ_3-based OLED,[1-5] the Emissive Layer (EML) of luminescent AlQ_3 is embedded between the Hole Injection Layer (HIL), and the Electron Transport Layer (ETL). The HIL usually consists of an aromatic amine of low ionization potential while the ETL is generally made of AlQ_3 (the Q ligand is a highly aromatic molecule with good electron-conducting properties). Holes are injected into the HIL by the anode made of Indium-Tin Oxide (ITO), a transparent material with a high work-function ϕ_1, while electrons come from the cathode, usually consisting of a metal plate of a low work-function ϕ_2 (Al or a Mg:Ag 10:1 alloy).

The application of an electric potential at the electrodes *(forward bias)* induces hole injection into the HIL and electron injection into the ETL. Under this potential difference charges start to migrate across the layers toward the opposite electrode, with hole transport occurring through the HOMO orbitals and electron transport through the LUMOs. Thus, the overlap of the HOMOs of the HIL molecules could be considered as a “valence band” of semiconductors whereas the overlap of the LUMO orbitals of the ETL originates the “conduction band”.

Depending on the velocity of the process and on charge mobility, the recombination of holes and electrons at the emitting layer generates an excited state (exciton), suitable to transfer the energy to the emitting molecule thus stimulating luminescence. In a “trapping” model each molecule represents a potential trap which can host the exciton. However, for efficient emission stimulation, the exciton should be confined into the emissive layer. The exciton migration across the diode can be blocked by

selecting proper hole-transporting molecular materials with a higher exciton level than that of the EML.[10-11] A scheme of the energy levels of a multi-layer diode is reported in Figure A.1.ii.

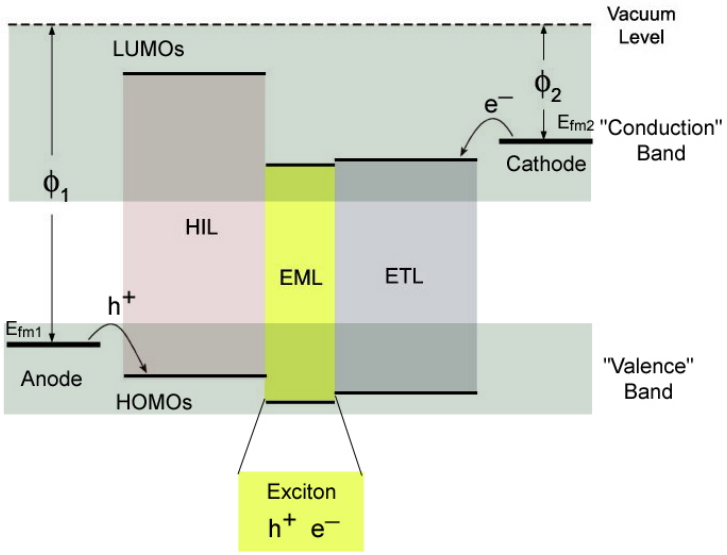

Figure A.1.ii: *Energy level diagram of a multi-layer diode.*

In general, for an organic material, the exciton corresponds to a singlet (S*) or a triplet (T*) excited state giving rise to radiative emission, namely fluorescence or phosphorescence. In electroluminescence experiments, the relative percentage of excited singlet (S*) with respect to excited triplet (T*) states formed upon voltage application is 25% to 75%. Hence, phosphorescence should be the main emission process even though this also depends on the nature of the emitting molecule.[2]

Recently, lanthanide complexes were also proposed as luminescent materials for electroluminescence devices and ErQ_3 (Q=8-quinolinolate) was used for the fabrication of the first lanthanide-based NIR-emitting OLED.[6-10] Lanthanide complexes have the advantage to originate sharp emission instead of the broad emissions bands of common organic dyes and d- or p-metal complexes. Lanthanide-centred emission can be stimulated by energy transfer from the ligand excited triplet state directly generated by carrier recombination into the diode. In principle, the efficiency of this process is close to 100%. Moreover, the use of lanthanide complexes as emitting centres in OLED devices allows to “fine-tune” the EL colors by selecting the proper lanthanide, without affecting the stability and the physical properties of the emitting material.[10-12]

Among the several techniques used for the fabrication of OLED devices, such as lithography or spin coating, the Vapor Phase Deposition (VPD), is, up to now, the most common. However, it requires a molecular material with high thermal stability as well as capability to form uniform and homogeneous thin films.

OLED devices are currently finding many applications both as signal amplifiers in telecom technology and as auto-luminescent components for a new-generation of ultra-thin and flexible displays (FOLED: *Flexible Organic Light Emitting Diodes*). One on the main advantages of this technology is undoubtedly the low operating cost which requires a very low voltage with almost no heat dissipation.

A.1.2 Optical fibres and amplifiers for telecommunication

In telecommunication systems, light is used to send information between different users at considerable distances.

Integrated optics technology allows to incorporate devices like splitters, couplers, multiplexers, demultiplexers and amplifiers, needed for signal manipulation, on planar substrates. Planar optical waveguides represent a basic element of a photonic integrated circuit (Figure A.1.iii).[13-15]

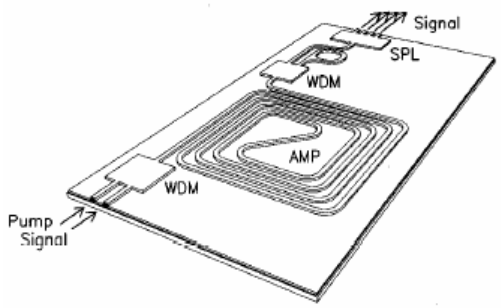

Fig. A.1.iii: *Representation of on-chip integration of an optical planar amplifier.*[15]

Optical networks based on silica fibres* are gaining popularity because of low-cost, convenience and accessibility. Moreover, they are flexible and can be bundled as cables. They allow signal transmission over longer distances and at higher data rates than other forms of wired and wireless communications. This is advantageous for long-distance communications,

* Waveguides can be made of silica glass or plastic materials (polymers), the latter having some advantages such as mechanical resistance and processing ease. However, only glass fibres are normally used for long-haul telecommunications since they have lower optical attenuation.

because light propagates through the fibres with lower attenuation than in electrical cables. Therefore, long distances can be spanned with few repeaters. NIR radiation (in the 1–1.6 μm range) is used to transport the signal since silica possess high transparency in this spectral region.

An optical fibre is a cylindrical dielectric waveguide that transmits light along its axis by total internal reflection. The fibre consists of a *core* of a high refractive-index material surrounded by a *cladding* layer of a lower refractive-index. The different refractive-index values of the waveguide and its cladding, ensure the confinement of the light beam into the core and optical signal trasmission occurs as a results of a light constant bouncing at the interface between the two layers.[16] Figure A.1.iv.

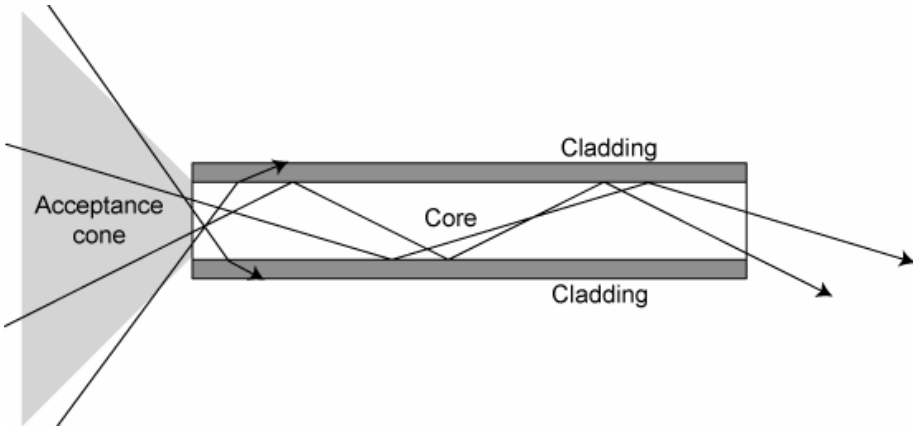

Fig. A.1.iv: Sketch of a typical optical waveguide.

Optical fibers are usually coated with a tough resin *buffer* layer which may be further surrounded by a *jacket* layer, usually plastic. These layers add strength to the fibre but do not contribute to its optical waveguiding properties. A light-absorbing ("dark") glass between the fibres prevents light that leaks out of one fibre from entering another. This reduces cross-talk between the fibers and therefore allows to avoid any signal interference and noise.

Although glass optical fibers are characterised by a very low optical attenuation compared to other optical waveguides, they suffer from optical losses arising from scattering or absorption phenomena mostly due to impurities in the glass (e.g presence of O–H groups). This calls for the integration of signal amplifiers in the waveguide. Signal amplification could be obtained by doping the guiding layer with an active element that (if pumped properly) gives rise to optical gain. Some trivalent NIR-emitting lanthanide ions (Er^{3+}, Yb^{3+}, Nd^{3+}) can provide signal amplification for optical communication.[13,17-19] Er-doped materials are very attractive for lasers systems operating in the third telecommunication window at 1.5 μm and are extensively exploited in telecommunications. Nowadays, EDFAs (Er-doped fiber amplifiers) are the most diffused amplification systems used in the long-haul telecommunication technology operating in the 1.5 μm window.

However, this technology presents some drawbacks that still result in the fabrication of long and expensive amplifiers. The first difficulty arises from the low solubility of lanthanide inorganic salts in all the matrices optical fibres are made of. This often leads to the formation of clusters and to

concentration quenching even at relatively low concentration.[17] In addition, lanthanide ions have very low absorption and emission cross-section that makes optical pumping, required to obtain laser population inversion and stimulated emission, very inefficient, difficult and costly. Lanthanide complexes with suitable antenna ligands represent a strategy to overcame these drawbacks since organic ligands make lanthanide compounds more soluble in the silica matrix and, at the same time, provide a way to enhance optical pumping by allowing an indirect mechanism of excitation of the metal ion. Therefore, optical gain can be achieved by using a readily available and rather inexpensive laser pump.

A.2 Electronic and vibrational spectra of erbium quinolinolates

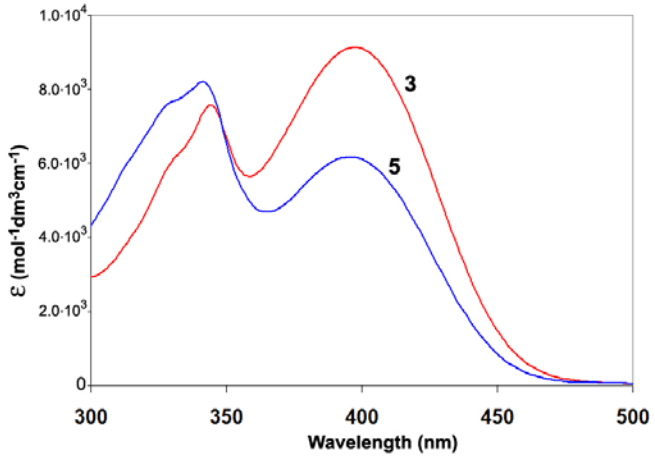

Fig. A.2.i: UV-visible spectrum of **3** (blue line) and **5** (red line) in MeOH solution.

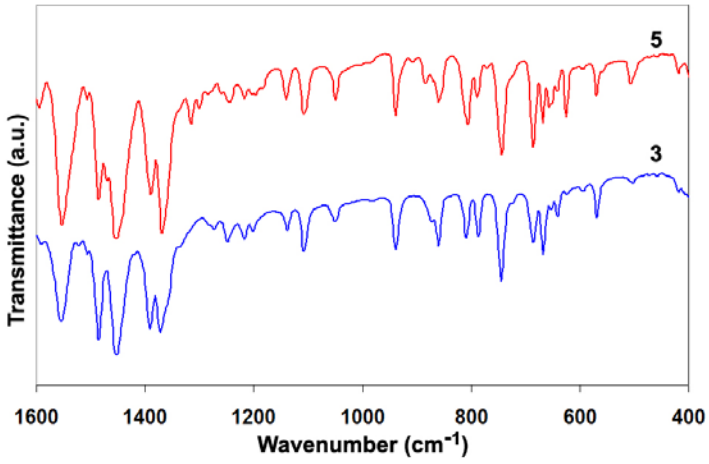

Fig. A.2.ii: FT-IR spectra of **3** (*tris* complex) and **5** (*tetrakis* complex).

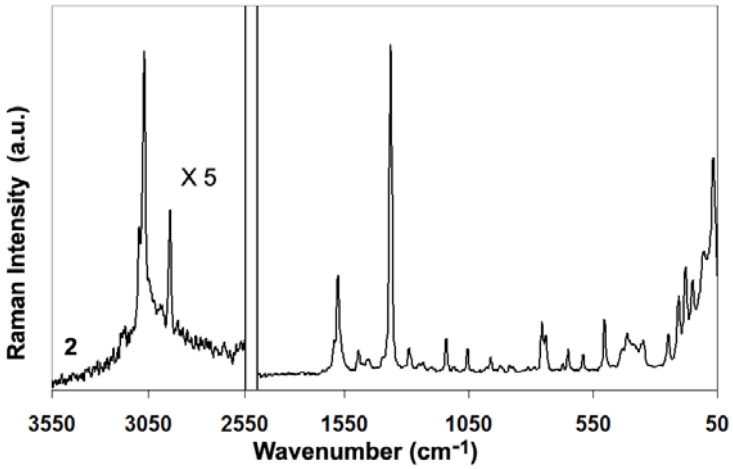

Fig. A.2.iii: FT-Raman spectrum of $[Er(5,7ClQ)_3(H_2O)_2]$ (**2**).

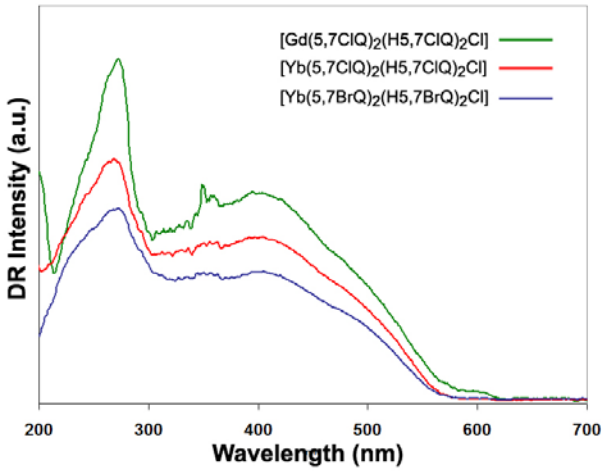

Fig. A.2.iv: Stacked DR spectra of *tetrakis* complexes of Gd^{III} and Yb^{III} in the 200-700 nm spectral region.

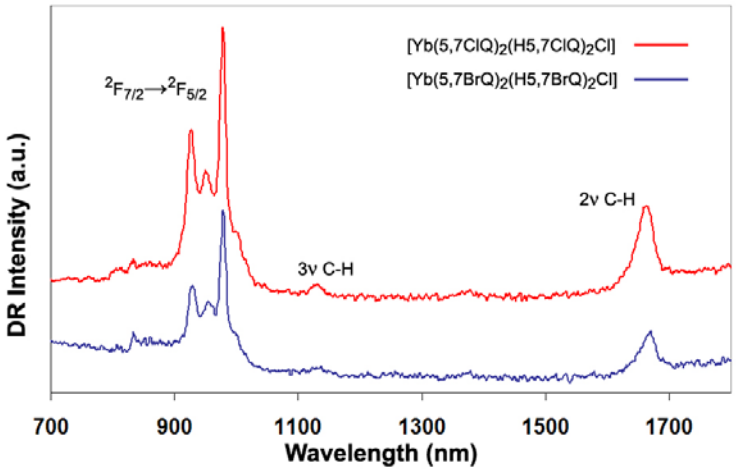

Fig. A.2.v: DR spectra of $[Yb(5,7XQ)_2(H5,7XQ)_2Cl]$ (X = Cl, red line, X = Br, blue line) in the 200-700 nm spectral region.

A.3 Molecular orbitals

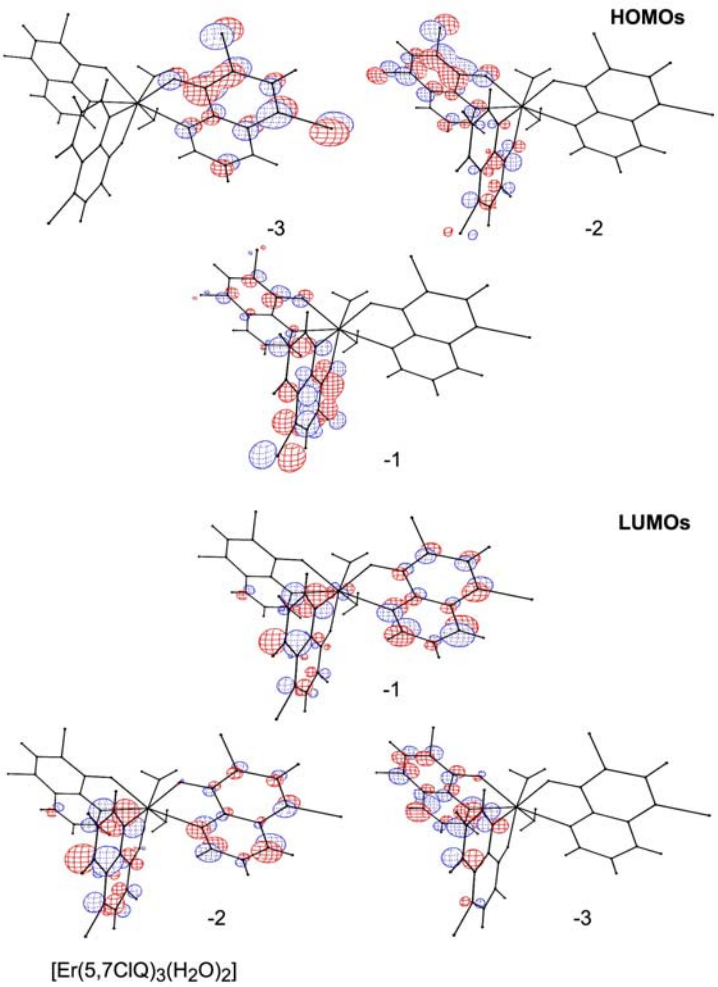

Fig. A.3.ii: The last three closely-spaced HOMOs and the first three closely-spaced LUMOs in **2**, calculated by using semi-empirical extended Hückel methods through the CACAO program.[20]

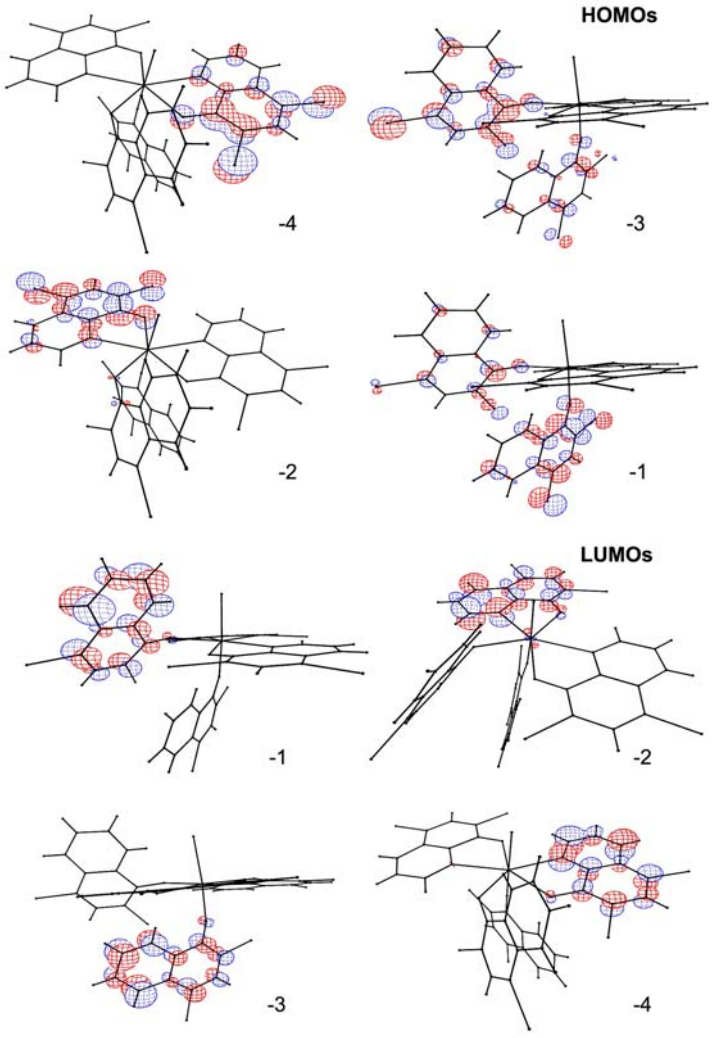

$[Er(5,7BrQ)_2(H5,7BrQ)_2Cl]$

Fig. A.3.ii: The last four closely-spaced HOMOs and the first four closely-spaced LUMOs in **5**, calculated by using semi-empirical extended Hückel methods through the CACAO program.[20]

A.4 Structure of $[ErCl_2(H_2O)_6]Cl$

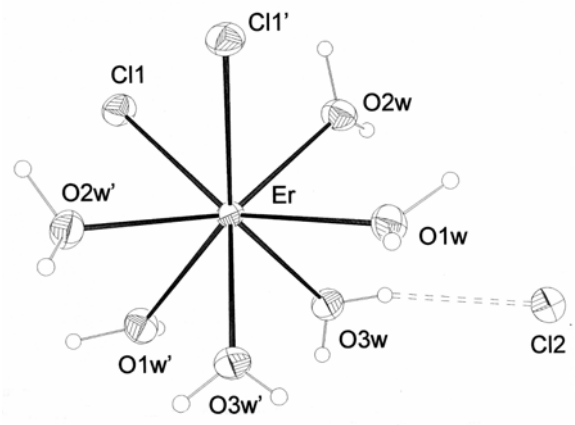

Fig. A.4.i: Ortep drawing of $[ErCl_2(H_2O)_6]Cl$ at the 30% ellipsoids level. The Erbium atom exhibits a square antiprismatic geometry. d(Er-O) = 2.338(3)-2.374(3) Å, d(Er-Cl(1)) = 2.735(1) Å.

A.5 Magnetic measurements

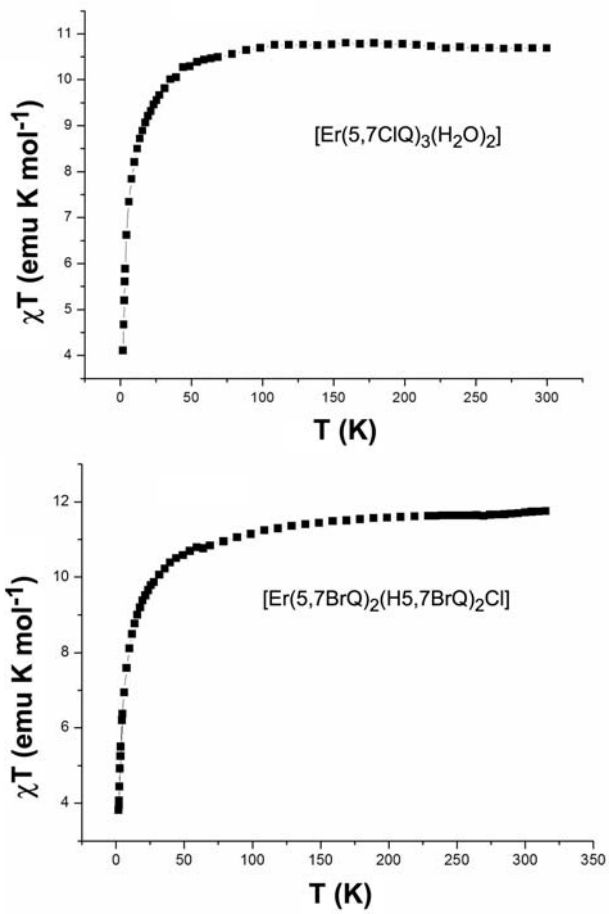

Figg. A.5.i,ii: Temperature dependence of the $\chi_M T$ product in the temperature range 2-300 K for $[Er(5,7ClQ)_3(H_2O)_2]$ (**2**), (above) and for $[Er(5,7BrQ)_2(H5,7BrQ)_2Cl]$ (**5**), (below).

A.6 Crystallographic data and experimental details for $K_2[Er(C_5O_5)(\mu_2\text{-}SO_4)(OH_2)_4]_2$

A.6.1. Crystallographic data

Crystallographic data for $K_2[Er(C_5O_5)(\mu_2\text{-}SO_4)(OH_2)_4]_2$	
Empirical formula	$C_5H_8ErKO_{13}S$
Formula weight	514.53
Crystal size (mm)	0.10 x 0.05 x 0.03
Crystal system; Space group	Monoclinic; $P2_1/a$
a, b, c (Å)	12.169(7); 7.866(3); 13.898(8)
α, β, γ (deg.)	90; 110.61(2); 90
V (Å³)	1245.2(11)
Z; ρ(calc) (Mg/m³)	4; 2.745
T (K)	293(2)
μ (mm^{-1})	7.314
θ range (deg.)	3.03 to 27.00
No.of rflcn/obsv F>4σ(F)	2807 / 2705
GooF	1.015
R1	R1 = 0.1249
wR2	wR2 = 0.1351

Table A.6.i: Summary of X-ray crystallographic data for $K_2[Er(C_5O_5)(\mu_2\text{-}SO_4)(OH_2)_4]_2$.

A.6.2 Experimental

Chemicals. All the reagents and solvents were purchased from Aldrich and used without further purification.

$K_2[Er(C_5O_5)(\mu_2\text{-}SO_4)(OH_2)_4]_2$: $KCr(SO_4)_2{\cdot}12H_2O$ (0.092 g, 0.184 mmol) and $Er(NO_3)_3{\cdot}5H_2O$ (0.163 g, 0.368 mmol) and potassium croconate ($K_2C_5O_5$, 0.182 g, 0.828 mmol) were dissolved in 100 mL of distilled water under gentle heating. After few minutes, a yellow precipitate began to form and the mixture was maintained under stirring at room temperature for 1 day. The precipitate was collected by filtration and then redissolved in 200 mL of water under heating. When all the product was dissolved, the solution was roto-evaporated up to half volume and then left standing to the air. After several days well-shaped yellow block crystals suitable for X-ray structural studies were obtained, washed with water/ethanol 1:1 mixture and dried in oven (60°C). **CHN**: Found (Calcd): C% 11.75(63.69), H% 1.65(1.57). **FT-IR spectrum** (cm^{-1}): 3341 s,br 3049 m (νC–H), 2079-2066 vs (split peak, νCN), 1651 mw, 1630 m, 1576 m, 1541 w, 1647 m (νC=O uncoordinated),[21] 1582 s (νC–O coordinated), 1475 br, vs (νC–O + νC–C),[21] 1409 ms, 1383 s, 1140-1097 s (split peak, δSO_4^{2-}), 833 mw, 644 m, 600 mw, 565 mw, 530 mw, 459 w. **DR spectrum** (nm): 449, (broad bands, ligand $\pi\rightarrow\pi^*$ transition); 519, 541, 652, 800, 971, 1507 (f→f); 1974 ($a\nu_1+\nu_2+b\nu_3$ H_2O).

Measurements. See Chapter 3, Paragraph 3.6.2.

Crystal structure determination of $K_2[Er(C_5O_5)(\mu_2\text{-}SO_4)(OH_2)_4]_2$ was performed by Dr. Luciano Marchiò, University of Parma, Italy.

A.7 d-complexes as ligands: synthesis and characterisation of cyano-bridged $[Fe(phen)_2(\mu\text{-}CN)_2Er(NO_3)_3(H_2O)]_2$

A.7.1 Molecular structure and crystallographic parameters for $[Fe(phen)_2(CN)_2]\cdot 2H_2O$

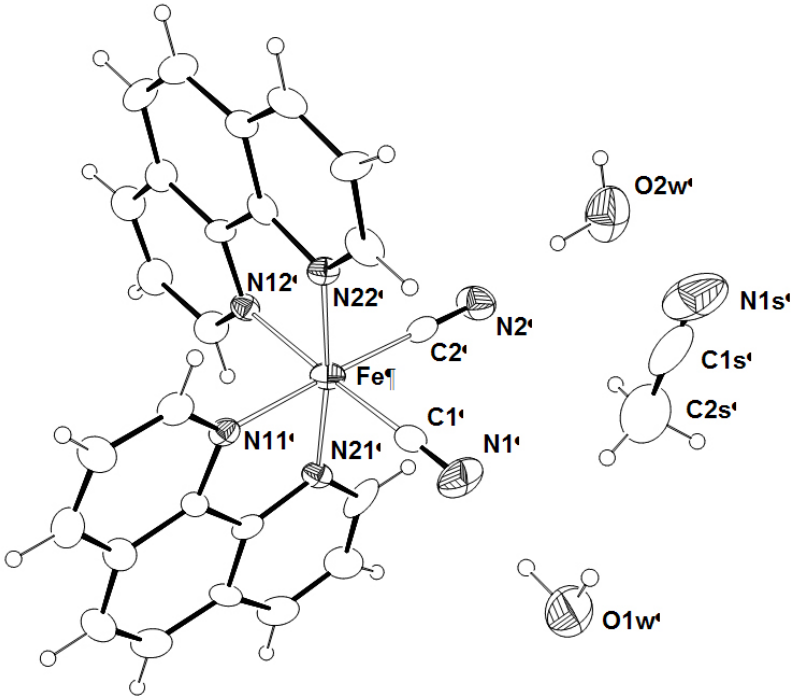

Fig. A.7.i: Crystal structure of $[Fe(phen)_2(CN)_2]\cdot 2H_2O\cdot CH_3CN$.

Crystallographic data for $[Fe(phen)_2(CN)_2]\cdot 2H_2O\cdot CH_3CN$	
Empirical formula	$C_{28}H_{23}FeN_7O_2$
Formula weight	545.38
Crystal size (mm)	0.10 x 0.08 x 0.05
Crystal system	Triclinic
Space group	P-1
a, b, c (Å)	10.266(4); 10.396(4); 12.107(4)
α, β, γ (deg.)	80.92(1); 78.75(1); 87.07(1)
V (Å^3)	1251.1(8)
Z	2
ρ(calc) (Mg/m^3)	1.448
T (K)	293(2)
μ (mm^{-1})	0.644
θ range (deg.)	1.73 to 24.04
No.of rflcn/obsv F>4σ(F)	11601/3934
GooF	0.892
R1	0.1572
wR2	0.0688

Table A.7.i: Summary of X-ray crystallographic data for $Fe(phen)_2(CN)_2$.

A.7.2 Crystallographic data for $[Fe(phen)_2(\mu\text{-}CN)_2Er(NO_3)_3(H_2O)]_2$ (Fe_2Er_2)

A summary of crystallographic parameters for **Fe_2Er_2** is reported in Table A.3. Intermetallic distances and angles are reported in Table A.4.

Crystallographic data for $[Fe(phen)_2(\mu\text{-}CN)_2Er(NO_3)_3(H_2O)]_2$	
Empirical formula	$C_{56}H_{42}Er_2Fe_2N_{20}O_{20}$
Formula weight	1761.32
Crystal size (mm)	0.20 x 0.10 x 0.05
Crystal system; Space group	Monoclinic; $P2_1/a$
a, b, c (Å)	10.74(7), 25.59(9), 11.74(8)
α, β, γ (deg.)	90, 100.26(3), 90
V (Å³)	3174(32)
Z; ρ(calc) (Mg/m³)	2; 1.843
T (K)	293(2)
μ (mm^{-1})	3.156
θ range (deg.)	3.07 to 25.00
No.of rflcn/obsv F>4σ(F)	6741/5575
GooF	0.768
R1	0.1550
wR2	0.0747

Table A.7.ii: Summary of X-ray crystallographic data for **Fe_2Er_2**.

Fe···Er(Fe'···Er')	5.470 Å
Fe···Er'(Fe'···Er)	5.359 Å
Fe···Er'···Fe' (Fe···Er···Fe')	86.52 deg
Er'···Fe···Er (Er'···Fe'···Er)	93.48 deg

Table A.7.iii: *Intermetallic distances and angles for* **Fe_2Er_2**.

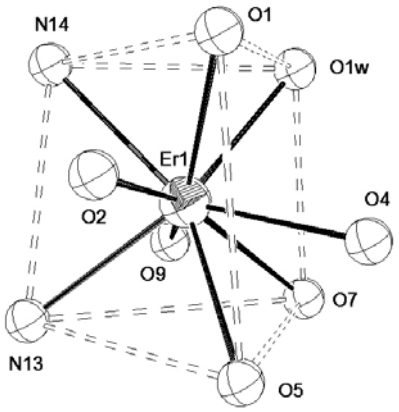

Fig. A.7.ii: Ortep drawing of the erbium coordination environment in **Fe_2Er_2**.

A.7.3 Experimental

Chemicals. All the reagents and solvents were purchased from Aldrich and used without further purification.

[Fe(phen)$_2$(CN)$_2$]·2H$_2$O: $Fe(NH_4)_2(SO_4)_2 \cdot 6H_2O$ (0.975 g, 2.5 mmol) and 1,10-phenatroline (1.5 g, 7.5 mmol) were dissolved in 100 mL of distilled water and the dark red mixture was heated to just below the boiling point. Afterward, a freshly prepared solution of KCN (2.5 g) in 5 mL of H_2O was added all at once. After 30' of stirring the reaction mixture was allowed to cool at room temperature, and violet crystalline platelets began to form. After 24 h the crystalline product was filtered, washed with water, and dried in vacuum at room temperature. **CHN**: Found (Calcd): C% 64.68(63.69), H% 3.84(4.52), N% 17.56(17.14). Dark-violet crystals suitable for X-ray studies were obtained from recrystallisation in CH_3CN. **FT-IR spectrum** (cm^{-1}): 3432 m,br 3049 m (νC–H), 2079-2066 vs (split peak, νCN), 1651 mw, 1630 m, 1576 m, 1541 w, 1507 w, 1454 m, 1429 s, 1409 ms, 1385 m, 1342 w, 1299 mw, 1254 w, 1206 mw, 1141 mw, 1097 mw, 1056 mw, 981 w, 915 w, 845 vs, 781 ms, 724 s, 668 vw, 645 vw, 558 w, 540 ms, 522 m. **UV-Vis spectrum** (nm; [mol^{-1} dm^3 cm^{-1}]): 226[(21.6±0.1)10^3], 265[(22.4±0.1)10^3], 364[(0.6±0.1)10^3], 524[(2.7±0.1)10^3], 593[(3.6±0.1)10^3]. **DR spectrum** (nm): 584, 641, (broad bands), 1126 w (3ν C–H), 1661 (3ν C–H), 1943 (aν_1+ν_2+bν_3 H_2O).

[Fe(phen)$_2$(μ-CN)$_2$Er(NO$_3$)$_3$(H$_2$O)]$_2$ (**Fe$_2$Er$_2$**)*:* $[Fe(phen)_2(CN)_2] \cdot 2H_2O$ (0.123 g, 0.243 mmol) was dissolved in 100 mL of $CHCl_3/CH_3CN$ 1:1 solvent mixture under gentle heating. When all the solid was dissolved, the dark violet solution was cooled down in an ice bath and a solution of $Er(NO_3)_3 \cdot 5H_2O$ in 20 mL of CH_3CN was slowly added. The reaction mixture turned suddenly red. After few minutes red crystals began to form and the mixture was left standing overnight at 4°C. Red crystals

suitable for X-ray studies were collected, washed with $CHCl_3$ to dissolve all the unreacted iron complex precursor, and dried in vacuum at room temperature. **CHN**: Found (Calcd): C% 37.13(37.02), H% 2.27(2.63), N% 14.56(14.94). **FT-IR spectrum** (cm^{-1}): 3401 m,br 3084 w (νC–H), 2426 vw, 2094 vs (νCN), 1653 mw, 1635 mw, 1577 w, 1559 w, 1521-1484 s (broad, νNO_3^-), 1428 ms, 1384 vs (νC(1)–C(2) phenanthroline), 1298 s (broad, νNO_3^-), 1212 vw, 1143 mw, 1031 mw, 847 ms, 814 mw (νNO_3^-), 775 w, 750 mw (νNO_3^-), 725 ms, 668 mw, 545 w. **UV-Vis spectrum** (nm; [mol^{-1} dm^3 cm^{-1}], ε calculated for the dimeric unit $[Fe(phen)_2(\mu\text{-}CN)_2Er(NO_3)_3(H_2O)]_2$): 475[$(6.2\pm0.1)10^3$], 520[$(6.6\pm0.1)10^3$]. **DR spectrum** (nm): 415, 531, (broad bands), 960 (broad band), 1508 (Er^{III} $^4I_{13/2}\leftarrow{}^4I_{15/2}$) 1661 ($3\nu$ C–H), 1922 ($a\nu_1+\nu_2+b\nu_3$ coordinated H_2O).

Measurements. See Chapter 3, Paragraph 3.6.2.

Crystal structure determinations of $[Fe(phen)_2(CN)_2]\cdot 2H_2O$ and $[Fe(phen)_2(\mu\text{-}CN)_2Er(NO_3)_3(H_2O)]_2$ were performed by Dr. Luciano Marchiò, University of Parma, Italy.

References

[1] C.W. Tang, S.A. VanSlyke, *Appl. Phys. Lett.* **1987**, *51*, 913.

[2] C. H. Chen, J. Shi, *Coord. Chem. Rev.* **1998**, *171*, 161.

[3] C. W. Tang, S. A. VanSlyke, C. H. Chen, *J. Appl. Phys.* **1989**, *65*(9), 3610.

[4] U. Mitscke, P. Bauerle, *J. Mater. Chem.* **2000**, *10*, 1471.

[5] T. W. Kelley, P. F. Baude, C. Gerlach, D. E. Ender, D. Muyres, M. A. Haase, D. E. Vogel, S. D. Theiss, *Chem. Mater.* **2004**, *16*, 4413.

[6] R. J. Curry, W. P. Gillin, *Appl. Phys. Lett.* **1999,** *75,* 1380.

[7] W. P. Gillin, R. J. Curry, *Appl. Phys. Lett.* **1999**, *74,* 798.

[8] O. M. Khreis, R. J. Curry, M. Somerton, W. P. Gillin, *J. Appl. Phys.* **2000**, *88*, 777.

[9] M. Iwamuro, T. Adachi, Y. Wada, T. Kitamura, S. Yanagida, *Chem. Lett.* **1999**, 539.

[10] O.M. Khreis, W.P. Gillin, M. Somerton, R.J. Curry, *Org. Electron.* **2001**, *2*, 45.

[11] J. Kido, Y.Okamoto*, Chem. Rev.* **2002**, *102*, 2357.

[12] C. Adachi, M.A. Baldo, S.R. Forrest, *J. Appl. Phys.* **2000**, *87*, 8049.

[13] J. Kido, K. Nagai, Y.Ohashi, *Chem. Lett.* **1990**, 657.

[14] L.H. Slooff, A. van Blaaderen, A. Polman, G.A. Hebbink, S.I. Klink, F.C.J.M. Van Veggel, D.N. Reinhoudt, J.W. Hofstraat, *Appl. Phys. Rev.* **2002**, *92*, 3955.

[15] A.Polman, *J. Appl. Phys.* **1997**, *82*, 1.

[16] L. Eldada, *IEEE Journal of Selected Topics in Quantum Electronics* **2000**, *6*, 54

[17] K. Kuriki, Y. Koike, Y. Okamoto, *Chem Rev.* **2002**, *102*, 2347.

[18] L.H. Slooff, A. Polman, M.P. Oude Wolbers, F.C.J.M. van Veggel, D.N. Reinhoudt, J.W. Hofstraat, *J. Appl. Phys.* **1998**, *83*, 497.

[19] R. Pizzoferrato, T. Ziller, R. Paolesse, F. Mandoj, A. Micozzi, A. Ricci, C. Lo Sterzo *Chem. Phys. Lett.* **2006**, *427*, 124-128.

[20] C. Mealli, D. Proserpio, *J. Chem. Ed.* **1990**, *67*, 39.

[21] R. West, M. Ito, *J. Am. Chem. Soc.*, **1963**, *85*, 2580-2584.

Acknowledgement

Firstly, I wish to thank very much all my research group. Thanks to my supervisor, Prof. Paola Deplano, for having proposed me this interesting research and for her precious guide. Thanks to Prof. Maria Laura Mercuri, Dr. Angela Serpe, Prof. Emanuele Trogu and to Drs. Luca Pilia and Marco Salidu for their constant support and the valuable advice.

I wish also to acknowledge Dr. Luciano Marchiò who performed the structural characterisation and the ESI-Mass spectra of the complexes and all the Prof. Bongiovanni's research group, in particular Dr. Riccardo Orrù, for the photoluminescence studies on the erbium quinolinolates.

I am grateful to Dr. Rik Van Deun and Prof. Koen Binnemans who gave me the opportunity to spend a research stay in their lab at the University of Leuven. In particular, I wish to thank very much Dr. Rik Van Deun, who suggested me to work on lanthanide doped-sol gel glasses, and for his help during my stay in Leuven.

Finally, my acknowledgement go to Prof. Andrea Caneschi and to Dr. Kevin Bernot for the magnetic measurements.

This research has been carried out thanks to the financial support of the Fondazione Banco di Sardegna, the MIUR (PRIN-2005033820_002 "*Molecular materials with magnetic, optical and electrical properties*") and the COST, which are gratefully acknowledged.